ENHANCED CONDITIONS FOR HIGH PERFORMANCE MACHINING

ENHANCED CONDITIONS FOR HIGH PERFORMANCE MACHINING OF HARDENED H13 DIE STEEL

By

AML ELFIZY, B.SC.

Cairo University, Egypt

A Thesis

Submitted to the School of Graduate Studies

in Partial Fulfillment of the Requirements

for the Degree

Masters of Applied Science

McMaster University

MASTER OF APPLIED SCIENCE (2008) McMaster University

(Mechanical Engineering) Hamilton, Ontario

TITLE: Enhanced Conditions for High Performance Machining of Hardened H13 Die Steel

AUTHOR: Aml Elfizy, B.Sc. (Cairo University, Egypt)

SUPERVISOR: Dr. Stephen Veldhuis

Department of Mechanical Engineering

McMaster University

NUMBER OF PAGES: xvii, 214

Abstract

The availability of sophisticated machine tools, together with advanced cutting tool designs and high performance coatings has allowed machining to meet many challenges. A significant remaining challenge is the competitive milling of hardened steels at moderate to high cutting speeds. This is of particular importance for the die and mould making industry. Despite the necessity to achieve higher production rates and improved surface finish, cutting speeds above the range of 300-600 m/min are still not possible. This limitation is due to the combination of high mechanical, thermal and chemical interactions that are taking place on the tool surface during cutting.

To address this situation, an extensive amount of research has been focused on developments associated with hard coatings such as nano-multilayered hard PVD coatings that exhibit novel mechanical and thermal properties. The development of methodologies for designing a cutting tool with a strong cutting edge micro-geometry has set guidelines for selecting proper cutting edge preparation for specific cutting applications.

The results indicate that, the development of new hard coating designs is the most effective way to improve the service life of coated carbide tools for hard high speed milling applications. The developments of both robust and rigid substrate designs with adaptive cutting edge micro-geometries assist the cutting tool performance by favoring the surface adaptability of the deposited coating. The developments of different strategies for dry air cooling that provide a "soft-cool" environment seem to have a

beneficial impact on cutting performance and tool life improvement. Dry air cooling is found to be more effective than chilled-air cooling and minimum-quantity-lubrication (MQL). Therefore, the utilization of a cutting environment tailored to meet the requirements of both the tool and the coating while providing sufficient air flow to remove chips from the cutting zone will complement the adaptability of the whole tool-workpiece-chip system.

To the Loving Memory of my Father, ***Abdul Rihiem*** 1935-2007

Acknowledgements

This thesis would not have been possible without the guidance and support of many people to whom I owe my sincere gratitude and respect.

I am most grateful to my supervisor Dr. Stephen Veldhuis for his continuous guidance, enthusiasm, support and patience throughout this research. His research motivation and critical reviews contributed immensely to this work. I would like to thank Dr. German Fox-Rabinovich for always being supportive and in particular for reviewing different topics of this research. Special thanks are due to my committee members Dr. Mo Elbestawi and Dr. Peidong Wu for taking the time to read and review this thesis.

I am deeply indebted to Dr. Allan Spence, Dr. Stephen Veldhuis, Dr. Peidong Wu, Dr. Philip Koshy and Dr. Mukesh Jain for the valuable knowledge they shared in the instruction of their courses.

I would also like to thank Warren Reynolds, Terry Wagg, Jim McLaren, Etienne Thomas and Jean-François Fritsch for their technical assistance.

Last, but certainly not least, I would like to acknowledge my family, friends and colleagues, whose constant love, aid and encouragement made this work possible.

Table of Contents

List of Figures

List of Tables

Chapter 1: Introduction

1.1 Motivation

The overall goal of modern machining is to achieve the highest material removal rate per overall process cost, while meeting geometrical, dimensional and surface quality requirements for the machined part. Productivity, cost and quality are all important considerations as are environmental, and health and safety issues. High performance machining concepts are ideally suited to meet these objectives. The high performance can be accomplished by using high cutting speeds and feeds in a dry environment using specially prepared tooling. High performance milling of hardened steels using carbide tools is still considered to be a relatively challenging machining operation, owing to the demanding properties of the workpiece material and the nature of the high speed interrupted cutting action.

Of particular concern is the rate of tool wear. If tool wear is too high, then the process is no longer viable from both an economic and quality standpoint. Tool wear is a result of a combination of mechanical, thermal and chemical activities taking place at the cutting edge. Several forms of tool wear can be controlled by using lower cutting speeds. However, lower cutting speeds offer less productivity. Therefore, finding ways to enhance tool life, while maintaining high cutting speeds, is critical to promoting high performance machining of hardened tool steels. An important aspect of this is strengthening the cutting tool and minimizing the aggressive nature of the surface interactions that take place by reducing friction. This can be achieved by using tough carbide grades with improved tool designs. These improved designs would include strong cutting edges and nano-scale mono/multi-layered hard coatings that exhibit adaptive properties under high temperatures and heavy loads. In addition, a well controlled favorable cutting environment can increase the cutting tool life by enhancing specific elements of adaptability and thus delay several forms of tool wear.

1.2 Research Objective

Tool design usually refers to three main aspects in modern machining applications: substrate design, coating design and cutting edge micro-geometry or the so-called "cutting edge preparation". Therefore, the main scope of this thesis is to investigate the influence of the three aforementioned aspects of tool design on the cutting performance of coated carbide tools during high speed milling of hardened Die Steel (AISI H13) with a hardness of (HRC 54-55) under different cutting environments. Different cutting speeds were utilized in this research in order to try to enhance the unique properties of the nano-multilayered TiAlCrN/NbN PVD coating used in this research and to identify the limitations in the operational cutting speeds.

Cutting edge preparation can have a big impact on tool performance. The improper selection of cutting edge micro-geometry can lead to higher rates of flank wear and correspondingly higher machining force components. This can have a detrimental effect on the machining accuracy, particularly in hard cutting, where higher magnitudes of cutting force are typical. Therefore, a methodology for designing a cutting edge geometry which exhibits geometric adaptive properties was studied. Opportunities for tool life and productivity improvement due to the beneficial interaction of the geometric adaptability of the tool with the self-adaptability of the coating were also explored. This was done by considering the influence of the cutting edge micro-geometry and coating properties on the cutting forces, surface roughness and chip morphology.

In light of its potential impact on the cutting performance, the cutting environment must be tailored efficiently to the cutting process. In order to reach this goal, an experimental investigation was conducted using different dry cooling and minimum-quantity-lubrication (MQL) cutting environments. The cutting performance of TiAlCrN/NbN PVD coated carbide tools was assessed under different dry air cooling strategies in order to develop a feasible strategy with both effective cooling and sufficient air flow to remove chips. The influence of these different dry air cooling strategies on dynamic cutting forces, surface roughness and chip morphology was investigated. The influence of mist lubrication on the cutting performance of TiAlCrN/NbN PVD coated carbide tool was investigated as well.

In addition, the experimental investigation focused on the mechanism of saw-tooth chip formation during hard cutting and discussed whether or not the mechanism is influenced by different cutting variables such as tool wear, cutting speeds, cutting tool design and cutting environment. Furthermore, a post-polished coated-carbide tool was utilized in order to investigate the influence of post-treatment polishing of coating surfaces on tool life improvement.

A class of commercially available hard Supernitride-HSN^2 PVD coatings was also tested. This class of coatings was considered due to the high chemical stability under elevated cutting temperatures that is achievable due to the advanced sputtering technology employed.

1.3 Thesis Outline

This thesis first provides a detailed literature survey on the machining of hardened steels. This then leads to discussion of the ongoing research related to the development of cutting tool designs, hard coatings and cutting environments for high performance machining. The rest of this thesis is then organized as follows: Chapter 3 provides a detailed description of the experimental setup and procedure; Chapter 4 is dedicated to the experimental investigations and discussions of the developments of various machining aspects that impact the machining of hardened steels for die and mould making applications; Chapter 5 summarizes the findings of the research and discusses some anticipated future research trends.

Chapter 2: Literature Survey

2.1 Machining of Hardened Steels

Manufacturing of dies and moulds for hot-working applications is influenced by the demanding properties of the working material such as its composition, structure and hardness. Hot-working tool steels which contain high carbide content within the tempered martensite matrix exhibit high resistance to abrasive wear, plastic deformation, thermal softening and fatigue cracking. In recent years the machining of hardened steels for the die and mould making industry has developed tremendously, owing to the vast development of machine tools, CAD/CAM integrated systems, hard coating materials, substrate designs and carefully controlled cutting environments.

All of these factors have made it possible to perform hard cutting more efficiently under improved cutting conditions with higher cutting speeds, better surface finishes and enhanced geometrical and dimensional accuracy. Thus, the conventional finishing processes of grinding and polishing can be reduced or even eliminated. Accordingly, high speed machining of hardened steel can be utilized effectively from roughing to finishing in one set-up. This is particularly evident in the production of forging dies due to their moderate size with relatively shallow cavities, [Altan et al, 2001]. Figure (2.1) shows the development and reduction of machining times during high speed milling of soft and hard steel for the forging die making industry using solid and inserted carbide ball nose end-mills.

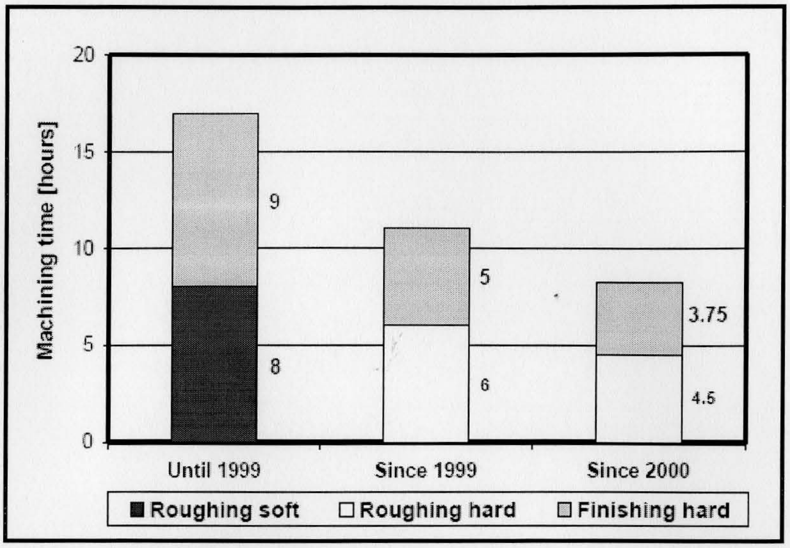

Figure (2.1) Development of machining times for die making industry, [Altan et al, 2001]

2.1.1 Machining of Dies/moulds (AISI H13 Die Steel)

AISI H13 belongs to group-H of Hot-Work Steels. It is a 5% Chromium-based high alloy steel that is commonly used for hot die working applications such as die casting and molding dies particularly dies for the extrusion of aluminum and magnesium, [Davis, 1998]. AISI H13 is directed at specific industries where high hot-hardness and high wear resistance are mandatory to withstand the high temperature, pressure and abrasion associated with the forming of metals. Therefore, the role of alloying is to improve hardenability and to improve the resistance to wear and thermal softening by adding chromium and strong carbide formers such as molybdenum and vanadium, [Davis, 1998]. AISI H13 has a relatively low coefficient of thermal expansion ($\approx$ 10.4-12.4 μm/m-K) and acceptable thermal conductivity ($\approx$ 28 W/m-K). Most chromium hot-working steels are air-hardened to the hardness required for their application areas (up to

60 HRC) and can be heat treated to strengths exceeding 2,070 MPa. Table (2.1) lists the hot hardness of H13 die-steel.

AISI Designation	Hardness, HRC				
		Hot hardness			
	Room Temperature	315 °C (600 °F)	425 °C (800 °F)	540 °C (1000 °F)	650 °C (1200 °F)
H13	55	49	47	42	22

Table (2.1) Hardness of selected H13 die-steel at elevated temperatures, [ASM Handbook, 1990]

High Speed Ball-End Milling

The manufacture of dies or moulds involves complicated shapes and geometries and as such a wide range of radii are required. Ball-end milling is usually utilized for rough, finish and semi-finish machining of these complicated geometries with free-form or sculptured surfaces. An example of a typical sculptured surface generated during ball-end milling is shown in Figure (2.2).

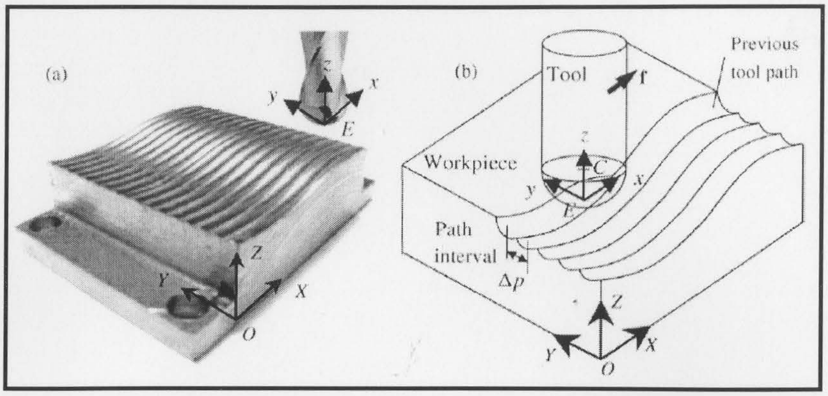

Figure (2.2) Machining of wavelike form surface using ball-end milling, [Fontaine et al., 2006]

2.1.2 Tool Materials and Coatings

Over the years, tool materials, coatings and tool geometries have been developed in order to offer improved cutting performance and an increase in metal-cutting productivity using high performance machining concepts. There are two factors affecting the high performance machining of hardened steels: namely, high cutting temperatures associated with high cutting speeds (up to 1600°C) and an increased workpiece hardness (45-70 HRC). Therefore, there is always a demand for a combination of substrate and coating designs that provides a coated tool with high abrasion wear resistance, fracture resistance, thermal shock resistance and improved lubricity along the chip-tool interface. In addition, a reliable tool design with strong micro-edge geometry reduces the risk of severe edge chipping.

Cubic boron nitride (CBN) tools have very good resistance to diffusion; therefore, they are more likely to be used in cutting applications where very high cutting temperatures are attained, [Movahhedy et al., 2002, and Ren and Altintas, 2000]. Ren and Altintas [2000] found that carbide and CBN tools were used successfully in cutting P20 Mold Steel up to 600 m/min and 1000 m/min respectively. However, the cutting length was more than doubled for the case of the CBN tools when compared to the carbide tools. This is attributed to the higher diffusion limit (i.e. 1600ºC) for Alumina as a binding material in CBN tools when compared to the Cobalt diffusion limit (i.e. 1300ºC) in carbide tools. In general, CBN tools are more prone to chip during hard machining due to their lower toughness. Therefore, strengthening the cutting edge by adding a small radius or chamfer is recommended to prevent tool breakage.

Polycrystalline cubic boron nitride (PCBN) material offers reliable cutting tools for high speed machining of hardened steels since they maintain high hardness and strength at elevated temperatures when compared to carbide tools, as shown in Figure (2.3). While, coated carbide tools offer a cheaper alternative with satisfactory performance for mass-production machining when compared to PCBN tools, especially for interrupted cutting applications with short operating cycles where a tool with higher toughness is recommended, [Dumitrescu, 1998].

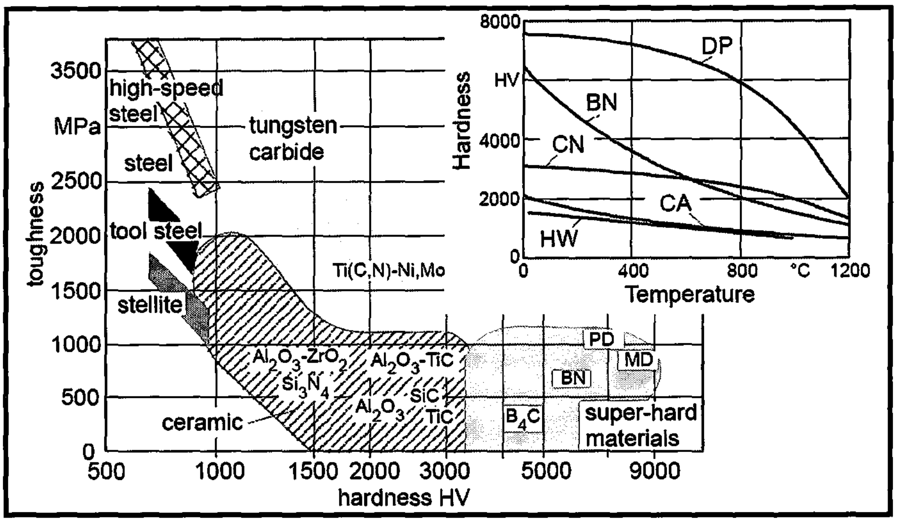

Figure (2.3) Toughness and Hot-hardness of hard tool materials, [Byrne et al., 2003]

Nevertheless, the ability of PCBN tools to maintain higher hardness at high cutting temperatures resulted in better abrasive wear resistance than carbide tools when milling hardened steel (HRC 48-56) at low/medium cutting speeds (60 to 100 m/min), [Braghini and Coelho, 2001]. Despite the higher conductivity of carbide tools as compared to PCBN tools, much smaller flank wear was developed on PCBN tools when compared to carbide. It can be concluded from this study that the increased hardness of PCBN tools outweighs the benefits from the improved toughness of the carbide tools under the cutting conditions used in this study.

Tungsten Carbide (WC) Tool Materials for Hard Cutting Operations

The grade of tungsten carbide tools is usually characterized by three main factors: binder content, hardness and grain size of the carbide particles; refer to Table (2.2). In general, hard milling applications require a hard carbide grade which possesses high abrasion resistance. Therefore, tooling with a uniform microstructure that is micro-grain in size (0.2-1 μm) is recommended for this type of application due to its increased hardness and increased carbide strength (hardness up to 2000 HV and transverse rupture strength up to 3000 N/mm^2), [Electronica Machine Tools Ltd., 2007].

GUIDE TO CARBIDE PROPERTIES		THIS IS WHAT WILL HAPPEN TO :				
		Cobalt %	Abrasion Resistance	Grain Size	Hardness	Fracture Toughness
WHEN YOU INCREASE :	Cobalt Content		↓		↓	↑
	Abrasion Resistance	↓		↓	↑	↓
	Grain size		↓		↓	↑
	Hardness	↓	↑	↓		↓
	Fracture Toughness	↑	↓	↑	↓	

Table (2.2) Characteristics of carbide cutting tools, [Electronica Machine Tools Ltd., 2007]

In addition to high wear resistance, milling cutting tools demand carbide substrates with high toughness (i.e. high impact or high transverse rupture strength[1]) in order to resist the mechanical cyclic loading that results from the interrupted cutting action associated with milling. Therefore, a combination of high cobalt (Co) content and sub-micron grains are preferred in this application.

Carbide tools are usually employed for the interrupted cutting of hardened steels due to their relatively higher toughness and lower price as compared CBN or PCBN tools. In general, WC/Co alloys having 5-12 wt% Co and carbide grain size range of 0.5-

[1] Transverse rupture strength (TRS) represents the maximum tensile strength the cutting edge can withstand before it fails by catastrophic fracture, [Dokainish et al., 1989]

5 µm are commonly used for machining steels. Another advantage comes from the short chips that are produced [Santhanaml, 2003].

Due to the heat generated in the cutting process there is degradation in the fracture strength of the tool. This usually occurs when the cutting temperature exceeds 500°C, [Acchar et al., 1999, and Tlusty and Masood, 1978]. The fracture strength degradation of carbide tools at elevated temperatures is related to the high oxidation rates that are encountered during cutting; refer to Figure (2.4). Given that the substrate material of the tool is working at its limit in these applications, the development of new coatings that offer improved thermal and mechanical properties is of great importance.

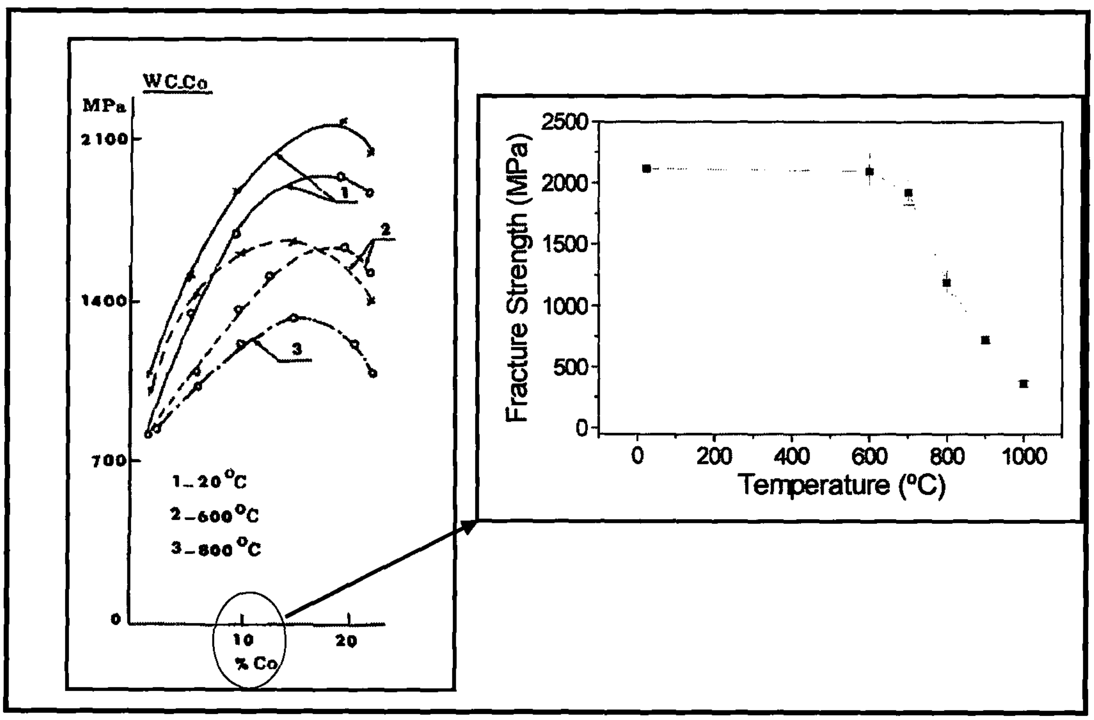

Figure (2.4) Transverse rupture strength of WC/Co alloys as a function of temperature and cobalt content, reproduced from [Acchar et al., 1999, and Tlusty and Masood, 1978]

Tool Coatings

Coatings serve to significantly enhance the cutting performance of tungsten carbide tools. The development of hard coatings with high hot hardness, high lubricity and improved surface adaptability hold great promise for improving machining productivity and tool life for high speed machining of hardened steels. The ideal coating for high speed machining of hardened steel should be as follows:

- Hard with an improved toughness and strong adherence to the substrate;
- Chemically stable with appreciable inertness for better diffusion resistance;
- Thin with ultra-fine grain size to prevent brittleness but thick enough to shield the cutting tool from any chemical and adhesion wear mechanisms during cutting.

2.1.3 Heat Generation

In metal cutting, the mechanical energy is mostly transformed into heat within the cutting zone (i.e. primary, secondary and tertiary shear zones). Since all tool wear mechanisms are activated under conditions of high cutting temperatures, the heat generated in the cutting zone is considered to be the most significant factor affecting cutting performance. Most of the heat generated within this thermally active environment is transferred into the chips with a lesser amount being conducted into the tool. Some of the heat is carried off by convection to the surroundings or conduction into the workpiece. In high performance milling applications, the high speed nature of the cutting action lowers the contact time between the tool and chip thus reducing the amount of time available for heat transfer. This serves to reduce the overall temperature but also increases the thermal fatigue.

Thermal fatigue occurs in milling when the cutting tool undergoes severe variation of temperature. In this case, thermal cycling is developed within the cutting and non-cutting periods and hence, tensile stresses are induced in the tool surface resulting in thermal fatigue cracking particularly when milling hardened steel with tungsten carbide tools. The thermal impact repeats itself every cutting cycle. The heating-up/cooling-off period depends on the cutting environment, as well as the value of tool immersion inside the workpiece, [Tlusty, 1999]. An experimental and numerical study in [Shaw, 2005] showed that the tool-face temperature did not go to zero at the end of the non-cutting period, which indicates that the dominant induced stresses are still compressive. It was revealed that the tensile thermal cracks are usually developed on the tool surface during interrupted cutting as a result of induced tensile stresses at the end of the heating-up period rather than at the end of the cooling-off period due to the thermal expansion of the heated zone.

Another very common factor that produces heat during dry milling is the development of seizure at the chip-tool interface. In this situation, dry frictional conditions are utilized resulting in a large contact area and more concentration of surface deformation. As a consequence, the heat starts building up significantly in the friction system. This causes the workpiece materials to stick intensively to the tool surface as a result of severe surface plastic deformation, [Fox-Rabinovich and Totten, 2006, and Trent and Wright, 2000]. At this point, material hardening occurs and causes build-up to form at the chip-tool interface (i.e. metallic bonding). Since cooling by metallic conduction is very efficient, more heat will tend to conduct away from the chips into the tool resulting in tool life deterioration, which negatively affects productivity.

Hard coatings diminish tool surface deformation at elevated temperatures and act as thermal barriers. Therefore, the development of hard coatings and efficient evacuation of chips from the cutting zone are mandatory for dry hard milling applications to protect the tool surface and avoid re-cutting of chips. In addition, large flank wear is always associated with more heat generated in the cutting zone. Accordingly, the geometry of the cutting edge (e.g. clearance angle or flank wear evolution) has tremendous influence on the heat developed between the tool and the newly generated machined surface.

2.1.4 Machining Under Dry and MQL Cutting Conditions

Coolant and lubricants for metal cutting applications can be classified into four main categories: gaseous lubricants, cutting fluids, plastic lubricants and solid lubricants, [Fox-Rabinovich and Totten, 2006]. Despite the environmental and health concerns, high pressurized coolant or cutting fluids (70 bar) are the ideal cutting environment for cooling and lubrication purposes when conventional machining of sticky materials such as low carbon steel, stainless steel or heat resistance alloys. The importance of cooling lubricants is to: improve tool life by reducing friction and lowering tool overheating; improve surface finish and part accuracy; ease chip-breaking and enhance chip ejection, [Klocke and Eisenblaetter, 1997].

In general, modern coated carbide tools usually perform better in a dry milling environment. Under high speed milling conditions, cutting temperatures can reach about 1200°C. Therefore, any cutting fluids will convert into steam and thus have little lubrication effect, [Shaw, 2005]. In addition, during high performance milling of hardened steel using carbide tools, thermal shocks will dominate when cutting fluids are used due to the increase in heat transfer between a solid and a liquid when compared to that between a solid and a gas.

Therefore, dry milling for die and mould making is beneficial not only for environmental and health aspects but also for lowering the thermal fatigue. Overall, this has a significant impact on production costs. Compressed or pressurized air is the best way to ensure perfect chip evacuation from the cutting zone while maintaining the conditions necessary for cooling (i.e. high speed air has higher heat transfer coefficient[2]) and lubrication (i.e. enhancing the generation of tribo-films on coated tool surface). The air stream is usually delivered to the cutting zone using a high pressure of about 100 to 140 PSI. Then it has to be properly directed to the cutting zone (e.g. air through the spindle or specially designed super air nozzles).

[2] High speed air has a heat transfer or convection coefficient of 100-2000 W/m^2K for driving pressure of 10-100 PSI, while low speed air (i.e. no forced air flows at maximum velocity of 22.5 m/sec) has a heat transfer coefficient of 10-100 W/m^2K, [Barnett-Ritcey, 2004]

Moreover, the use of gaseous lubricants or minimum-quantity-lubrication (MQL) can be another alternative for minimizing the amount of cooling lubricants while reducing the friction in the contact zones, [Weinert et al., 2004]. Better performance of coated carbide tools for die and mould making can be achieved by using high-pressurized oil mist, which has an appreciable penetration into the cutting zone with an improved cooling capacity and lubricious effect.

2.1.5 Chip Configurations

Chips are initially formed by shear deformation within the so-called "shear zone" extending ahead of the cutting edge to the upper surface of the chip. The analysis of chip formation in terms of chip shape, morphology and dynamics has a significant impact on studying the material behavior and improving cutting performance. In addition, the estimation of chip surface temperature based on chip colors has been proved to be an effective and simple technique to judge cutting temperatures.

2.1.5.1 Chip Formation in Ball Nose End-milling (Chip Shape)

In metal cutting, the cutting action occurs firstly by the tool approaching the workpiece in a certain way/strategy. Once the cutting edge engages with the workpiece, mechanical and thermal stresses start to develop within the cutting zone where the work-material yield strength is reached (i.e. thermal softening versus strain hardening). Consequently, elastic and plastic deformations of the workpiece material are established within the primary shear zone and hence, the chip formation begins with the machined surface being generated. Then the deformed workpiece material (i.e. chips) starts to flow along the tool rake face (i.e. flow zone) where the secondary deformation zone is established under sticking and sliding conditions. These conditions are associated with rapid heat build up, which initiates other tool wear mechanisms such as adhesion (i.e. seizures), diffusion and eventually abrasion.

Finally, the chips flow along the tool rake face under certain criterion that depends mainly on the behavior of workpiece material under specified cutting parameters (e.g. material strength, un-deformed chip thickness and rake angle). In addition, chip control is very essential in some cutting processes such as turning and drilling while in milling the nature of cutting action relatively eases chip control by naturally producing small individual chips. According to the ISO Standard 3685, chips are categorized based on their geometries in terms of curling mechanisms and shapes; elemental chips are more likely to be produced during ball nose end-milling as will be discussed later.

In ball end-milling, the chip is produced with a semi-conical shape that matches both the shape of the in-cut segment and the geometry of the ball-part of the end-mill, especially if no tilt angle is employed in cutting. This is attributed to the nature of the shearing process (i.e. axial and radial chip thickness thinning), as shown in Figure (2.5). Owing to the work-material hardness and cutting tool geometry, chips with continuous or segmental cross-sections are produced during hard milling. More details regarding chip formation mechanisms will be discussed later.

The geometry of ball-end mills have another significant influence on cutting parameters due to the variation in the effective cutting speed with radius (ranges from cutter radius "r_{max}" to zero), as shown in Figure (2.5). For more illustration, the ball part of the tool is divided incrementally into a number of segments. It is obvious that the cutting speed ($V_c = 2\pi N r_{effective}$) varies along the cutting edge resulting in chip load and cutting force variation across each segment.

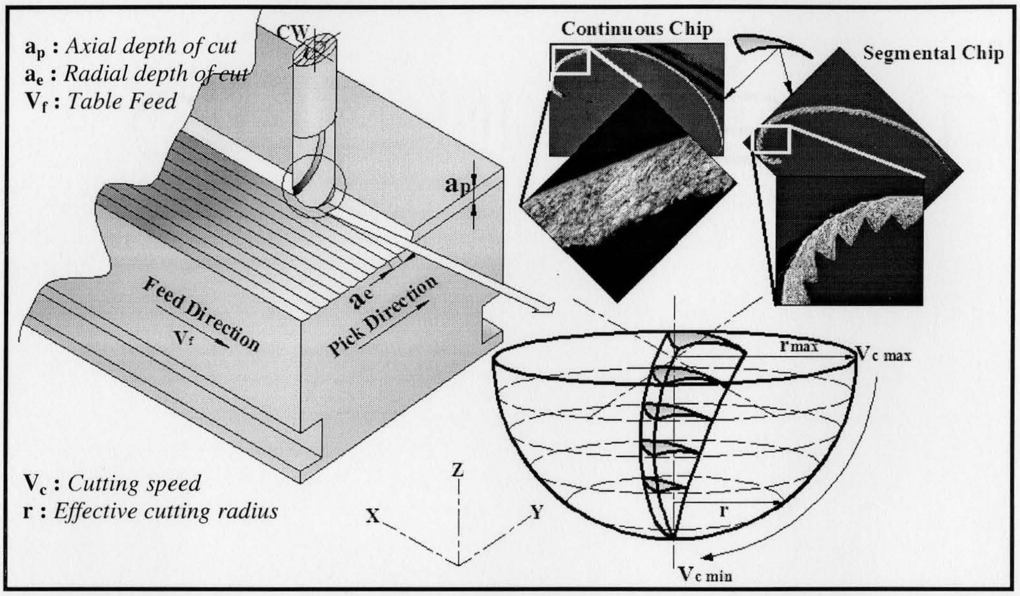

Figure (2.5) Kinematics of three-axis ball end-milling and chip geometry

In order to avoid this variation in mechanical and thermal loads, the tool can be inclined with respect to the workpiece to minimize the range of cutting speed variation. This technique can be applied with the aid of four-axis and five-axis milling kinematics. In general, machined surfaces in end-milling are generated due to the engagement action between the rotary tool that has multi-cutting edges and the workpiece. The cutting action in end-milling usually takes place along the periphery as well as the end of the cutting tool. Figure (2.6) shows an example of down-milling (the tool and workpiece are moving in the same direction) using an end-mill that has two teeth. It can be seen that three differential cutting force components are responsible for the cutting action: namely, axial, radial and tangential cutting force.

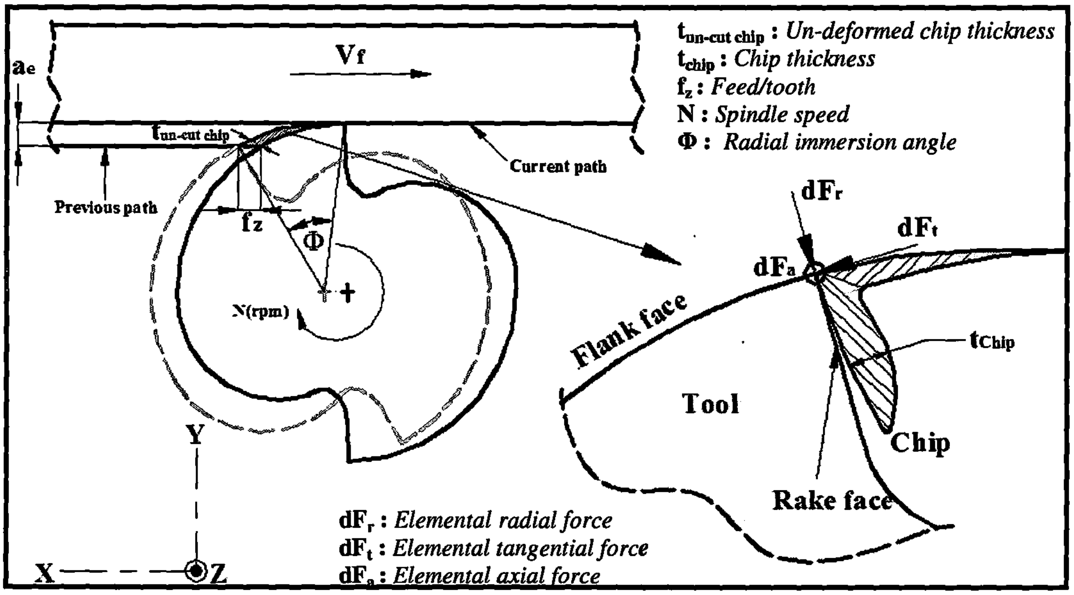

Figure (2.6) Schematic illustration of in-cut segment, chip formation and force analysis during milling

The thermal effect during cutting has a tremendous influence on chip curliness and radius of chip curvature. Generally, under stable cutting conditions elemental chips tend to be curled in the radial and axial directions. This is due to the fact that within a very small chip thickness (on order of micrometers), the chip experiences a significant temperature gradient between both chip surfaces: namely, inside-surface (i.e. free dull surface) which is exposed to the surrounded cutting environment and the backside-surface (i.e. bright surface adjacent to the tool rake face) where the highest heat is involved along the chip sticking-sliding zone, [Ning et al., 2001]. Therefore, chips with "double comma shapes" are more likely to be produced under these conditions. Figure (2.7) shows SEM (scanning electron microscopy) images of chip shapes and surfaces generated during ball end-milling of hardened steel-AISI H13 (HRC 55).

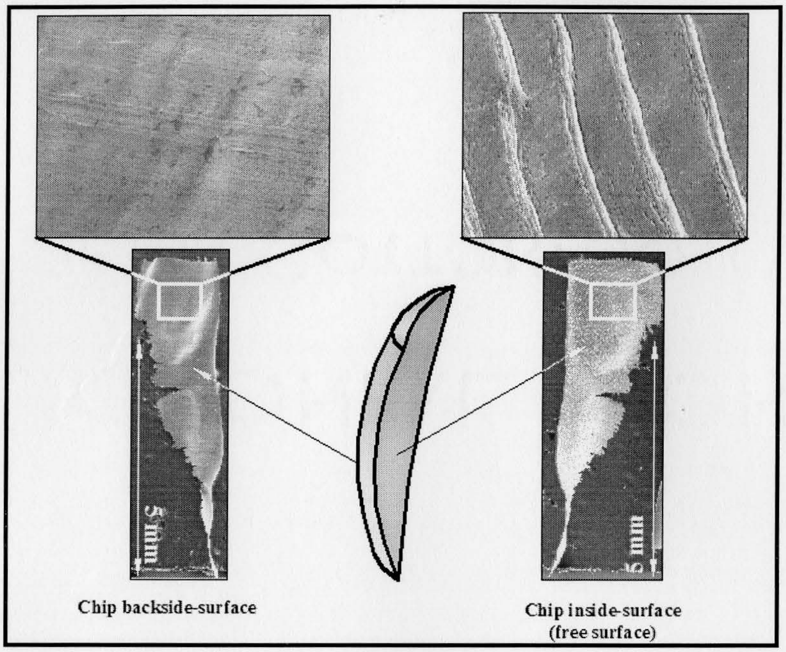

Figure (2.7) Elemental chip geometry and Under/in-side surface textures

2.1.5.2 Mechanisms of Chip Formation

The chips produced in metal cutting vary mainly from continuous to serrated and finally to discontinuous chips, as shown in Figure (2.8). Meanwhile, the mechanism of chip formation depends on many aspects in machining: namely, the behavior of the tool-workpiece material combination, cutting tool design and process parameters.

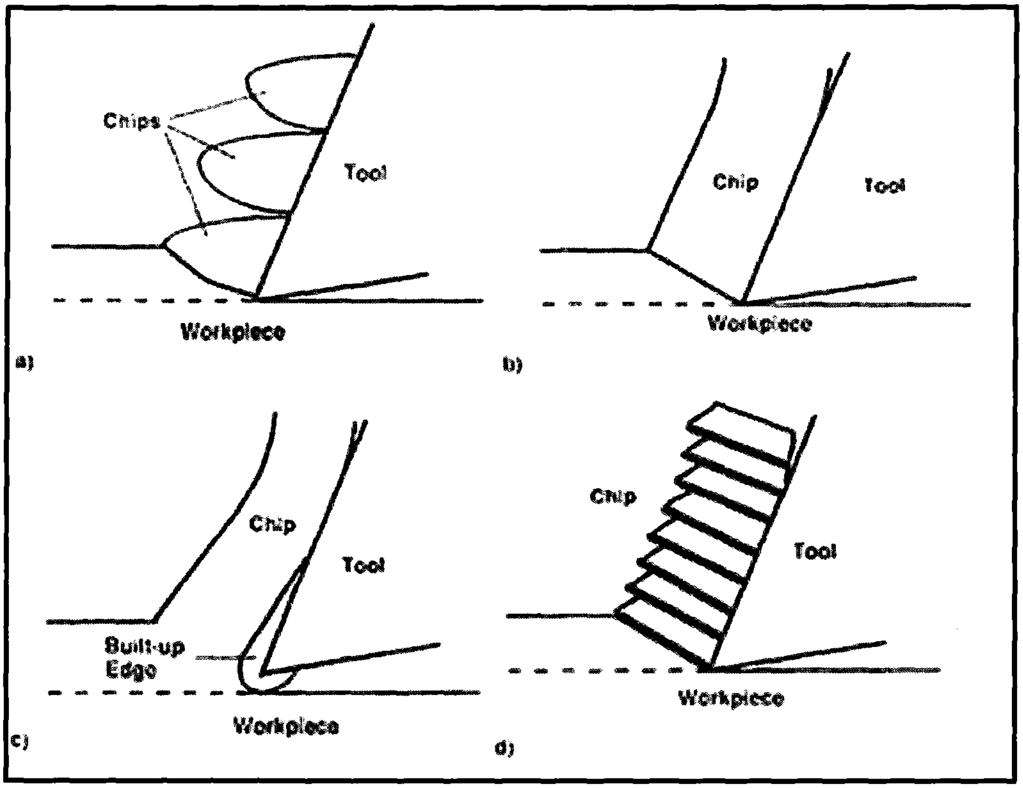

Figure (2.8) Chip types a) Discontinuous chip b) Continuous chip c) Continuous with built-up edge chip d) Serrated (shear localized) chip, [Stephenson and Agapiou, 1997]

Continuous chips are usually formed under high cutting speeds, where excessive heat generation enhances the work-material ductility. In addition, continuous chips with a built-up edge are usually formed under conditions of excessive adhesion between the tool and workpiece at moderate cutting speeds. While, discontinuous chips are formed when machining brittle material such as Cast Iron or when machining ductile materials under dry cutting conditions and very low cutting speeds, [Armarego and Brown, 1969].

A serrated chip is the term usually used by researchers to describe other types of chips produced when workpiece materials experience some instability during plastic deformation. These chips are classified based on their formation mechanisms as, [Komanduri and Brown, 1980]:

- Wavy chip:

  As the name implies a wavy chip has a sine wave geometry as a result of cyclic variations induced in the un-deformed chip thickness. This type of chip is mainly formed within a machine tool with less rigidity where cyclic vibrations are induced in the system;

- Catastrophic shear chip:

  This type of chip is an indication that unstable plastic deformation occurs within the primary shear zone at very high cutting speeds (i.e. critical speeds in terms of workpiece material characteristics). Catastrophic shear chips tend to be formed when machining Titanium alloys where a lot of heat is induced due to very low thermal conductivity which leads to catastrophic failure along the shear plane;

- Discontinuous chip:

  A discontinuous chip is a catastrophic-shear chip where the sheared chip segments are being separated either during high speed cutting of brittle materials or during low speed cutting of ductile materials;

- Segmented chip (shear localized/ saw-tooth chips):

  Shear localized chips are considered to be a special case of continuous chips which are formed under catastrophic failure conditions. These failure conditions involve a ductile fracture and a large strain plastic deformation that leads to heavily deformed material and eventually to localized deformation. This type of chip is common when cutting hardened materials such as hardened steels, titanium alloys and nickel-iron based super alloys at relatively high cutting speeds, [Barry and Byrne, 2002, and Stephenson and Agapiou, 1997].

2.1.5.3 Chip Segmentation in Hard Cutting (Chip Morphology and Dynamics)

Segmented chip morphology and dynamics are of great importance when considering the chip forming criterion during high performance cutting of hardened materials. The properties of the workpiece material such as high hardness and lower thermal conductivity are among the factors promoting the formation of saw-tooth chips. In addition, chip segmentation tends to be influenced by higher shear strain values attained during cutting, [Komanduri and Brown, 1980]; the higher the cutting speed and negative rake angle the higher the tendency for saw-tooth chip formation, [Dumitrescu, 1998].

In the literature, there are two theories describing the root cause of saw-tooth chip formation: namely, adiabatic shear theory and cyclic crack propagation theory, [Barry and Byrne, 2002, Shaw, 2005, Shaw and Vyas, 1998, and Vyas and Shaw, 1999]. The adiabatic shear theory refers to the catastrophic thermoplastic instability that leads to repetitive catastrophic strain localization during chip formation, [Davies et al., 1997, Davies et al., 1996, and Shaw and Vyas, 1998]. Based on this theory, an increase in the rate of thermal softening due to higher cutting speeds leads to higher strain rates (i.e. rapid plastic flow) coupled with a lower amount of heat being conducted away during the plastic deformation of the workpiece material. In this case, the rate of thermal softening then exceeds the rate of strain hardening. Accordingly, the material will experience local deformation and eventually catastrophic shear "slip", [Chen et al., 2004]. Therefore, the workpiece material flow is highly affected by the yield and strain hardening property of the workpiece material. Meanwhile, the transition between thermal softening and strain hardening depends on the time being assigned for the material to flow and the heat that needs to be dissipated during deformation, [Trent and Wright, 2000].

However, the thermal-based analysis is not able to completely describe the criterion of saw-tooth chip formation, since this type of chip was found to be produced at relatively low cutting speeds with a correspondingly lower temperature, [Shaw, 2005] and since under some cutting conditions the adiabatic shear bands don't seem to fully propagate towards the free surface so as to cause catastrophic failure, [Barry and Byrne, 2002]. In addition, the micro-fracture theory was proven to be involved not only in the formation of serrated chips but also in the formation of continuous chips with micro-cracks which are re-welded during material plastic flow, [Shaw and Vyas, 1993]. Shaw and Vyas [1993] showed evidence of micro-cracks being formed on the side surface of continuous chips. In the study carried out by Barry and Byrne [2002], it was also shown that both the severity of the cutting conditions (particularly cutting speed) and workpiece material hardness are the two main factors affecting the mechanism of saw-tooth chips. Therefore, the adiabatic shear theory can be used either as a stand-alone theory or coupled with the periodic fracture theory to describe the initiation and formation of saw-tooth chips.

Owing to the cyclic crack propagation theory, the chip is produced due to a crack initiated at the chip free surface (i.e. surface where the least compressive stresses are being involved), as shown in Figure (2.9). First, the micro-crack originates as a result of imperfections and irregularities within the plastically deformed material such as void nucleation, dislocations and grain boundary fracture. Second, the micro-crack starts propagating towards the tool tip while facing mechanical resistance (i.e. compressive stresses) as the workpiece material is being plastically deformed. Then the resistance reaches a point where the crack propagation stops due to the increase in compressive stresses acting on the shear plane (i.e. transition between brittleness and ductility due to severe plastic deformation [Elbestawi et al., 1996]), while the material is being extruded and displaced along the rake face, [Dumitrescu, 1998]. Elbestawi et al. [1996] supported the idea that the mechanism of saw-tooth chip formation is basically a result of a crack initiated at a point on the chip free surface where the critical surface layer energy is attained at a very low cutting pressure.

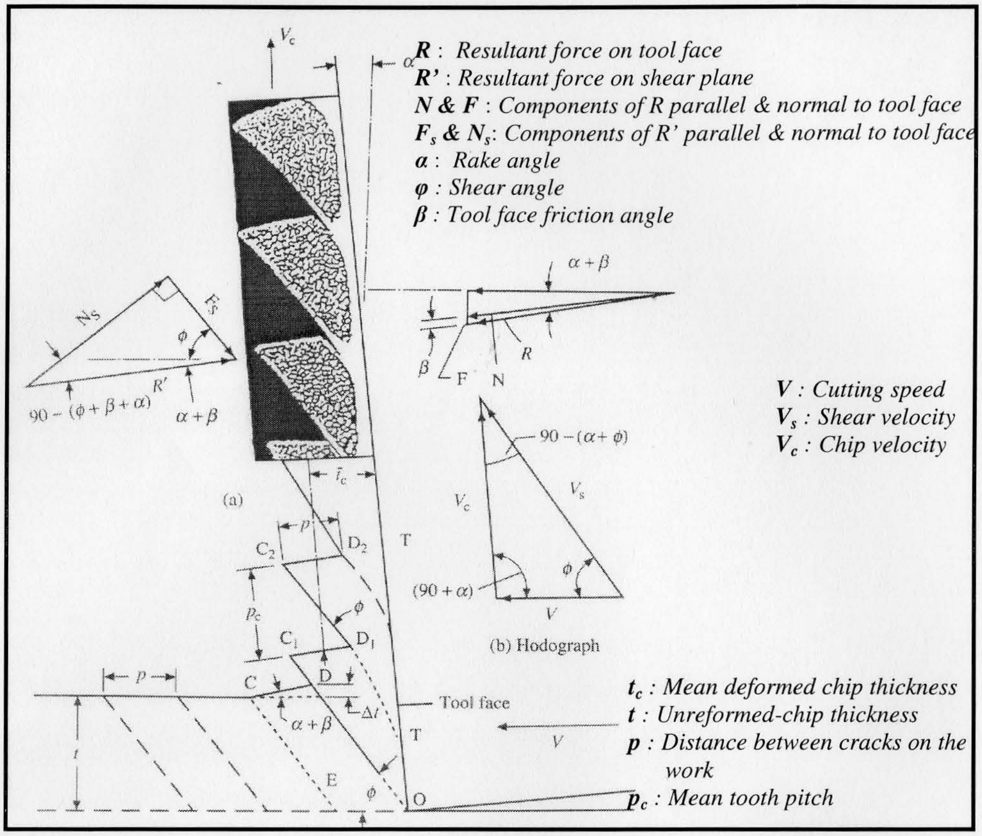

Figure (2.9) Cyclic crack mechanism during saw-tooth chip formation under orthogonal cutting conditions, [Vyas and Shaw, 1999]

Saw-tooth chips usually experience inhomogeneous deformation within the entire chip. While the core of the segment is barely deformed, a highly deformed zone is formed between each segment and along the chip surface adjacent to the tool rake face, [Trent and Wright, 2000]. This is where adiabatic shear theory is involved, as shown in Figure (2.10). The inhomogeneous deformation is supported with the non-uniform temperature distribution within the saw-tooth chips especially with the existence of bands between the saw-tooth segments, [Chen et al., 2004]. These bands resulting from highly concentrated shear action are usually referred to as white layers. The material within these bands shows little resistance to plastic deformation under a localized shear with higher temperature contours between segments, [Chen et al., 2004]. This is attributed to the fact that each band between segments can be considered as an extension to "the non-continuous micro-crack" in the secondary deformation zone, [Shaw and Vyas, 1993]. In addition, the heat generated along the tool rake face promotes the formation of the other band adjacent to the tool face.

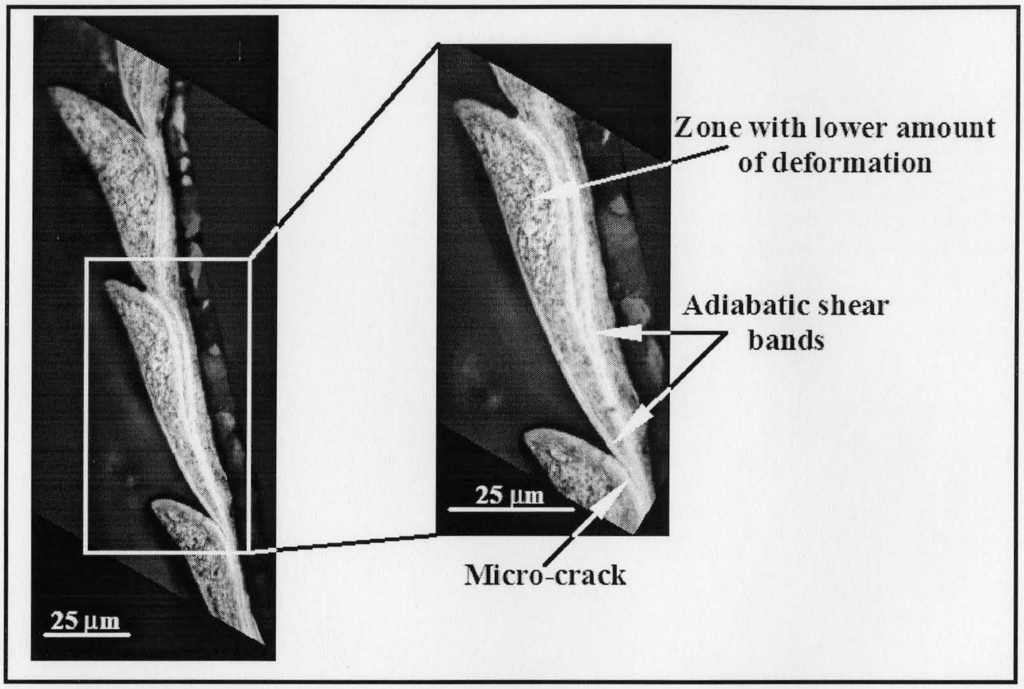

Figure (2.10) Optical microscope image of chip produced in hard ball end-milling of AISI H13 (HRC 57) using a chamfered cutting edge (-15° rake angle) under the following cutting conditions: cutting speed of 300 m/min, feed rate of 0.06 mm/tooth, table feed of 1146 mm/min, axial and radial depth of cut of 5 and 0.6 mm respectively and flank wear of 0.1 mm

The formation of "non-etching/structureless" white layers within the chips during the machining of hardened steel is associated with some heating and rapid cooling regimes (i.e. temperature in these bands exceeds the transformation temperature where the diffusion of carbides and ferrite is transformed into untempered martensite and retained austenite), [Shaw, 2005]. Since these layers are harder than the rest of the chip material, cutting forces, tool life and surface integrity may be negatively affected. White layer formation doesn't necessarily activate the conditions for an aggressive abrasion wear mechanism, since high temperatures (i.e. above the austenite transformation temperature) are attained during chip formation which offers a material with little resistance to deformation. However, during white layer formation, diffusion wear mechanisms tend to occur under conditions associated with high transformation temperatures and increased chip speed along the tool rake face, especially when the cutting ratio exceeds one, [Shaw, 2005]. In addition, the attrition tool wear mechanism may be activated on carbide tools by the formation of saw-tooth chips. This is mainly attributed to the fatigue loading exerted on the cutting edge once this type of chip starts to form, [Trent and Wright, 2000].

2.1.5.4 Chip Colors (Estimated Chip Surface Temperature)

In metal cutting, the workpiece material undergoes severe plastic deformation during the chip forming process (primary shear zone). Once the chip starts forming, severe frictional conditions are attained at the interface between the formed chip and the tool rake face resulting in more heat generation (secondary shear zone). Depending on the thermal conductivity of both the workpiece and cutting materials, 80% of the heat generated during cutting is carried off by the separating chips. Oxide-films are formed on the chip surface under dry cutting conditions which result in a variety of colored chips being formed. The higher the cutting speed and thus the temperature, the higher the oxidation rate, which in turn results in darker colored-chips, [Ning et al., 2001]. Colorless chips usually result when the oxidation process is interrupted due to either the presence of cutting fluids or from chips experiencing severe sticking conditions with the tool.

Estimating chip surface temperature based on post-process chip color is a simple technique when compared to other techniques such as embedded thermocouple or infra-red scanning. It is particularly useful if the objective is to build a comparative study in order to evaluate cutting performance.

Venkatesh et al. [1993] based their chip study on the ability to estimate the variation in chip surface temperatures based on the colors of iron-oxides formed on the chips. They conducted dry turning tests on AISI 1018 steel (0.18 %C) using carbide inserts. The micro-structures of the chips were studied as well. Next, the sampled chips were analyzed using Auger Electron Spectroscopy (AES). Then, the colors were obtained and classified using the standard HIS (hue-intensity-saturation) color space system and image processing software. The study showed that as the temperature ranges from 829°C to 981°C; the steel chip color changes from light-golden-brown (i.e. thinner oxide films) to dark brown and blue and finally to dark blue (i.e. thicker oxide films and highly strained chip). Similar observations were reported by Yeo and Ong [2000].

In addition, the coating thermal conductivity has an influence on the heat generated at the interface between the tool and workpiece, and consequently on chip color. Coatings with lower thermal conductivity result in more heat diffused into the chip and different oxide thicknesses. An example of this is the darker blue chips (i.e. 718°C) and thicker white layers formed when using TiN coating with a thermal conductivity of 19 W/mK as compared to those obtained when using TiCN coating with a higher thermal conductivity of 36 W/mK, [Yeo and Ong, 2000].

2.1.6 Tool Wear

In metal cutting, the machined surface is obtained when the workpiece materials are being plastically deformed under high mechanical and thermal stresses. Meanwhile, friction and rubbing zones are created at the interface between the cutting tool and the workpiece during chip forming and flowing processes. Therefore, significant mechanical and thermal loading is generated within the cutting zone, as well as the tool-workpiece surface interface. This thermally active environment enhances the activation of several forms of tool wear mechanisms by chemical and mechanical reactions resulting in different tool wear types being developed on the surface of the tool.

2.1.6.1 Tool Wear Mechanisms and Types

Tool Wear Mechanisms

- Abrasion wear mechanism

Abrasion occurs mainly during cutting materials that have hard particles in the form of hard grains or inclusions such as carbide inclusion in steel. Those hard particles are activated when a temperature gradient is present between the machined surface (i.e. less temperature) and the tool flank surface, [Tlusty, 1999]. The interaction between the hot cutting tool and the machined surface results in an abrasive loading action exerted on the tool surface. Also there is some speculation that the abrasion wear mechanism might occur by an erosive interaction between the abrasive particles in the cutting fluids and the tool surface, [Stephenson and Agapiou, 1997].

- Adhesion wear mechanism

Adhesion is commonly caused by the heat generated at the tool-workpiece interface under severe sticking and friction interaction between the tool (i.e. the harder surface) and the workpiece (i.e. the repeatedly formed new surface). Owing to the increase in cutting pressure and the higher temperatures involved in the chip forming process, the asperities on both surfaces tend to be welded together and form junctions. These junctions are more likely to be sheared off during cutting. However, the severity of tool surface damage depends mainly on the severity of the load that causes the shearing mechanism, [Armarego and Brown, 1969].

In other words, with the increase in cutting pressure, the bonding between the particles of the tool surface becomes less strong than the one between the two mating surfaces. As a consequence, some particles start to be removed from the tool surface resulting in tool wear. It is of interest to note that the adhesion wear mechanism is usually followed by an increase in abrasion activity which is then responsible for accelerating the mass transfer between the two mating surfaces, [Shaw, 2005].

- Diffusion wear mechanism

High cutting speeds represent the main condition for the diffusion mechanism to take place because of the intense heat generated. This heat accelerates the diffusivity of the material (i.e. workpiece/tool material affinity). This results in atoms moving from a region of high concentration to a region of lower concentration in the crystal lattice, [Tlusty, 1999]. For instance, diffusion wear conditions are created between steel (i.e. working material) and tungsten carbide (i.e. tool material) under high cutting speeds, where the affinity between the iron and carbon is increased when a transformation between α-iron to γ-iron takes place. This enhances the solubility of carbon into iron. In this case, the chips absorb the carbon and cobalt from the tool (i.e. binder of the tool material) while the iron penetrates into the tool material. This type of wear mechanism is mostly coupled with abrasion wear and results in a weakening of the tool surface layer. This eventually leads to extensive tool surface damage especially on the rake face where crater wear is formed very deeply. This is attributed to the absorption of carbon into the chips, which results in stronger chips, [Shaw, 2005]. A diffusion wear mechanism generally initiates and accelerates crater wear.

- Oxidation wear mechanism

Oxidation occurs usually around the tool surface area that is mostly exposed to air. Once, the chip is formed, the area corresponding to maximum depth-of-cut is the first to lose contact with the work-material. Hence, oxygen has access to this hot area. The existence of oxygen in the cutting zone results in the formation of oxide films especially those containing the constituents of the tool such as the Cobalt in the tungsten carbide or the Aluminum in the Al-rich coatings, [Sandvik Coromant, 1994]. Unlike the Aluminum-oxide, the cobalt-oxide is weak and it tends to be worn out very quickly. This usually leads to notch wear especially at the maximum depth of cut where the air can access the cutting zone very easily.

Abrasion wear can also be accelerated by the oxidation wear mechanism. This usually occurs due to the oxidation of workpiece material debris. The hard oxides formed in this process have the same abrasive effect as the hard inclusions, which may result in intensive flank wear, [Stephenson and Agapiou, 1997].

- Fatigue wear mechanism

The fatigue wear mechanism is caused by the cycling of thermal and mechanical loading. It usually results in the formation of cracks which propagate over time across the surface of the tool. These cracks are created by cyclic loading applied to the tool-workpiece surface asperities which serve as initiation sites. Under friction and sliding conditions, the interaction between those asperities result in tensile and compression stresses induced in front of and at the back of each tool surface asperity respectively, [Armarego and Brown, 1969, and Sandvik Coromant, 1994]. The fluctuations in loading are more likely to reach a critical limit, particularly for interrupted cutting, as the tool continually engages and leaves the workpiece. At this point, the cracks start to distribute excessively in parallel and perpendicular to the cutting edge and eventually result in massive breakage of the cutting edge.

Tool Wear Types

Figure (2.11) shows the most common types of tool wear.

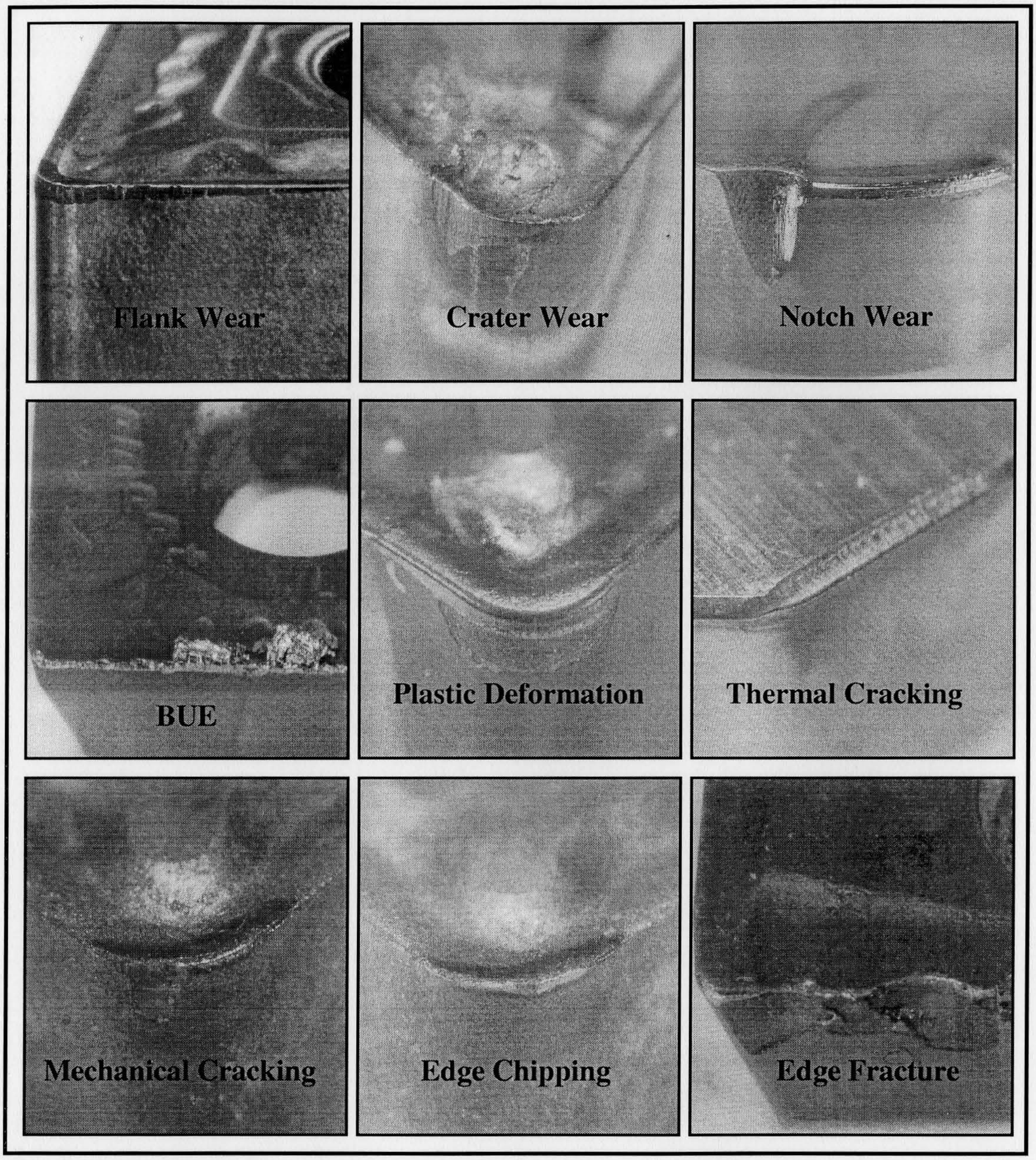

Figure (2.11) Different types of tool wear, [Sandvik Coromant, 1994]

- Flank wear

Flank wear is associated with an abrasion wear mechanism. It forms on the cutting tool flank face (i.e. leading edge, trailing edge and nose) due to the abrasive rubbing between the cutting tool and the workpiece material during the chip forming process and afterwards. Since flank wear leads to the deterioration of the clearance between the tool and the workpiece, an intensive rubbing zone forms at the interface. As a consequence, the temperature and the cutting forces tend to increase with the progression of flank wear, [Armarego and Brown, 1969].

The abrasion resistance is directly related to the hardness of the tool and the coating materials used. This is considered to be the key factor to minimize flank wear. Therefore, a cutting tool with a hard coating and a hard substrate material has to be selected for the cutting application to maintain stable flank wear progression. Carefully controlled selection of cutting conditions will also contribute to a more predictable flank wear rate, [Stephenson and Agapiou, 1997].

- Crater wear

Crater wear is associated with diffusion and abrasion wear mechanisms. It forms on the rake face where extremely hot chips are flowing. Consequently, two wear mechanisms are excited in this case: namely, abrasion by hard particles and diffusion between the chip and the tool material. Under extreme cutting conditions of high cutting speeds and excessive heat generation, the two mechanisms occur simultaneously resulting in severe crater wear. Severe crater wear weakens the cutting edge since it changes the natural shape of the tool rake face by increasing the effective rake angle. Consequently, the flow direction of the chips will be altered and the cutting forces may tend to decrease and change direction as well. This tool wear mechanism is prone to sudden fracture due to the lack of support around the cutting edge, [Sandvik Coromant, 1994, and Stephenson and Agapiou, 1997].

The hot hardness of the cutting tool material and chemical affinity between the tool and workpiece material are effective parameters when considering crater wear. The use of coatings that produce Al-oxide films on the tool surface has been shown to be beneficial for enhancing diffusion wear resistance. In addition, the selection of a suitable cooling system for a cutting application such as the directing of a copious quantity of coolant or air flow towards the chip-tool interface plays an essential role in reducing diffusion wear.

- Notch wear

Notch wear is usually associated with abrasion and oxidation wear mechanisms. It is considered to be a special type of flank wear where localized wear develops on the flank face of the tool adjacent to the workpiece surface, ISO 8688-1. At the end of each cut, air has access to the tool that is still relatively hot. If the exposed area of the tool is not coated or coating layers were delaminated, the substrate would be exposed. If this occurs, diffusion wear mechanism can take place. For instance, a cobalt-oxide (i.e. weak at resisting cutting loads) is formed for the case of tungsten carbide tools. In addition, notch wear could result from other wear mechanisms such as, adhesion or abrasion wear mechanisms, [Sandvik Coromant, 1994]. During the machining of hardened materials; the formed chips may have an abrasive action against the tool surface, which results in areas of notch wear.

Changing the tool approach in terms of tool entry angle and using harder coatings and tool materials are commonly used approaches to protecting the tool surface against notch wear. Moreover, the reduction in cutting speed is the most effective way to reduce notch wear, [Sandvik Coromant, 1994].

- Built-up edge (*BUE*) and build-up layer formations

BUE is mostly associated with an adhesion wear mechanism. Owing to a relatively high affinity between the tool and workpiece materials, layers of workpiece materials tend to stick/adhere to the tool surface. The pressure developed during cutting welds those layers to the tool. In general the lower range of cutting speeds provides a suitable environment for those layers to keep accumulating and building-up, [Sandvik Coromant, 1994]. Meanwhile, sticky-unstable structures of BUE act as a shield for the cutting edge. However once this structure reaches a critical size, it is prone to be torn away causing damage to the tool surface by removing particles of the tool (i.e. edge chipping). Deeper structural damage to the tool can also occur, further weakening the surface region of the tool.

Built-up layers are another form of adhesion wear, where particles/layers of workpiece material start forming and accumulating on the tool rake and flank faces. As these welded asperities grow they are more likely to be split off and removed from the tool surface during cutting, resulting in severe damage to the tool, [Tlusty, 1999].

In order to avoid BUE formation, a proper estimation of the cause has to be defined. In most of the cases, the increase in cutting speed is one of the techniques to overcome BUE formation. Flood coolant is also very beneficial especially when machining stainless steels, [Sandvik Coromant, 1994].

- Thermal softening

Thermal softening results in a significant increase in abrasion wear and if extreme enough, then plastic deformation of the cutting edge can occur. The hardness of the cutting tool material drops as excessive heat starts developing in the cutting zone. The excessive heat is usually coupled with high compressive loads being exerted on the cutting tool. Therefore, certain cutting edges tend to be plastically deformed because of the relatively lower hot hardness of the tools. The deformed cutting edge changes the cutting geometry and affects the surface finish. Also once the edge is critically deformed it becomes more prone to being sheared-off unpredictably.

Thermal softening and edge plastic deformation can be avoided by selecting cutting tool materials with higher hot hardness. Thermal softening is associated with weaker binder material. Therefore, a reduction in binder content typically improves the hot hardness of the cutting tool when mixed-metallic crystals are used for binding the hard particles, [Stephenson and Agapiou, 1997]. However, the compromise between hardness and fracture toughness of the cutting tool materials has to be taken into consideration when selecting harder tool materials for certain cutting applications. In addition, edge plastic deformation can be managed by reducing the cutting feed, increasing coolant supply and using low-friction coatings, [Stephenson and Agapiou, 1997].

- Thermal and mechanical fatigue cracking

Thermal and mechanical cracks are commonly developed on tool surfaces by thermal and mechanical fatigue wear mechanisms. In the former, the cutting tool undergoes thermal cycling especially with interrupted cutting processes. This results in the formation of thermal fatigue cracks perpendicular to the cutting edge. Once the size of these cracks reaches a certain limit, excessive edge chipping start to dominate. On the other hand, the initiation of mechanical cracks is affected by the variation in both the magnitude and direction of the cutting force components. Once an excessive fluctuation level is reached cracks start to form parallel to the cutting edge, [Sandvik Coromant, 1994].

The use of coolant intensifies the magnitude of the thermal cycle loads by providing rapid cooling as the tool leaves the cutting zone. Therefore, a dry cutting environment can be utilized to reduce the magnitude of thermal shocks. In addition, using smaller cutting feeds and tougher tool grades are two important factors to avoid tool failure by fatigue wear mechanisms. In milling, the length of the heating cycle is reduced when a smaller radial immersion is used. This has a beneficial impact on heat related wear mechanisms such as thermal fatigue cracking. For coated tools, thermal fatigue cracks usually cause "spalling" of the coating surface. This usually occurs with coatings that exhibit lower thermal shock resistance, [Stephenson and Agapiou, 1997]. In addition, mechanical cracking can be minimized by selecting the best tool entry for the cutting application.

- Cutting edge chipping

Brittle tool materials are more prone to failure by edge chipping. Chipping is more likely to be a mechanical type of wear. In interrupted cutting, the cutting edge continually enters and leaves the workpiece. Therefore, repeatable cycling of loading and unloading results in edge fragmentation (*i.e. spalling*) due to the mechanical shocks that are exerted on the cutting edge while entering and leaving the workpiece, [Stephenson and Agapiou, 1997].

On the one hand, in more ductile machining applications the load exerted on the cutting edge when it exits the workpiece is more critical than the one at the entrance. In other words, the tools are more likely to undergo the so-called "exit failure", especially those with zero or positive rake angles. The reason is the existence of a "negative shear zone[3]" by the end of the cut where higher values of plastic strain, specific cutting energy and temperature are attained. Accordingly, the resistance of the workpiece material starts decreasing very rapidly which corresponds to a release in tool loading. Therefore, induced tool stresses tend to reverse direction to maintain loading equilibrium. At this point, the maximum tool stress will be reversed from compressive to tensile and eventually will result in massive breakage of the cutting edge, [Shaw, 2005].

[3] This negative zone is usually formed in front of the cutting edge as the shear angle starts decreasing in the negative direction.

On the other hand, the so-called "entry failure" is more pronounced in the applications of machining hardened materials with zero and positive rake angles, [Stephenson and Agapiou, 1997]. In addition, vibrations induced inside the system (usually due to an increase in the cutting forces) lead to edge chipping and eventually to accelerated flank wear progression. Chipping can be reduced by using tougher cutting tool materials with a strong cutting edge micro-geometry while maintaining stable cutting by increasing system stiffness. Moreover, the cutting conditions can be adjusted to avoid early edge chipping by reducing the feed rate during the running-in stage, [Sandvik Coromant, 1994].

- Tool fracture

Brittle fracture is a catastrophic failure of the cutting tool by massive breakage of the cutting edge or part of the tool under excessive thermal and mechanical loads. This type of failure usually causes severe damage to the workpiece and affects the dimensional accuracy of the machined surface. In general, the tool cutting edge tends to fracture when it is no longer able to withstand the mechanical load. Severe chipping can also be considered as an indication that the probability of edge fracture is increasing.

In order to prevent the edge from being prematurely fractured, stable cutting is mandatory. In addition, the reduction in feed or depth of cut has a beneficial impact on tool life. However, the resulting reduction in speeds and feeds adversely affects productivity. Therefore, other techniques for cutting tool edge strengthening have to be adopted. For example, the selection of a cutting tool with higher fracture toughness (e.g. higher cobalt content in tungsten carbide) is mandatory to increase the resistance against mechanical shocks. However, the increase in the binder content has some detrimental influences on the resistance against abrasive and chemical wear mechanisms, [Stephenson and Agapiou, 1997].

Surface Damage of Tungsten-Carbide (WC/Co) Tools

Abrasion, diffusion and oxidation are the most common wear mechanisms when using WC tools to cut ferrous work materials. Abrasion commonly occurs by hard abrasive particles in the workpiece material, while the diffusion wear mechanism is activated by the heat generated during cutting. The heat enhances the diffusivity of an element especially those with high affinity to each other such as iron in the workpiece material and carbon in the WC tool. For uncoated WC tools, oxidation is more likely to occur than with coated ones. The oxygen in the cutting zone results in the formation of instable cobalt-oxide. This oxide tends to be removed very easily by rubbing which has a detrimental effect on the tool binder (i.e. weakens the tool matrix), [Stephenson and Agapiou, 1997].

In addition, edge chipping and massive breakage are very common in carbide tools especially when machining hardened steels at high cutting speeds. Edge chipping is usually developed on the cutting edge due to high shear stresses flowing through the cobalt layer. Massive breakage of either cutting edge or tool tip in carbide tools is a result of excessive tensile loading exerted across the carbide grains. Therefore, chipping can be considered to be ductile failure while breakage is definitely brittle failure, [Tlusty, 1999].

High cutting speed is usually associated with a higher cutting temperature. Therefore, different types of wear mechanisms can be correlated with the cutting speed; refer to Figure (2.12). Regardless of the cutting operation, it can be noticed that adhesion and abrasion are the two dominate tool wear mechanisms at low and moderate cutting speeds, while at higher cutting speeds, the "thermally induce loss of strength" mechanism starts to be more pronounced in continuous cutting than in interrupted cutting due to the nature of each cutting operation.

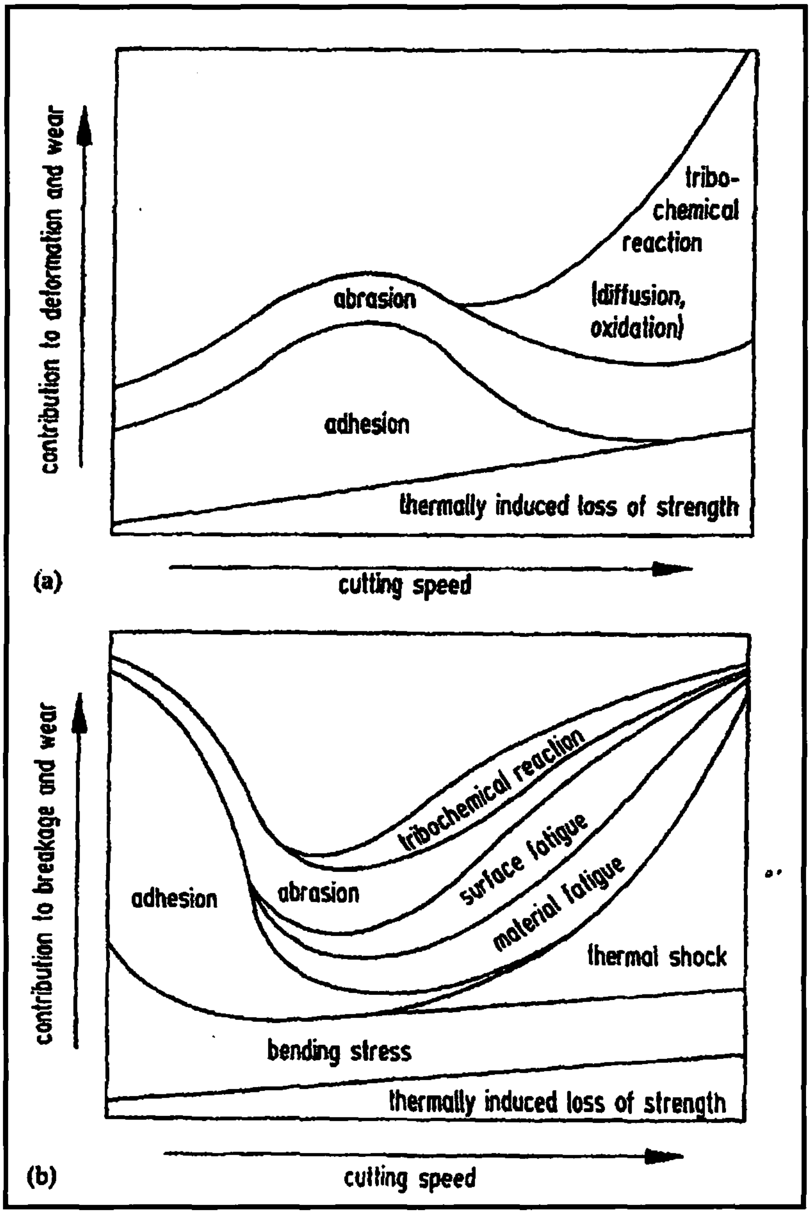

Figure (2.12) The correlation between different tool wear mechanisms and cutting speed in (a) continuous cutting and (b) interrupted cutting, [Löeffler, 1994]

Under high speed cutting conditions, coated carbide tools generally experience a longer tool life with lower wear rates than the uncoated ones. Hard coatings are protecting the tool against all forms of wear mechanisms; refer to Figure (2.13) for different types of tool wear observed when high speed cutting of hardened steel. However, the failure of a coating layer is still possible. For example, in interrupted cutting hard coatings tend to fail by spalling due to mechanical or thermal fatigue, diffusion (i.e. crater wear) and oxidation wear mechanisms, [Stephenson and Agapiou, 1997]. Owing to its ability to resist diffusion wear as an inert-kind of oxide, Aluminum-oxide is considered to be one of the most favorable oxide layers formed on coated tungsten carbide tools, [Sandvik Coromant, 1994].

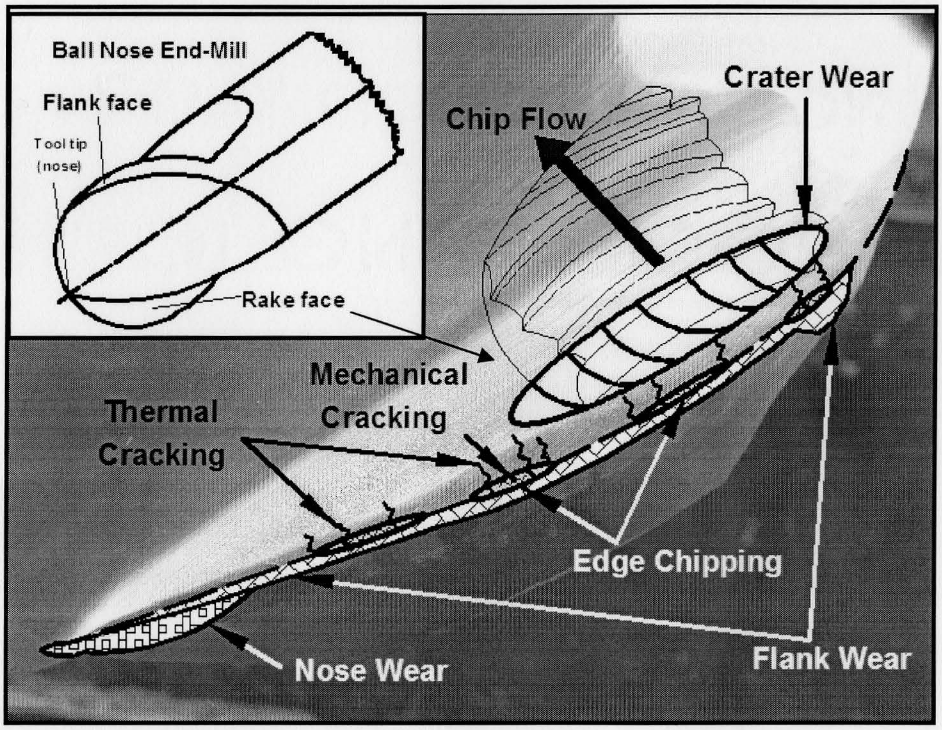

Figure (2.13) Schematic of tool wear distribution on the cutting edge of tungsten carbide ball nose end-mill

2.1.6.2 Tool Life Criterion

Tool life is the criterion that is most commonly used to evaluate cutting performance. The life criterion is the ability of the cutting tool to maintain a reasonable performance with a steady wear rate and predictable tool life. However, machined surface accuracy and surface finish are considered to be the parameters limiting the tool life criterion, particularly in finish hard cutting. Flank wear width and crater wear depth are the most commonly used criteria in the assessment of tool deterioration. In addition, cutting edge chipping and notch wear are the two other forms of tool wear that commonly developed during the machining of hardened materials under high cutting speeds.

The flank wear evolution depends on the tool/workpiece combination and cutting conditions. The typical variation of flank wear over cutting time consists of three defined stages: namely, the running-in stage, post running-in stage and unstable wear stage; refer to Figure (2.14) for details. First, the initial tool wear rate increases rapidly. Then, the wear rate tends to stabilize and form stable or steady-state wear. Finally, a severe progression in tool wear occurs, which marks the end of tool life in most cases.

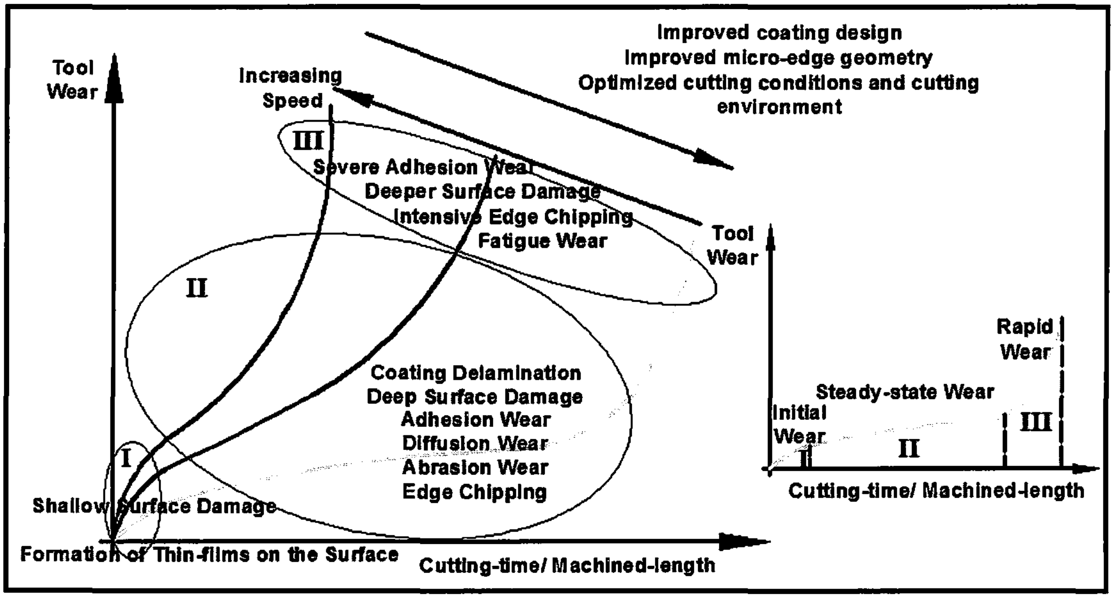

Figure (2.14) Progression of wear on coated-tools for hard cutting applications

2.1.6.3 Friction in Metal Cutting

The cutting system undergoes severe mechanical and thermal loads especially at the interaction surface between the cutting tool and the workpiece material. A pressure as high as the yield strength of the working material is developed at the friction surface while the temperature tends to build-up to the softening or melting point of the working material.

For two mating surfaces, there are two forces involved in the friction action: namely, frictional force and normal force. The latter is usually compressive force applied perpendicularly on the interface, while the former is the force needed for sliding to occur over asperities and to initiate the shearing of the bonds formed at the interface peaks (i.e. the real area of contact) under compressive loading conditions. Therefore, the frictional force is proportional to the normal force and to the real area of contact (very small compared to the apparent area of contact). This is known as a "classical friction model"; ($F_f = \mu N_f$), where the stress imposed on the apparent contact area is significantly lower than the yield strength of the material-pair; refer to Figure (2.15).

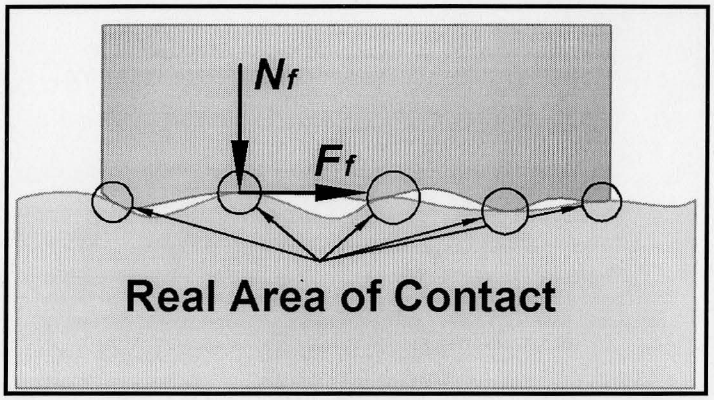

Figure (2.15) Schematic illustration of the frictional and normal forces exerted at the interface between the mating surfaces

Owing to the difference between workpiece and tool material strengths the classical friction concept is not necessarily valid in metal cutting, where very high normal stresses are acting on the interface between the tool and the workpiece material. Accordingly, the real area of contact is not proportional to the normal force any more, while the frictional force becomes directly dependent on the shear strength of the weaker material across the real area of contact (i.e. shear area). For instance, the presence of zones of sticking material on the tool surface in the form of adhered layers or fragments is mainly attributed to the fact that the tensile strength of the metallic bonds at the interface is higher than that of the workpiece material, [Trent and Wright, 2000].

The formation of these metallic bonds (i.e. seizures) at the interface can be interrupted by the formation of oxide layers or the existence of contaminated layers such as oils or lubricants between the two mating surfaces, [Trent and Wright, 2000]. However, this is not always the case in metal cutting where fresh and hot workpiece material surfaces are permanently present during cutting. Therefore, the formation of such metallic bonding is more likely to occur to some extent during cutting regardless of the utilized cutting environment (i.e. wet, dry or MQL).

The development of the seizure process on the friction surface is very common in dry machining, where dry frictional conditions are utilized. Under those conditions, surface plastic deformation and intensive tool wear are more likely to occur. First, the plastic deformation occurs. Next, the interface surface tends to be damaged due to the destruction of the thin protective films formed during the severe interaction between the two contact surfaces. Last, an initial stage of seizure starts forming resulting in more contact area and more concentration of surface deformation. The reduction of plastic deformation resistance enhances the seizure process, where intensive interaction leads the surface asperities to adhere to each other. This results in zones of build-up. Consequently, the bonds tend to deteriorate between these asperities due to the developed shear stresses causing the materials to shear-off, [Fox-Rabinovich and Totten, 2006].

2.1.6.4 Surface Adaptability for High-Performance Machining

For specific combinations of workpiece-tool materials, the ability of one surface to adapt to the other is of great importance under severe frictional conditions. This ability is initiated by alterations in the surface microstructure as well as the mechanical properties. Consequently, the adaptability is developed by the formation of tribo-films. Tribo films are films that are produced on the surface of a tool in response to intensive frictional conditions: namely, heavy load and high temperature. Tool wear can be stabilized by introducing the concept of self-adaptability into the tool-workpiece system during the cutting action as a way to enhance the formation of favorable tribo-films. Through the formation of these films some of the detrimental effect of mechanical, thermal and chemical loads, which are exerted during the cutting action can be limited, [Fox-Rabinovich and Totten, 2006].

Three levels of adaptation are considered during cutting: namely, the "macro-level", the "micro-level" and the "nano-level". The "macro-level" refers to the level within the secondary deformation zone or the area of interaction between the cutting tool and the chips. It also refers to the ability of the cutting edge to preferentially wear during the first stage to minimize wear in later stages. This plays an important role in the macro-level as will be discussed later. The "micro-level" refers to the surface finish of the friction surfaces. The "nano-level" refers to the zone of the "tribo-film" formation. Each of the aforementioned levels has a significant influence on cutting performance. Therefore, the correct combination of the three levels has the potential to lead to a tremendous improvement in productivity, tool life and machined surface quality, [Fox-Rabinovich and Totten, 2006].

2.1.7 Cutting Forces

Cutting forces represent an important aspect in metal cutting. It is important to analyze (i.e. measure or estimate) the cutting forces acting on the cutting tool to estimate the energy required for cutting and to design a stable machine tool system. There are three main force components acting on the cutting edge: namely, tangential, longitudinal and radial force components. Refer to the cutting force component description for a ball-end mill in Figure (2.16). In recent years, the development of analytical and mechanistic force models for ball-end milling has attracted many researchers, [Lamikiz et al., 2005, Lazoglu and Liang, 2000, Lee and Altintas, 1996, Wang and Zheng, 2003, and Zhu et al., 2001]. Despite the geometric complexity of ball nose end-mills, there has been extensive attention to incorporate many cutting aspects into those models, such as the variation of cutter helix angle, the cutter axis inclination and the machining direction.

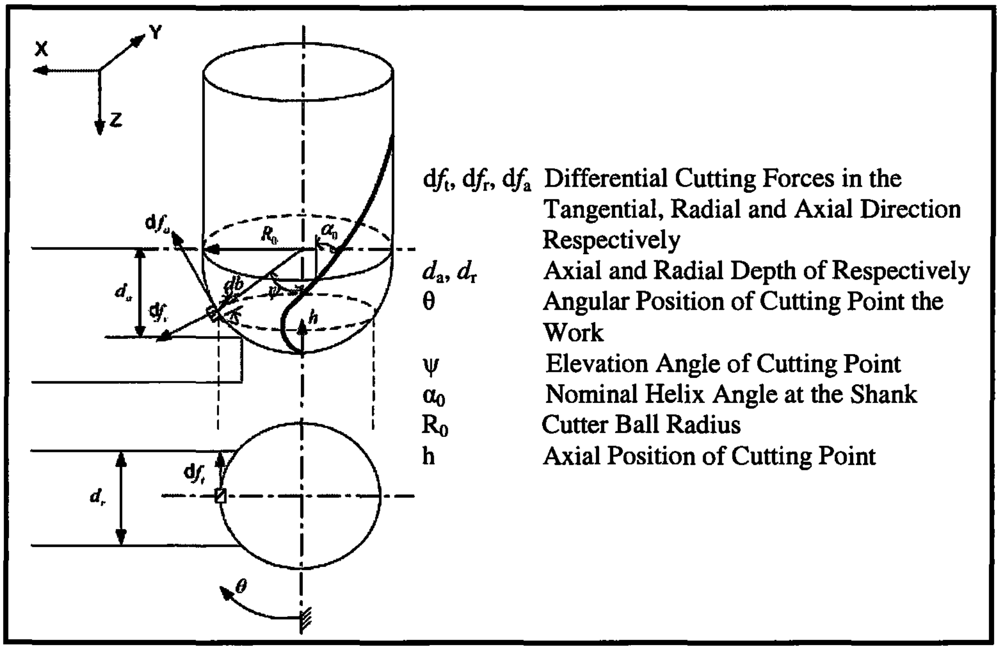

Figure (2.16) Cutting force components for a ball-end mill, [Wang and Zheng, 2003]

2.1.8 Machined Surface Quality

Surface quality is an important aspect of final product quality as it often affects final product performance. Surface finish is certainly one aspect of surface quality and it can be assessed by studying the surface shape, surface waviness and surface roughness profile of the machined part. It is important to achieve a smooth sculpture surface finish with minimum cusp or scallop height when high performance machining of hardened steel for die and mould making applications; refer to Figure (2.17) for a typical form of surface scallop generated on the machined surface during the ball-end milling process. The other important aspect is the residual stresses induced in the machined surface. The term residual stress refers to the stresses remaining in the material after releasing the externally applied loads. The applied loads could be forces, stresses, or displacements due to a temperature gradient, or from workpiece fixturing. In machining or metal cutting, the compressive and tensile residual stresses are mainly produced in the machined surface due to various plastic deformations and temperature gradients respectively.

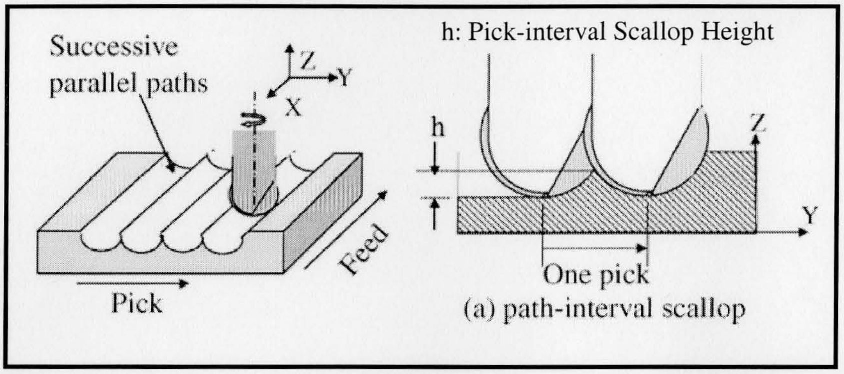

Figure (2.17) The path-interval scallops generated on the machined surface during ball-end milling, [Chen et al., 2005]

Extensive attention has been paid in the literature to investigate all these aspects in an effort to improve surface finish and to generate favorable residual stresses in the machined surface and subsurface. In order to do that, cutting tools (e.g. cutting tool geometry, cutting tool materials and coatings) and cutting conditions (e.g. feed, radial depth of cut, speed and cutting environment) have been investigated extensively. Moreover, the process kinematics and workpiece materials should be considered when developing the process.

2.2 Development of Cutting Edge Micro-Geometry

Cutting tool design is a combination of three different main areas: namely, cutting edge preparation, coating design and substrate design.

2.2.1 Introduction to Cutting Edge Preparation

Cutting edge preparation is an important component of cutting tool design; it refers to a controlled geometry on the cutting edge. First, edge preparation was applied as a finishing stage to remove any defects along the cutting edge in order to get a smoother tool surface with the least irregularities. These defects are usually produced on the tool surface during the tool/insert manufacturing process. For instance, ceramic and carbide cutting tools have some irregularities along their cutting edge due to either the flash formed during pressing and sintering operations or the burrs formed during the grinding operation. These defects can be eliminated by honing or polishing of the rake and flank surfaces.

Moreover, edge preparation has been extended to the cutting edge shaping process in which a Radius or Chamfer/T-Land is applied to an up-sharp cutting edge. This is done to strengthen it against fracture by reducing the stress concentration on the cutting edge (i.e. introducing more surface area to support the mechanical and thermal loads). In addition, edge rounding enables some coatings such as chemical vapour deposition (CVD) to stick properly to the cutting edge, [Beard, 1993].

Three designs of cutting edge preparation are mostly adopted in cutting applications: namely, Sharp, Honed and Chamfer/T-Land cutting edges, as shown in Figure (2.18). Edge preparation is applied to turning or milling inserts/tools with almost the same forms.

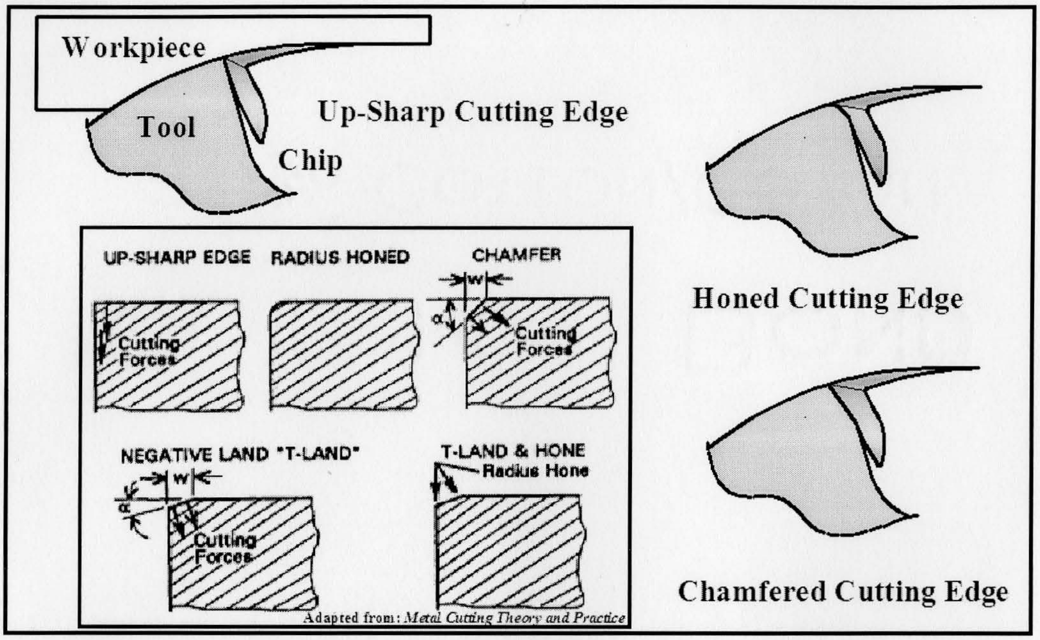

Figure (2.18) Cutting edge preparation, [Stephenson and Agapiou, 1997]

A chamfer/T-Land geometry is produced using a 5-axis CNC grinding machine or using a diamond file under a stereo microscope. The negative T-land is similar in shape to the chamfer. However, the chamfer is ground on the insert by eliminating the cutting edge corner; unlike the land which is a relief added to the insert face. The size of the chamfered cutting edge is defined by two main dimensions: namely, chamfer width and chamfer angle (i.e. primary rake angle) that ranges between 5° to 45°, [Beard, 1993, Gen, 2004 and Stephenson and Agapiou, 1997]. The chamfer width and angle usually vary in accordance with both the cutting application and cutting parameters; however, providing a very steep chamfer angle or a very large width to the edge geometry results in a larger radial cutting force. As a consequence larger deflections result in less accuracy and the tendency to generate chatter within the machine tool system, which in turn leads to an increased rate of flank wear.

2.2.2 Modeling of Metal Cutting

Experimental and modeling techniques (e.g. empirical, analytical, mechanistic and finite element analysis modeling) are extensively utilized techniques to examine existing conditions, study new cases and predict metal cutting performance. Experimental techniques have been conducted to analyze metal cutting processes over the years in the literature. However, the integration between several techniques has proved to be very essential to building an understanding and for analyzing the cutting action from a better prospective.

There have been many attempts to model the cutting action and to study the behavior of work materials during cutting; starting by Ernst and Merchant, followed by Lee and Shaffer, then by the more realistic models done by Oxley. However, none of these models account for the cutting edge micro-geometry, as the cutting mechanics in all of those models is based on cutting with tools having a sharp cutting edge preparation. Since the cutting models for a tool with a sharp cutting edge can be no longer used with honed/chamfered edge geometry, modeling techniques have been developed to examine the effect of cutting edge preparation on cutting performance. However, the development of a perfect model, which can be applicable over wide range of cutting conditions, is practically impossible. Since the focus of this study is on the chamfered cutting edge, some of the modeling techniques that have been addressed in the literature for machining with chamfered tools will be reviewed.

The formation of the so-called "dead metal zone (DMZ)" was studied by [Fang and Wu, 2005, Ren and Altintas, 2000, and Zhang et al., 1991]. The DMZ refers to the work-material which is trapped under the chamfer edge and acts as a cutting edge, [Ren and Altintas, 2000]. Since the cutting mechanics can be relatively affected by the new formed zone, a new three-zone model and a slip line field were developed by Zhang et al. [1991]. The developed model accounts for some aspects in machining with chamfered cutting tools such as: the energy consumed by excessive deformation and friction around the non-sharp cutting edge as well as the temperature and strain rate associated with the material flow stress. It was noticed that the existence of the DMZ is not dependant on the cutting speed, tool rake angle, or chamfer angle. However, the geometry of the DMZ is mainly dependant on the negative-land rake angle.

In the same way, Ren and Altintas [2000] proposed an analytical model based on Oxley's slip line field to study the cutting mechanics when a chamfered cutting edge is considered. The model was able to predict the shear angle, cutting forces and temperature at a specific cutting condition. It was revealed that the material flow around the chamfered cutting edge is simplified as a dead metal zone (Zone-BHO), as shown in Figure (2.19), where α_1 and b_{cf} are the chamfer or primary rake angle and chamfer length respectively. In the proposed model, the material flow stress was identified as a function of strain, strain rate and temperature, while the shear angle was estimated based on the minimum energy dissipation in the three deformation zones (i.e. primary shear zone, DMZ and tool/chip interface zone).

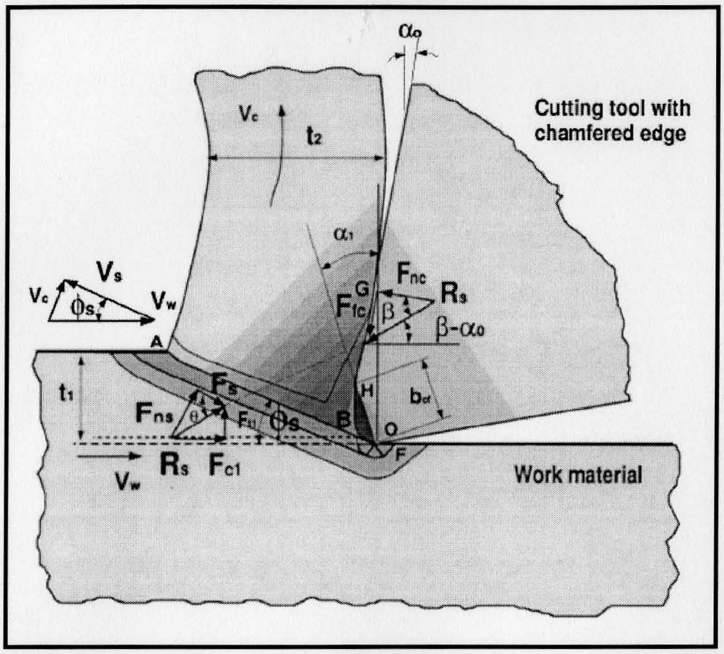

Figure (2.19) Proposed model of chip formation for cutting with chamfered tools, [Ren and Altintas, 2000]

Arbitrary Lagrangian Eulerian (ALE) finite element formulation has been applied by some researchers to simulate orthogonal cutting using a cutting tool with a chamfered cutting edge [Chen et al., 2006 and Movahhedy et al., 2002]. The advantage of using the ALE formulation is seen in the ability to model cutting with chamfered and rounded edge geometries more efficiently and realistically. The underlying reason is that no chip separation criterion is required in the model in this case. However, only continuous chip formation can be simulated using this technique, [Chen et al., 2006].

2.2.3 Influence of Cutting Edge Preparation on Cutting Performance

The evaluation of cutting performance is essential to improving productivity, tool life and final part quality. Therefore, the influence of chamfered-cutting edge preparation on some aspects in metal cutting has to be evaluated in order to implement new designs that have the ability to achieve process improvements.

Influence of Chamfered Cutting Edge Preparation on the Behavior of Work-Material

The influence of the cutting edge preparation on the deformation zones and chip formation has been addressed by many researchers in the literature, [Chen et al., 2006, Hirao et al., 1982, Movahhedy et al., 2002, Ren and Altintas, 2000, Yen et al., 2004 and Zhang et al., 1991]. Hirao et al. [1982] were among the authors supporting the DMZ hypothesis, they conducted turning tests on different workpiece materials (Steel 1112, 1045 and 4340) using chamfered and un-chamfered sintered carbide grade P30 tools to study the influence of a chamfered cutting edge on the chip formation. The obtained data revealed that the metal shearing and chip ratios are not significantly affected by the chamfered cutting edge. This was attributed to the formation of DMZ which enables the cutting edge to act as an up-sharp edge. Therefore, the chip production was not drastically affected by the edge geometry, as shown in Figure (2.20).

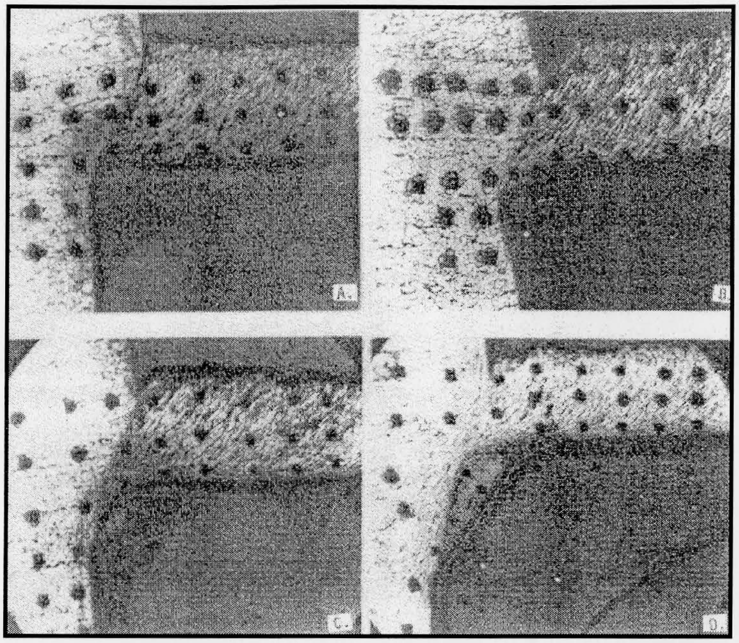

Figure (2.20) Effect of chamfer angle on chip formation for steel 1112 using carbide tools with chamfer width of 0.4mm and chamfer angle of (A) 0°, (B) 22°, (C) 41° and (D) 60° under the following cutting conditions: 100m/min cutting speed; 0.25 mm feed/rev, [Hirao et al., 1982]

In the same way, the formation of a DMZ on the negative land resulted in the same shearing action in the primary shear zone regardless of the variation in the chamfer angle. The experimental and predicted data in [Movahhedy et al., 2002 and Ren and Altintas, 2000] showed that the shear angle is not affected by a change in the chamfer angle when machining P20 mold steel (HRC 34) with carbide tools. A decrease of about 2° - 3° in the predicted shear angle was reported for the case of a chamfered-edge tool when compared to cutting with up-sharp tools. This was also supported by the experimental study of Zhang et al. [1991]. The velocity profile around the cutting edge was used in the study done by Movahhedy et al. [2002] to investigate the formation of a

DMZ. It was revealed that the velocity of the material trapped under the chamfered edge is almost 10 percent of the maximum speed. Moreover, the stress and strain rate values are almost constant over the wide range of negative chamfered-angles. However, the hypothesis of a DMZ was argued by the same authors Movahhedy et al. [2002]. They observed that the DMZ no longer exists at higher cutting speeds.

It is of interest to note that a DMZ is formed under a different mechanism compared to the one by which the conventional build-up edge (BUE) is formed, [Zhang et al., 1991]. On the one hand, under ordinary turning conditions the BUE is usually formed on the rake face when machining soft ductile metals or under relatively low cutting speeds of about 0.3 m/s. Moreover, BUE disappears either when it passes off with the chip after reaching a critical size or when thermal softening occurs under higher cutting speeds of about 1.2 m/s and a higher tool-chip interface temperature, [Stephenson and Agapiou, 1997]. On the other hand, when cutting no. 45 steel under a cutting speed of about 100 m/min, the DMZ formed on the negative primary land still exists unlike the BUE which disappeared at a cutting speed over 28 m/min, [Zhang et al., 1991].

The effective stress distribution within the working-material and around the cutting edge was utilized by some authors to study the influence of the chamfered-edge on the material behavior in the vicinity of the cutting zone, [Chen et al., 2006, Dokainish et al., 1989, Kishawy et al., 2002 and Movahhedy et al., 2002]. It was found that for a low carbon steel workpiece the introduction of a chamfer to the cutting edge did not prevent the negative rotation of the shear zone which is the main reason of tool exit failure during interrupted cutting, [Dokainish et al., 1989]. There was no exact interpretation mentioned for these results. However, the distribution of stress fields within the cutting zone depends mainly on the strain rate, strain hardening and thermal softening effects. The effective stress fields are usually higher within the primary shear zone while they maintain lower values within the secondary deformation zone and close to the tool tip where thermal softening effects start to dominate material deformation [Kishawy et al., 2002 and Movahhedy et al., 2002]. Therefore, further experimental studies are needed to support the numerical results obtained in [Dokainish et al., 1989].

Influence of Chamfered Cutting Edge Preparation on Cutting Forces

On the macro and micro-machining level, the cutting edge is not perfectly sharp. There is always a small cutting edge radius. Therefore, two terms in machining should be addressed for conditions where uncut-chip thickness is less than the edge radius: namely, a "ploughing force" and a "size effect". The latter refers to the increase in the specific cutting energy with the decrease in the uncut-chip thickness and the decrease in shear angle. In addition, an increase in workpiece material shear flow stress was also found to have an effect on the increase in the specific cutting energy with the decrease in uncut-chip thickness. For instance, when the uncut-chip thickness is reduced from 0.2 to 0.01 mm, the specific cutting energy is more than doubled, [Arsecularatne, 1997]. The significant increase in the specific cutting energy can be related to the energy needed to shear and plastically deform the material under a large negative rake angle. The ploughing force or non-cutting force refers to the cutting force component that corresponds to a zero uncut-chip thickness.

The geometry of the cutting edge preparation has a relatively significant influence on the cutting force components. Therefore, numerous studies in the literature have analyzed the machining forces based on the cutting edge geometry used. Most of these studies have emphasized how the machining forces are different for tools with chamfered or honed edges when compared to those having up-sharp cutting edges. The major role of applying a chamfer on the cutting edge is to increase the cutting edge strength by providing a wider surface area with an effective negative rake angle to support the cutting loads. Accordingly, the thrust force and cutting force components will be affected due to the effective negative rake angle effect, [Hiaro et al., 1982]. Hiaro et al. [1982] observed that the chamfer width has more influence on the thrust force (F_t) than the cutting force (F_c). They observed a drastic increase in the thrust force as the chamfer length increases.

Therefore, the chamfer width has to be selected carefully especially in hard machining applications where the thrust force component is usually the highest. In addition, the feed rate has to be optimized in terms of the utilized geometry in order to achieve a stable cutting process. In the study done by [Elbestawi et al., 1997], the effect of a negative effective rake angle on the force is emphasized during ball nose end milling of AISI H13 tool steel (HRC 45-55) using PCBN tools with different cutting edge preparations. The cutting tool with a honed-radius generates the highest average force due to the contribution of the ploughing force component. On the other hand, the chamfered cutting edge results in the lowest average force when a higher feed rate was employed as a result of a more stable cutting process. Similarly, the machining force components (particularly the thrust component) tends to increase as the chamfer angle increases due to the increase in the cutting pressure within the chamfered zone due the friction between the DMZ and chips, [Movahhedy et al., 2002, Ren and Altintas, 2000, and Zhou et al., 2003].

Further investigations were conducted on how the cutting edge geometry contributes to the machining of hard materials [Özel et al., 2005, Shatla et al., 2001, and Thiele and Melkote, 1999]. Thiele and Melkote [1999] studied the cutting force components as a function of cutting edge geometry, workpiece hardness and cutting conditions in finish hard turning of AISI 52100 Steel (HRC 41-57) using low-CBN content inserts. The data obtained showed that the thrust and tangential force components increase as the cutting edge radius increases. However, the thrust force is highly affected by the cutting edge geometry compared to the tangential force. The study revealed that the combination between the honed and chamfered cutting edges results in a higher thrust force component than that for the honed edge. This was attributed to the considerable increase in the effective negative rake angle. Shatla et al. [2001] reported a similar observation when hard turning AISI H13 tool steel using a PCBN tool. Overall, the up-sharp cutting edge usually results in lower machining force components when compared to those generated by chamfered or honed cutting edges.

Influence of Chamfered Cutting Edge Preparation on Stresses in Cutting Tools

Up-sharp cutting tools have more stress concentration than tools with less sharpness. Therefore, the study of stress distribution is of great importance to analyze the stress concentration (i.e. maximum localized stress) along the tool and tool-workpiece interface. Rounding the cutting edge was proved to relieve the stress concentration around the cutting edge. However, an excessive increase in the cutting edge radius resulted in a localized stress near the flank face due to less efficient cutting, [Shatla et al., 2001].

Therefore, the cutting edge geometry has to be optimized in terms of lowering the effective stresses around the cutting edge, while maintaining efficient cutting. The study presented by Zhou et al. [2003] suggested that a 15° chamfer angle has the smallest principle stresses acting on the cutting edge. Hence, it experienced the minimum tool wear. Zhou et al. conducted experimental and numerical studies under fine cutting conditions. A bearing steel (60-62 HRC) was turned using PCBN inserts with different chamfer angles and tool life criterion of $V_B = 0.25$ mm.

Kishawy et al. [2002] conducted a numerical investigation on orthogonal machining of 304L stainless steel using ceramic tools. The effect of three different edge geometries: namely, sharp, chamfered and honed on the equivalent stress distribution was studied. In all cases, the maximum equivalent stress was induced on the flank face and closer to the cutting edge. However, the sharp cutting tool exhibited the highest maximum stress followed by the chamfered, then by the honed cutting edge.

Influence of Chamfered Cutting Edge Preparation on Temperature Distribution

In metal cutting, the material plastic deformation and chip production are initiated by the mechanical energy while the heat in the cutting zone is generated from the friction at the workpiece/tool and chip/tool interfaces. This heat has a great influence on tool wear, since tool wear mechanisms are mostly activated under conditions of high cutting temperatures. Therefore, the temperature distribution in the chip, workpiece and cutting tool is one of the main aspects in metal cutting. However, the determination of temperature distribution near the cutting edge is technically difficult. Therefore, numerical and modeling techniques have been used extensively to predict the flow of cutting heat and temperature distribution.

Ren and Altintas [2000] predicted the temperature distributions during orthogonal high speed turning of P20 Mold Steel workpiece material using sharp and chamfered carbide tools. Regardless of the cutting speeds used the temperature distributions in the primary shear zone and at the tool-chip interface were not drastically affected by the variation in the chamfer angle. For instance, the temperature at the tool-chip interface showed an increase of about 100° to 200°C when the chamfer angle changes from 0° to -40°. This was attributed to the constant predicted friction angles. However, the temperature at the tool-chip interface shows a high degree of dependency on the cutting speed. The temperature increased from 1350°C to 1700°C when the cutting speed increased from 240 m/min to 600 m/min. This was found to be related to the adiabatic thermal process where less time is allowed for the heat to be conducted through the chips (i.e. localized heat along the chip-tool interface), [Movahhedy et al., 2002].

Yen et al. [2004] found that the maximum tool temperatures for chamfered tools is shifted from the upper chamfer corner to the lower corner as the chamfer angle increases to 25° and chamfer width increases to 0.2 mm. Increasing the chamfer width and angle was found to have the same bluntness effect on temperature distribution as the one obtained with the tool having a higher cutting edge radius of 0.1 mm.

Influence of Chamfered Cutting Edge Preparation on Tool Wear

Brittle and ductile fractures are the most common failure modes for Carbide, PCBN and CBN tools in hard machining applications. These forms of tool failure are more likely to occur in interrupted cutting where thermal and mechanical shocks are periodically exerted on the cutting edge while entering and exiting the workpiece. In this case, adding a chamfer or small negative land to the main cutting edge will strengthen it against chipping and gross fracture as well as improve its heat dissipation properties. However, this geometry causes higher machining forces especially in the thrust direction. Therefore, a hard substrate grade with appreciable toughness and high abrasion resistance is mandatory for such applications.

Sikdar et al. [1992] conducted face milling experiments on C25 Steel (AISI 1025) using coated carbide face milling inserts. Three geometrical parameters were investigated at different cutting speeds and feeds: namely, chamfer length, chamfer angle and cutting edge radius. The cutting edge preparation parameters seemed to have a considerable influence on the growth of tool wear. An increase in the chamfer length resulted in more crater wear on the negative land due to an increase in the chip-tool contact length. Optimized chamfered-edge geometry was proposed where longer tool life and less chipping were achieved.

However, the study done by Elbestawi et al. [1997] revealed that honed and chamfered edge geometries resulted in lower tool performance when compared to that of a sharp tool. They used two grades of PCBN ball-nose tools with three different edge preparations (sharp, honed radius of about 0.025 mm and a negative land with effective rake angle of about -30°) in high-speed end milling of H13 Tool Steel. The lower performance of the chamfered edge was caused by the extensive wear developed on the rake face as a result of a large negative rake angle. In general, for hard machining applications the chamfered cutting edge outperformed the honed edges, [Chen et al., 2006 and Elbestawi et al., 1997].

Ren and Altintas [2000] conducted turning tests for machining P20 Mold Steel with CBN and carbide tools with chamfered cutting edges. It was observed that higher forces and friction energy were associated with larger chamfer angles, while weak cutting edge was associated with a zero and smaller chamfer angle. They found that the optimal tool performance and the minimal flank wear were achieved at a -15° chamfer angle. Similar observations were revealed by Zhou et al. [2003].

Influence of Cutting Edge Preparation on Surface Roughness

Surface roughness is partially dependant on cutting feed and nose radius. Some applications such as finish hard cutting require that other factors are considered: for example, the cutting edge geometry and the workpiece hardness. For the former, the influence is remarkable since in finish machining, the cutting edge radius is nearly the same order of magnitude as the uncut-chip thickness. An increase in the cutting edge radius will result in more ploughing action and hence the surface roughness will be detrimentally affected.

Ozel et al. [2005] investigated the effect of workpiece hardness, feed and edge preparation on machined surface roughness. They conducted hard turning experiments on AISI H13 Hot Work Tool Steel using CBN inserts with two different edge preparations (honed radius of 10.5 ± 4 μm and chamfered edge of $20° \times 0.1 \pm 0.03$ mm). They found that the honed tool and lower workpiece hardness resulted in a better surface roughness. There was no clear explanation why the honed edge geometry results in better surface roughness when compared to the chamfered geometry. However, this could be attributed to the wear developed on the tool surface, since surface finish is influenced by flank wear progression.

Arunachalam et al. [2004] investigated the effect of insert shape, cutting edge preparation, tool rake angle and nose radius on both surface finish and residual stresses generated by a facing operation on age hardened Inconel 718 with two grades of coated carbide tools. Honed edge geometry resulted in the best surface finish when compared to sharp and chamfered edge geometry in both cases of wet and dry machining. A sharp cutting edge was worn away due to excessive chipping that resulted during the machining of this heat resistant super alloy. In turn the surface roughness was affected drastically. Conversely, a chamfered edge geometry resulted in a better surface finish when compared to a sharp edge due to the higher temperatures developed by the chamfered tools. A similar result was established in [Almeida et al., 2005].

2.2.4 Geometrical Adaptation of Cutting Tools

During tool wear progression, changes in the cutting edge geometry are associated with the following: deterioration of the up-sharp edge line, appearance of the wear-land and an alteration in the effective rake angle. The geometrical adaptation of the cutting tool refers to the availability of an adaptive geometry that accounts initially for the alteration that occurs in the cutting edge geometry during the running-in wear stage. For the tool geometry to be adaptive, the cutting edge geometry has to correspond to the shape of the natural wear at the transition point between the two stages of tool wear (i.e. running-in and steady-state), [Fox-Rabinovich and Totten, 2006]. In order to do that an elimination of the cutting edge corner can be performed by adding a relief (i.e. facet or chamfered-edge) to the tool face or a honed radius to the cutting edge, or a combination of both of them. Consequently, a modified cutting edge that corresponds to the shape of natural wear at the transformation point[4] is obtained. In order to achieve a more stable and less intense wear rate the utilized edge geometry has to be optimized with respect to the cutting application, as will be discussed later in the results and discussion chapter.

2.3 Development of Hard PVD Coatings

Developments in hard coatings have provided tungsten carbide tools with improved performance during high speed machining of hardened steels. First, coatings

[4] The point of transformation from the running-in wear stage to the steady-state wear stage

with high hardness improve tool life by diminishing tool surface deformation at elevated temperatures. Next, coatings act as thermal barriers which have a beneficial impact on tool life by reducing both the diffusion and adhesion wear mechanisms. Finally, an improvement in friction surface adaptability is attained due to better friction control and heat dissipation.

2.3.1 Hard PVD Coating Deposition Processes

Two main coating technologies have been utilized for applying coatings onto cemented carbide tools: namely, chemical vapor deposition (CVD) and physical vapor deposition (PVD). The CVD process provides thicker coatings with better adhesion to the substrate than those deposited by the PVD process. The PVD process is applicable for a wide range of substrates due to its lower deposition temperature (<550°C) as compared to a CVD deposition temperature in the range of 970 – 1000°C, [Koenig et al., 1992 and Santhanaml, 2003]. The high deposition temperature can cause strength degradation in the WC tool at the coating-substrate interface and eventually can lead to lower transverse rupture strength. Therefore, the PVD process offers a reliable coating deposition technique for high speed steel (HSS), brazed or solid WC tools, [Stephenson and Agapiou, 1997].

2.3.2 Enhancing Properties and Tribological Performance of Hard PVD Coatings

PVD coatings are mostly recommended for milling applications due to the induced compressive residual stresses in the coating layers resulting in more resistance against crack propagation (i.e. impact resistance), [Santhanaml, 2003, and Stephenson and Agapiou, 1997]. Therefore, sub-micron solid substrates coated with PVD TiAlN-based coatings are currently the ideal cutting tools for high speed milling (e.g. machining of dies and molds) because of the improved toughness of the substrate and the improved hardness and wear resistance of the deposited coating, [Altan et al., 2001 and Cselle and Barimani, 1995]. Owing to its flexibility, PVD coatings can be processed using a wide range of elemental compositions with a wide variety of mono/multilayered designs, [Fox-Rabinovich and Totten, 2006].

2.3.2.1 Self-Adaptability of Coatings

The term "coating adaptability" refers to the ability of a coating to adapt to the mechanical and thermal loads experienced during cutting operations. Adaptability corresponds to the alteration in the structure and property of the coating during its running-in stage, which is followed by the formation of thin protective layers on the friction surfaces (i.e. tribo-films). These films have a tremendous influence on improving the life of the cutting tool by stabilizing the tool wear rate and improving the lubricity of the coated tools. However, these thin layers must be generated continuously during the running-in stage as well as the post running-in stage since they are constantly being removed, [Fox-Rabinovich and Totten, 2006].

Tribo-films are formed on the surface mostly because of diffusion and chemical reactions with the Oxygen found in the cutting environment. Strong films usually promote the stabilization of wear by acting as thermal barriers, as well as enhancing the lubricity between the friction surfaces when elevated temperatures are attained. Meanwhile, the change in the microstructure lowers the thermal conductivity as a result of the amorphous-like or a nanoscale-grained structure. Therefore, these films have a beneficial impact on improving the friction and heat dissipation in the cutting zone by directing more heat into the chips, [Fox-Rabinovich et al., 2005].

However, the formation of weak oxide films can negatively affect the tool surface due to the tendency of such films to be worn away very quickly. An example of this is when cobalt-oxide forms on the uncoated areas of tungsten carbide tools. Accordingly, the thin films are supposed to be hard and to have a low-intensity interaction with the mating surface to direct the friction stresses towards the elastic zone rather than the plastic zone of deformation. In addition, these thin films have to be supported by a well-engineered substrate material to protect the surface effectively, [Fox-Rabinovich and Totten, 2006].

2.3.2.2 Post-Treatment of a Coating Surface

Coatings with an improved surface integrity (i.e. surface finish) can be developed by the pre-treatment of the substrate surface and post-treatment of the coating surface. The latter treatment is utilized to remove any particles that stick to the coated surface, while the former treatment is used to provide a substrate with a smoother surface in order to enhance the adhesion of the coating, [Santhanaml, 2003]. Bouzakis et al. [2005] studied experimentally and numerically the influence of micro-blasting of PVD films deposited on micro-blasted polished substrates. An improvement was achieved in the performance of these specially treated coated cemented carbide tools during dry milling of 42CrMo4V steel. Endrino et al. [2006] reported an improvement in tool life by post-polishing of coated cutting tools. In this case post-treatment-polishing was utilized to remove the macro-particles formed on the coated-tool surface during deposition.

2.3.3 Nano-Scale Mono and Multi-layered Hard PVD Coatings

The coating microstructure and composition are essential to maintaining acceptable performance. The selection of the alloying elements has to be done properly to ensure a coating with a wide range of applicability to different cutting conditions. The improved performance of the nano-scale mono-layered TiAlCrN coatings with high Al-content is attributed to the improved oxidation resistance and the improved plasticity and lubricity due to its lower coefficient of friction at temperatures of up to 1000°C, [Fox-Rabinovich et al., 2005 and Kovalev et al., 2006]. The formation of $(AlCr)_2O_3$ complex oxides on the tool surface will enhance the oxidation resistance of the TiAlN-based coatings due to their high thermodynamic stability, [Fox-Rabinovich et al., 2005].

Multi-layered coatings represent a coating system that offers an optimum coating performance by combining different materials with different features. For instance, when Al_2O_3 is added to TiC, this results in a coating that has better adhesion and provides better diffusion resistance (i.e. good thermal barrier), [Stephenson and Agapiou, 1997]. Owing to the finite thickness of each individual layer, nano-scale multi-layered coatings are considered to be tougher (without compromising on hardness) than coatings of several micrometers. Thus, they are ideal for arresting crack propagation, [Santhanaml, 2003].

In high speed machining (HSM), the cutting tools are subjected to enormous thermal and mechanical loads. Therefore, the development of nano-multilayered coatings has been the trend in the current research for coated tools, [Fox-Rabinovich et al, 2008, Fox-Rabinovich et al., 2006, Ning et al, 2007, Ning et al., 2007 and Yamamoto et al., 2005]. For instance, the incorporation of tungsten (W) to nano-structured multilayered *(TiAlCr)N-based* coatings in the form of transitional metal such as (W)-based nitride resulted in a considerable improvement in cutting tool performance during HSM of hardened steel (HRC 50), [Fox-Rabinovich et al., 2006 and Ning et al., 2007].

2.4 Development of Dry and MQL Cutting Environments

The development of dry machining and MQL conditions offer cleaner and more economic cutting environments and if administrated properly they can result in better cutting performance (i.e. extended cutting tool life and better machined surface finish and dimensional accuracy). The cooling capacity of the pressurized gas can be increased by delivering chilled or refrigerated air to the cutting zone using vortex guns or chilled gases, such as carbon dioxide or nitrogen. MQL or mist lubrication can be used in order to improve the cooling and lubricity by incorporating a small quantity of cutting oils to the fast flowing air stream. Another technique is to use devices with very high blowing capability such as super-air or high-jet nozzles for improving the volumetric flow rate of the air stream.

2.4.1 Conditions for Better Coolant and Chip Evacuation

Significant ongoing research has been devoted to the implementation of dry and MQL machining operations. A better understanding of the cutting process mechanism and proper adjustment of cutting conditions are essential in order to realize the full benefits of dry and MQL machining. Machado and Wallbank [1997] studied the effect of five different lubricant conditions on force components and surface finish, when turning medium carbon steel at a cutting speed of 200 m/min and a wide range of feed rates (0.05 to 0.4 mm/rev) using uncoated cemented carbide inserts. The results showed that the largest beneficial effect of using air and soluble oil environment was found on the cutting force components at higher feed rates (0.3 to 0.45 mm/rev), when compared to those found under a dry environment, while no significant improvement was observed in surface finish. The only noticeable improvement was found under lower cutting speeds (30 m/min).

In the same way, Rahman et al. [2002] tested three cutting environment strategies, dry cutting, MQL (oil-air mixture) and flood coolant (fully synthetic water soluble coolant) during end milling of ASSAB 718HH Steel (HRC 35) using uncoated carbide inserts under a cutting speed range of (75 to 200 m/min) and a feed rate range of (0.01 to 0.03 mm/tooth). The results showed that dry and MQL cutting environments resulted in similar tool wear at higher feed rates regardless of the cutting speed, while flood coolant resulted in localized chipping due to relatively higher thermal stresses. The overall findings included: first, the MQL effectiveness was evident under low feeds and speeds; second, MQL and dry cutting had almost the same beneficial impacts on cutting performance under higher speeds and feeds when compared to that obtained under flood coolant conditions.

Similar observations were revealed in [Diniz and Micaroni, 2002] except for the finding regarding higher cutting speeds. Dry cutting was recommended over flood coolant when turning 1045 Steel (HRD 55-59) using coated carbide inserts under lower cutting speed and relatively higher feeds (0.1 to 0.14 mm/rev). The improved dry cutting performance when higher feed was attained was due to better heat dissipation as a result of a larger area of the tool being exposed to the heat generated during cutting, which eased the cooling of the cutting zone.

The adaptation of compressed chilled or refrigerated air in the cutting environment has been investigated by a number of researchers in the literature, [Kim et al., 2001, Liu et al., 2007, Rahman et al., 2003 and Su et al., 2007]. Kim et al. [2001] studied the influence of four different cutting environments on tool life and cutting temperature when ball-end milling die steel (HRC 42) using PVD-TiAlN coated carbide tools at a cutting speed of 210 m/min. Chilled air of (-9 °C) yielded the best cutting tool performance (*i.e. longest tool life and normal wear pattern*), while chilled air of (-35 °C) had severe wear patterns similar to those obtained under wet cutting condition. The severe edge chipping in both cases was attributed to thermal fatigue due to excessive cooling conditions.

Similar observations were revealed in the experimental study conducted by Rahman et al. [2003]. They employed compressed chilled air of (-35 °C at 6.67E-3 m^3/sec) during rough and finish end-milling of ASSAB Mould Steel (HRC 35) using uncoated tungsten carbide inserts. The overall findings included: first, the cooling capacity of chilled air was more pronounced at lower feed rates and resulted in lower flank wear when compared to dry or flood coolant conditions; second, more chipping appeared on the inserts using chilled air at higher cutting speeds, which reflects the negative impact of a thermal gradient for the case of chilled air. The surface roughness was beneficially affected when chilled air was employed at higher feed rates.

Further investigation was conducted to asses the feasibility of using refrigerated air during finish turning of Inconel 718 Nickel-based Super Alloy (HRC 41) and end-milling of AISI D2 Cold Work Tool Steel (HRC 62) using PVD-TiAlN coated carbide tools, [Su et al., 2007]. Cooling air cutting environments resulted in a 78% and 130% improvement in tool life[5] over dry cutting, when machining Inconel 718 and AISI D2 tool steel respectively. The surface roughness was improved as well. It is of interest to mention that, the term "dry cutting", in all the previously reviewed studies, refers to a cutting environment that has no forced air flow rate and no lubrication.

[5] A 0.2 mm flank wear was used as tool life criterion.

Chapter 3: Experimental Setup and Procedure

The performance of different cutting tool designs (i.e. substrates, tool geometries, cutting edge preparations and coating designs) were evaluated during ball end-milling of Hardened AISI H13 (HRC 54–55). Different dry and MQL cutting environments were also investigated in order to improve the machining performance. In addition, cutting tests were conducted at different cutting speeds in order to identify the limitations in the operational cutting speeds. The general machining setup is shown in Figure (3.1).

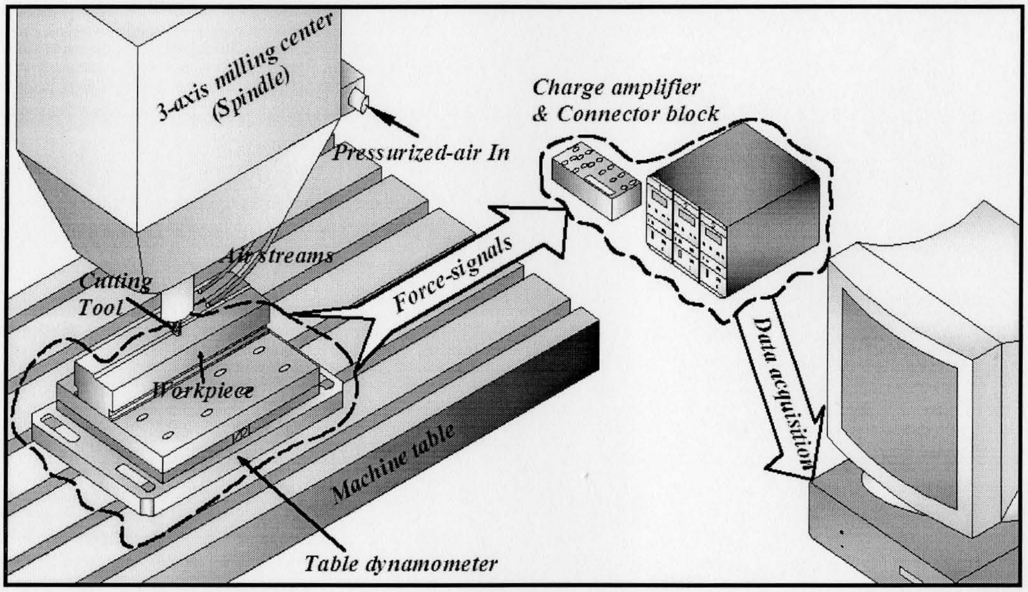

Figure (3.1) Schematic illustration for the machining setup

3.1 Cutting Parameters

Climb/Down milling strategy was applied in all cutting tests, where the tool and the workpiece are moving in the same direction, as shown in Figure (3.2).

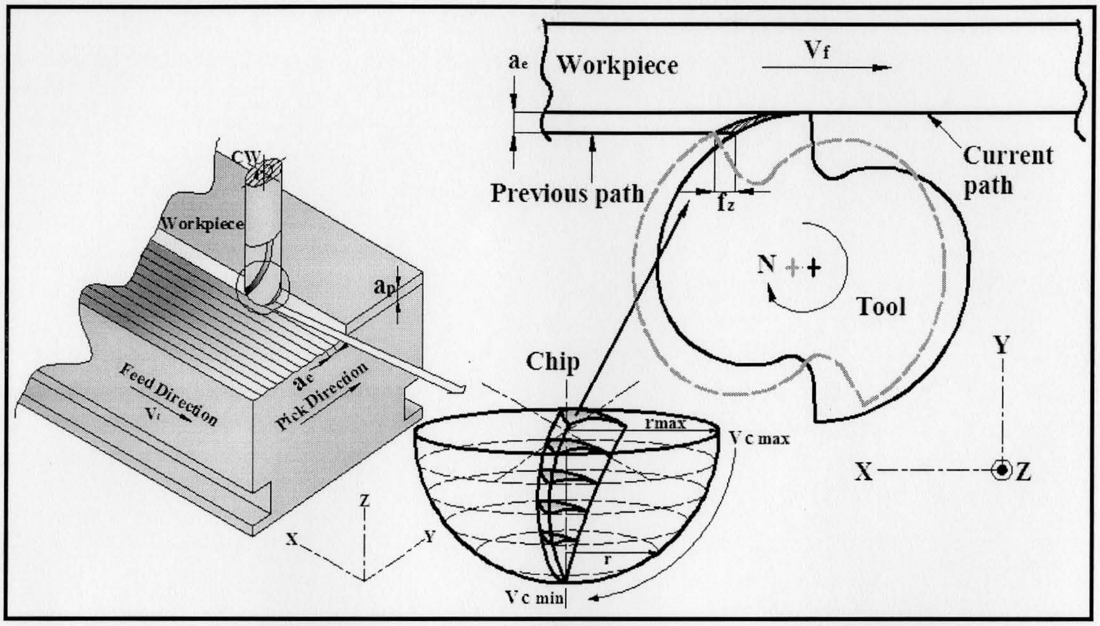

Figure (3.2) Schematic illustration of tool-workpiece configuration and chip geometry

A straight cutting path was employed with zero tilting-angle and with axial depth of cut equals to the radius of the tool ball-part to ensure that the whole ball is engaged in cutting so as to achieve the maximum cutting speed. The cutting conditions selected for ball end milling experiments are listed in Table (3.1).

Cutting speed ($V_{c\,max}$), (*m/min*)	300	350	400
Feed /tooth (f_z), (*mm/tooth*)	0.06		
Spindle speed (N), (*RPM*)	≈ 9,550	≈ 11,141	≈ 12,733
Table feed (V_f), (*mm/min*)	≈ 1,146	≈ 1,337	≈ 1,528
Axial depth of cut (a_p), (*mm*)	5		
Radial depth of cut (a_e), (*mm*)	0.6		

Table (3.1) Cutting parameters

3.2 Machine Center

All the cutting tests were conducted using a 3-axis milling center Matsuura FX-5G with maximum spindle speed of 27,000 RPM, spindle power of 27 HP, rapid feed rate of 25 m/min, high precision and high rigidity.

3.3 Cutting Tool Design

3.3.1 Substrate Design

Micro-grain cemented tungsten carbide (WC-12 at% Co) substrates with high wear resistance and high toughness were selected for the cutting tests. Different ball nose end-mills were used for the experimental work. The geometries, microstructures and hardness[6] are presented in Figure (3.3). The mechanical and thermal properties of cemented carbide are mostly dependent on the microstructural composition, the amounts of binding element and the grain size, [Davis, 1998]. The thermal conductivity was found to be in the range of (80-100 W/m-K) for most of the tested cemented carbide grades.

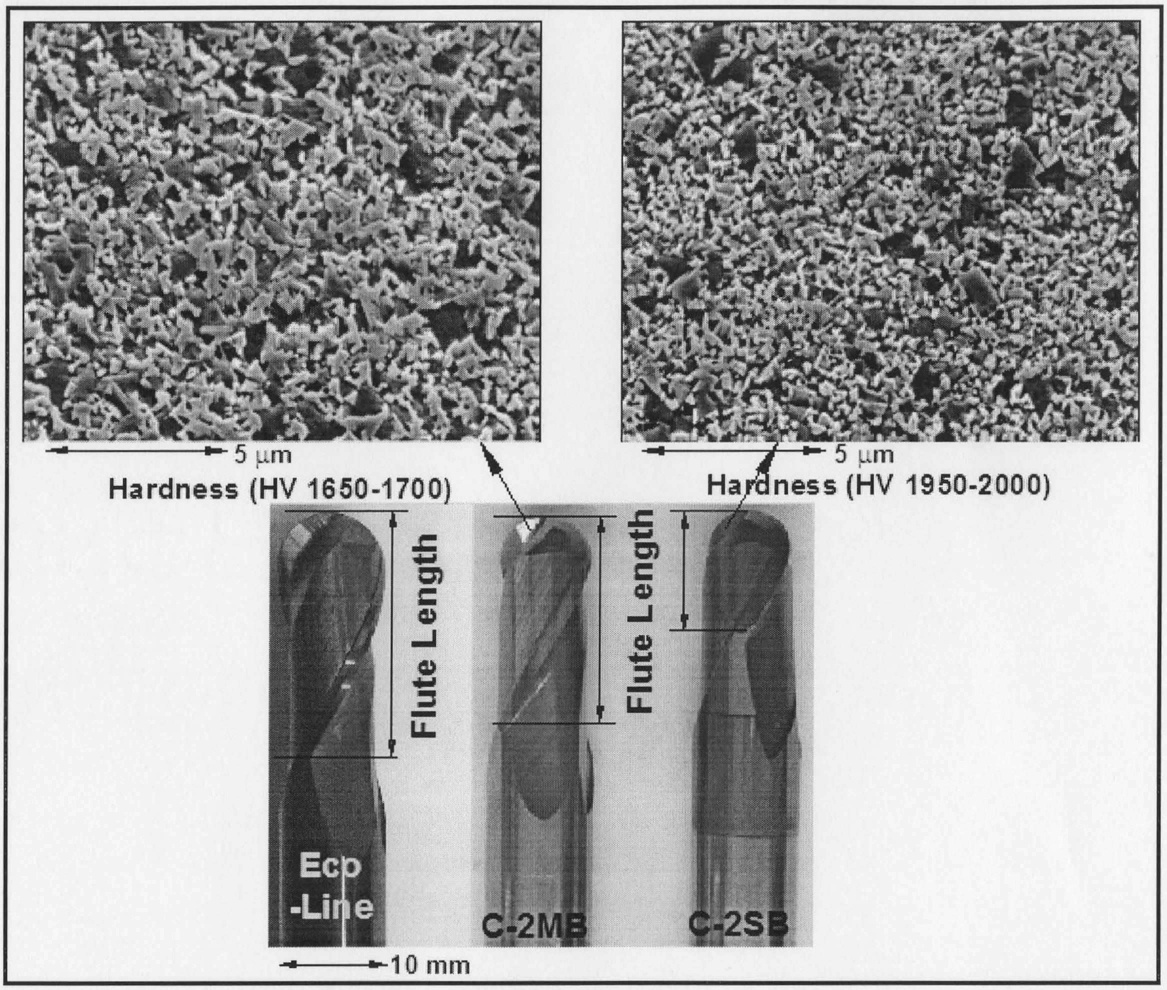

Figure (3.3) Different tool geometries and microstructures used for experimental work

[6] The hardness was measured using Micro hardness Shimadzu tester with applied load of 1 N.

Table (3.2) summarizes the geometrical parameters of the cutting tools used throughout the experimental work.

Cutting tool supplier	**Wolf-Gruppe tool**	**Mitsubishi Carbide tools**	
Specifications Tool	**Eco-Line**	**C-2MB**	**C-2SB**
Radius of ball nose (*r_{max}, mm*)	5	5	5
Shank diameter (*D, mm*)	10	10	10
Flute length (*L_f, mm*)	23	18	10
Overall length (*L_O, mm*)	100	100	100
Number of flute (*Z, teeth*)	2	2	2
Helix angle (*Straight Part*)	30°	30°	30°
Helix angle (*Ball Part*)	0° - 30°	0° - 27°	0° - 27°
Radial rake angle	0°	0°	0°
Tool weight (*grams*)	101.72	99.75	108.66

Table (3.2) Geometrical parameters of ball end-mills used for experimental work

Tool Clamping

All cutting tests were conducted using high precision (Mega New Baby Chuck BIG BBT40-MEGA13N-90 and BIG BBT40-MEGA20N-60) tool holders with cutting tools mounted on an overhang lengths of 33, 28 and 22 mm from the collet for Eco-line, C-2MB and C-2SB designs respectively. The tool run-out was kept within the range of 5-7 μm.

3.3.2 Cutting Edge Preparation

Figure (3.4) shows the three cutting tool edge preparations used for the experimental work: namely, Up-sharp edge, Facet A and Facet B. Most of the cutting tests were conducted using ball end-mills with an up-sharp cutting edge.

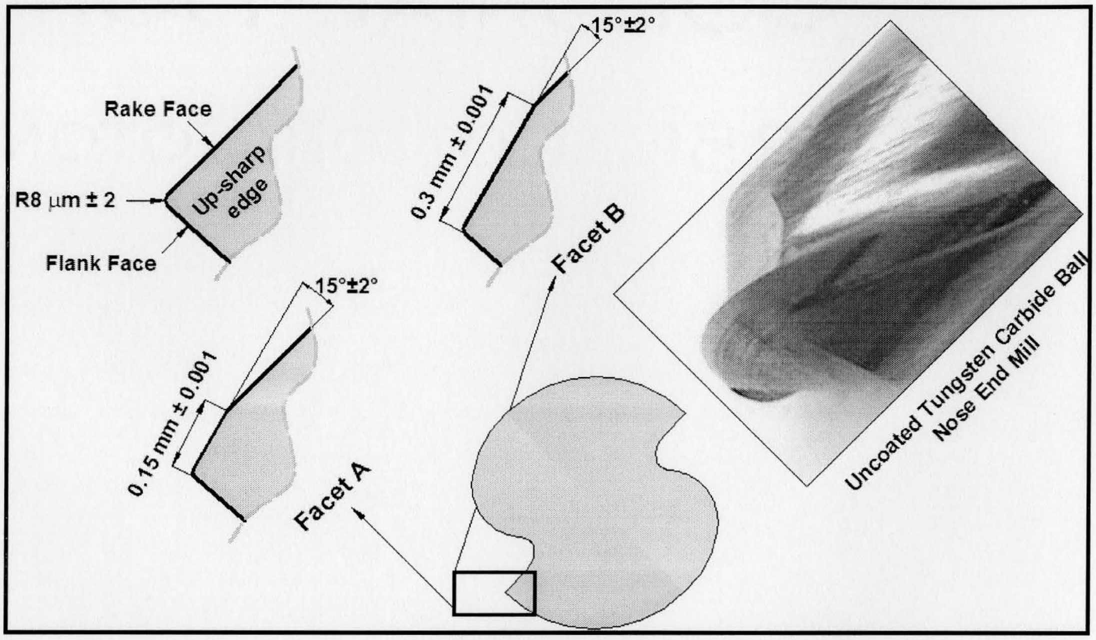

Figure (3.4) Different cutting edge geometries used for experimental work

Owing to severe edge chipping, C-2MB coated ball end-mill failed catastrophically by edge and ultimately shank fracture, as shown in Figure (3.5). Therefore, two facets were applied to new C-2MB substrates in order to investigate the influence of chamfered cutting edge preparation on strengthening the cutting edge against fracture.

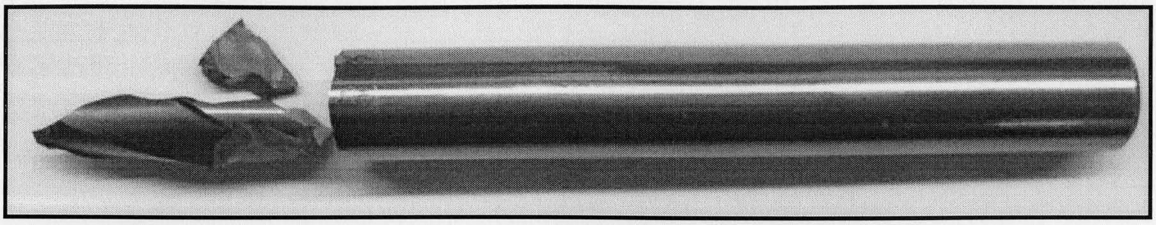

Figure (3.5) Catastrophic failure under the following cutting conditions: cutting speed of 300 m/min, feed rate of 0.06 mm/tooth, table feed of 1146 mm/min, axial and radial depth of cut of 5and 0.6 mm respectively and last measured flank wear of 0.163 mm

The geometry of the adaptive cutting edge geometry was selected based on tool wear evolution data obtained with the up-sharp cutting edge. The selection was also based on the concept of geometrical adaptation of cutting tools, [Fox-Rabinovich and Totten, 2006]. More details will be presented in the results and discussion chapter. Moreover, the chamfer negative angle was kept within 15°-18°, which was recommended by some researchers in the literature [Ren and Altintas, 2000, Sikdar et al, 1992 and Zhou et al., 2003]. This is attributed to the fact that a steeper chamfer angle can lead to an increased rate of flank wear due to larger radial forces. Moreover, Zhou et al. [2003] showed that 15° chamfer angle has the lowest principle stresses acting on the cutting edge when hard turning bearing steel (60-62 HRC) using PCBN tools.

In order to add the facets, the two new substrates were sent for cutting edge preparation. Each negative chamfered-facet was performed along the cutting edge by diamond filing under a stereo-microscope. It is of interest to note that, in ball end-milling the cutting speed and the chip load vary along the cutting edge with minimal values at the tool tip. Therefore, a facet with variable chamfer width was performed along the cutting edge, as shown in Figure (3.6). Since the chip load is usually diminished at the tool tip, then the chamfer size must be smaller with almost no facet applied once the tool tip is approached. This contributes to the minimization of the rubbing zone and thus excessive heat generation (i.e. ploughing or non-cutting action) that would be formed close to the nose tip due to the addition of a negative rake angle effect. In the literature the technology of having a variable edge preparation size is referred to as Engineered-Micro-Geometry (EMG) technology, [Benes, 2005, Conicity Technologies, 2006 and Kennedy, 2004].

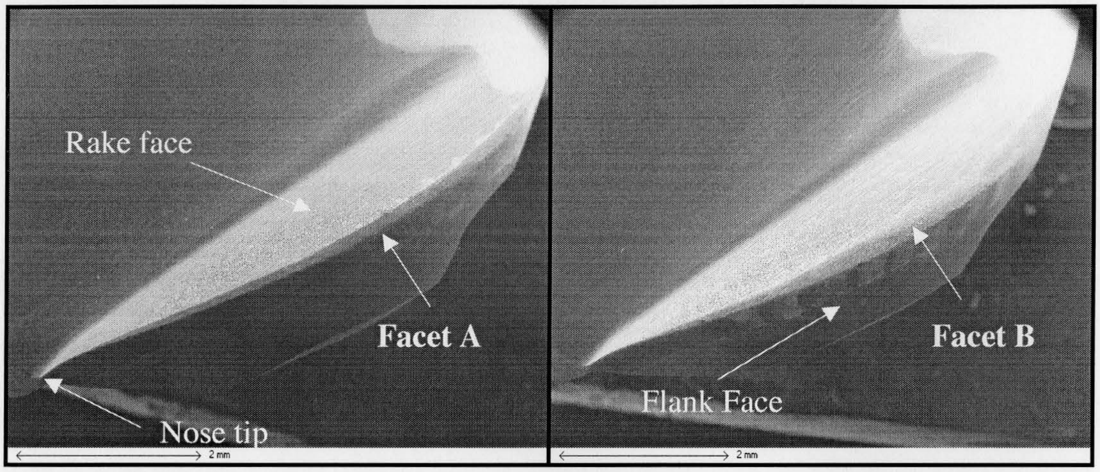

Figure (3.6) SEM images showing the variable size of each facet along the cutting edge

3.3.3 Deposited Coating

Two different PVD hard coatings were utilized on cutting tools tested in the presented study. The influence of using these hard coatings on cutting performance was investigated. The influence of a post-treatment process (i.e. coating surface polishing) on coating performance was examined as well. All the characterization analysis for the

Kobelco deposited coatings were provided by Kobe Steel Ltd., Japan. and the research group at McMaster University.

3.3.3.1 Coating Material

Most of the cutting tools were coated with Nano-structure PVD hard coatings (TiAlCr)N/(Nb)N. This experimental coating was developed and deposited by Kobe Steel Ltd., Japan and the research group at McMaster University. It is a nano-structured multilayered (Ti,Al,Cr)N-based coating with a transitional metal Nb-based nitride. Another coating deposition was supplied by Wolf Tool/Coating technology LLC., Germany. In that case the coating was PVD Supernitride-HSN^2. This is a multi-layered (Ti,Al)N-based coating with a fine-grained nano-composite structure. This coating was used for a comparative study.

3.3.3.2 Coating Deposition

The TiAlCrN/NbN coating deposition was conducted in Kobe Steel Ltd. The coating deposition was applied simultaneously using the plasma enhanced arc-cathode technique [Yamamoto et al., 2003], as shown in Figure (3.7) and the unbalanced magnetron sputtering (UBM) method [Yamamoto et al., 2005].

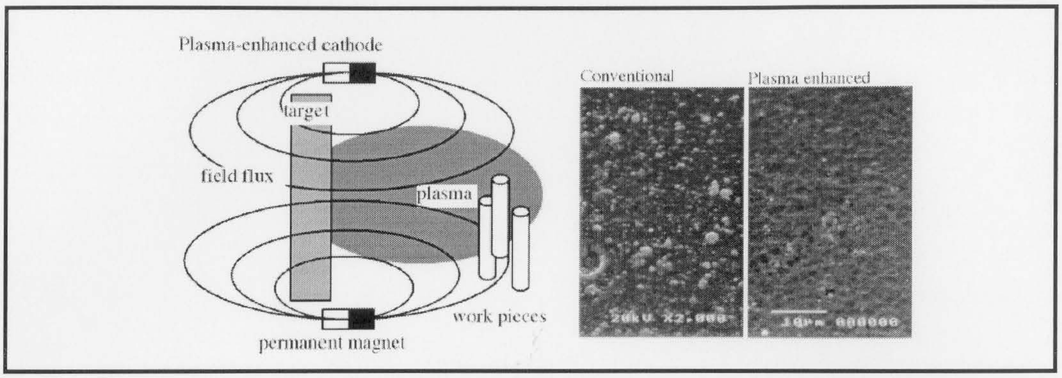

Figure (3.7) Schema of Plasma-enhanced cathode with an SEM image of the coating surface quality typically obtained, [Yamamoto et al., 2003]

First, the substrates were mirror polished and cleaned ultrasonically in ethanol. Next, the polished samples were preheated up to 773 K and placed inside an evacuated chamber. Then the samples were mounted on a sample holder rotating at 5 rpm and cleaned by an Argon (Ar)-ion etching process. Finally, the combined coating deposition process was applied on the passing samples. During the deposition, Ar-N_2 mixture gas was fed into the chamber at a pressure of 2.7 Pa with a N_2 partial pressure of 1.3 Pa. At this point in time a hot pressed TiAlCr target was employed as an arc cathode with an arc current of 100 A (for a target with 100 mm in diameter), while a material such as Niobium (Nb) was sputtered alternatively by UBM sputter source with a DC input power of 1 KW (for a target with 160 mm in diameter). Meanwhile, the substrate bias was kept at 30 V throughout the deposition. At the end, a 3 μm multi-layered coating film was deposited with a total of about 200 layers (≈15 nm period with grain size range of 10-12 nm); refer to Figure (3.8) for more details. Owing to the lower deposition rate, the layers deposited by the UBM evaporation source were thinner than those deposited by the enhanced arc method, [Fox-Rabinovich et al., 2006].

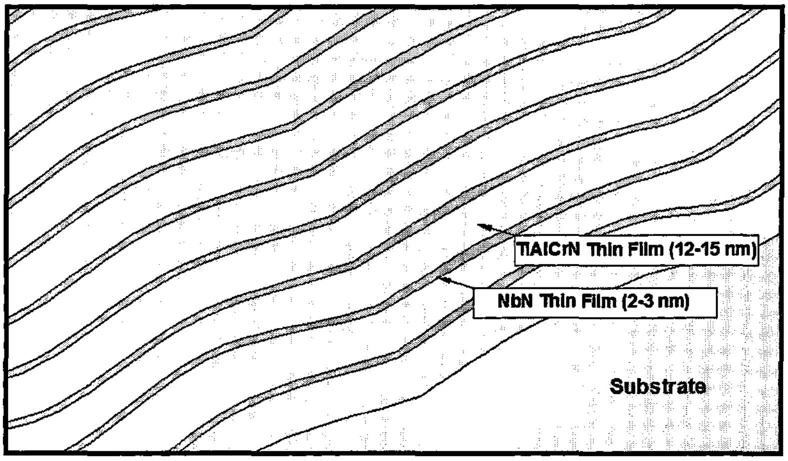

Figure (3.8) Schematic diagram for the cross-section of the TiAlCrN/NbN coating

3.3.3.3 TiAlCrN/NbN Coating Characterization

Compositional and Structural Analyses

EDS analysis was conducted to determine the aforementioned coating composition. SEM analysis was conducted to investigate the coating surface morphology before and after each cutting test.

Tribological Analysis

In order to study the tribological characteristic of the developed coating, the change in friction coefficient with temperature was monitored using the apparatus described in [Fox-Rabinovich et al., 2006]. The apparatus was designed to simulate the frictional conditions at the interface between the coated-tool and the workpiece. A sample of rotating coated substrate was placed between two polished specimens made of AISI H13 Die Steel with a hardness of 50 HRC and heated up to 1,200 °C by resistive heating, while a standard force of 2,400 N was maintained during the test. Under frictional conditions, zones of adhered asperities tend to be formed at the interface between the tool surface and the workpiece. Accordingly, the friction coefficient was calculated as the ratio between the shear strength of the adhered asperities and the normal load exerted on the contact interface at different heating temperatures (25 °C to 1,200 °C). The test was repeated up to three times with data scatter of approximately 5%.

Despite using plasma enhanced arc-cathode technique for coating deposition, the coating still experienced the formation of some "macro-particles" on its surface during deposition. These particles can lead to coating delamination under the high contact stresses involved in cutting. Therefore, a post-treatment process was applied to reduce the intensity of these droplets on the coating surface. A TiAlCrN/NbN coated tool was sent for polishing where a Nylon brush was used to create a droplet-free surface. The influence of this post-treatment process on coating performance was then investigated.

Mechanical and Chemical Analysis

A micro-hardness of 31.67 GPa was measured using a micro-indentation tester (micro-hardness with normal load of 25 gf). The oxidation resistance was estimated based on short-term oxidation tests. A weight gain of 0.055 mg/cm^2 at 900 °C was obtained after annealing in air for 60 min.

3.4 Workpiece Material

Hardened AISI H13 (5% Chromium Hot Work Tool/Die Steel) was used in all cutting tests as a workpiece material with the chemical composition as listed in Table (3.3).

	C	Mn	Si	Cr	Mo	V
Composition (at), %	0.39	0.36	1.13	5.14	1.24	0.83

Table (3.3) Chemical composition of workpiece material

First, the workpieces were received in the form of blocks (Width: 101 mm, Height: 106 mm and Length: 260 mm). Then the annealed blocks (BHN 219) were sent for hardening (hardened at 1,060 °C, quenched in vacuum/air and tempered at 500 °C twice during 1 hr). The obtainable hardness is within the range of HRC 54-55. For hardened AISI H13, the thermal conductivity is within the range of (28.6-28.7 W/m-K) for temperature range of (215-605 °C) and the coefficient of thermal expansion is within the range of (10.4-12.4 μm/m-°K) for a temperature range of (100-650 °C), [ASM Handbook, 1990].

3.5 Cutting Environment

The cutting tests were performed under dry and MQL cutting conditions. For chip evacuation and cooling purposes, a stream of air was initially driven at the cutting zone by pressurized air of 100 PSI (≈ 0.69 MPa) through an open copper tube (1/4" ≈ 6.35 mm in diameter and positioned at almost 80 mm from the cutting edge). The air was directed at the cutting zone at a volumetric flow-rate of almost 934 LPM (≈ 15.5E-3 m^3/sec and at room temperature ≈ 22 °C). In all of the cutting tests, the air blast was flowing normal to the tool rake face (black arrows), as shown in Figure (3.9).

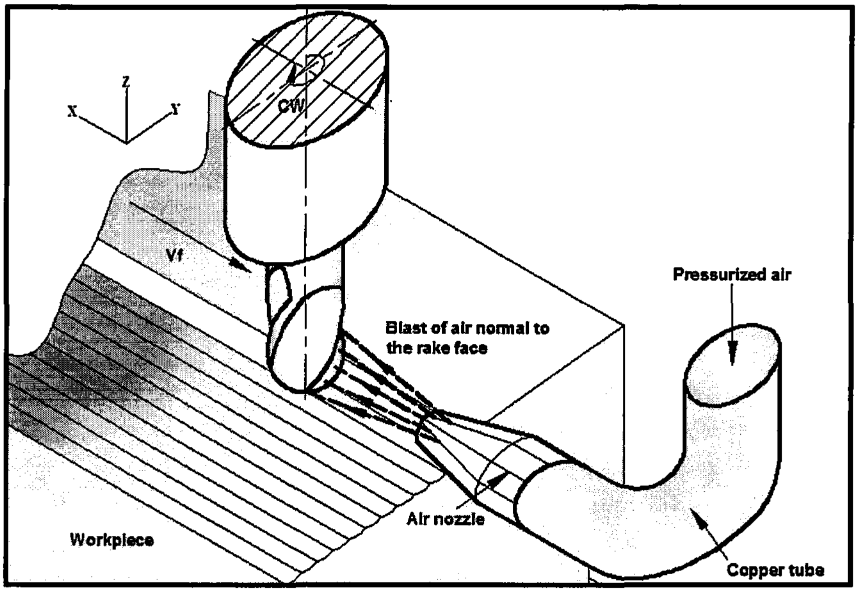

Figure (3.9) Schematic configuration for the Air-flow pattern

The next set of cutting tests was performed using two different compressed-air settings: namely a vortex tube and a super air nozzle. The configurations for the two devices used are listed in Table (3.4). The vortex tube is basically functioning by using delivered compressed-air (normally 80-100 PSI) as a power source in order to eject two streams of cold and hot air. In order to test for a low inlet pressure that would cause poor performance, a pressure gauge was placed right before the compressed-air inlet of the vortex tube. The stream of cold air can be adjusted to deliver a refrigeration effect to the cutting zone with a wide range of cold temperatures, while maintaining good flow rates for chip removal.

Similarly, the super air nozzle is functioning by using delivered compressed air. This nozzle has a certain aerodynamic design that enables the air to be ejected towards the cutting zone with amplified blowing capability and "hard-hitting force" (e.g. 850 grams for this model).

	Exair® Vortex tube		**Exair® Super air nozzle**
Air Blast	Dry chilled air Temp. (-5 °C ± 2)	Dry chilled air Temp. (-15 °C ± 2)	Dry air Temp. (≈ 22 °C)
Volumetric Flow Rate	15.1 E-3 m^3/sec ≈ 906 LPM	11.3 E-3 m^3/sec ≈ 680 LPM	18.3 E-3 m^3/sec ≈ 1100 LPM
Extension copper tube	Diameter : 3/8" ≈ 9.525 mm Positioned at almost 40 mm from the cutting edge		Diameter : 1/2" ≈ 12.7 mm Positioned at almost 50 mm from the cutting edge
Model	Model 3240	Model 3230	Model 1104

Table (3.4) Details of different configurations used for air blowing

Another set of experimental tests was conducted under MQL cutting conditions. The oil-air mixture was delivered to the cutting zone by using a commercial mist generator (Accu-Lube Precision Applicator). The oil-mist applicator dispensed a controlled amount of (Accu-Lube LB-2000) oil by using a stream of pressurized air (80 PSI). This natural oil was recommended for the environmentally safe machining of ferrous metals.

3.6 Tool Wear Monitoring

Throughout each cutting test, the cutting tool was examined regularly under an optical toolmakers microscope (Mitutoyo TM) to monitor the flank wear progression and to track the progression of other visible tool wear patterns (e.g. chipping, notch wear and crater wear).

In most of the cutting tests, flank wear was more predominant than any other type of tool wear. A maximum flank wear land width of (VB_{max}) of 0.3 mm was selected as a tool life criterion in accordance with ISO 8688-1. However, the selected tool life criterion was altered in a few cutting tests where catastrophic fracture of cutting tool (i.e. edge/shank fracture) occurred or was likely to occur due to a significant variation in cutting force and severe edge chipping.

In order to analyze tool wear mechanisms and coating deterioration, Scanning electron microscopy (SEM) images of new and worn cutting tools were taken using a Philips-SEM-515-LAB6-Gun provided with Link analytical pentafet energy dispersive x-ray for energy dispersive spectroscopy (EDS). Optical microscopic images were taken using a Zeiss Stemi 2000-C stereo microscope.

3.7 Cutting Force Measurement

Cutting force components were measured frequently during each cutting test to monitor the variation in forces throughout the tool life. For measuring the three orthogonal components of cutting force, the workpiece was clamped to a KISTLER three-component table dynamometer (9255B) with a maximum natural frequency of 2 KHz in the x and y axes and 3.3 KHz in the z-axis. The forces were sampled at a rate of 290-350 sampling-points per revolution over the tested range of cutting speeds. The force-signals were amplified using a KISTLER 5814B1 three-channel dual mode charge amplifier with a (180 KHz) plug-in filter. For data acquisition (DAQ), a National Instruments BNC-2110 adapter was connected to a DAQ device for analog input to digital output signal conditioning. LabView software was used for acquiring and analyzing the signals.

Cutting Dynamics

The measured and the resultant cutting forces, and their Fast Fourier Transforms (FFT) were investigated. In order to identify the nature of the vibrations induced during cutting, the underlying frequency content and its peaks were analyzed with respect to the following frequency modes:

- Tooth passing frequency (i.e. cutting frequency) and its harmonics;
- Frequency associated with chip formation process (i.e. chip segmentation);
- Frequencies associated with oscillations arising from the tool-clamping system.

More details on how to calculate these frequencies can be found in Appendix A.

3.8 Surface Roughness Measurement

Machined surface roughness was measured during some selected cutting tests using a portable surface roughness tester (Mitutoyo SJ-201P Surface Roughness Profilemeter) with a cut-off length adjusted to 0.8 mm and an evaluation length of 4 mm. The average surface roughness was measured at different cutting lengths throughout the cutting test along the pick-direction (path or pick-interval scallops) and at 4-different points distributed along the tested cutting paths. The sculptured surface finish (the surface finish produced by a finite increment between the successive tooth feeds) was also monitored during cutting.

3.9 Chip Analysis

Chip samples were collected throughout the cutting tests to estimate chip surface temperature based on chip colors at different machined lengths. SEM images were taken in order to analyze the shape of both the bright and dull chip surfaces facing upward. The cross sections of the chips were prepared to study and to track changes in chip morphology and dynamics under different cutting conditions and tooling designs. First, chips were mounted in Epoxy resin and kept as orthogonal as possible to the radial cutting direction. Next, the specimens were automatically ground and polished. Finally, the specimens were etched with a solution of 2% Nital for at least 10 seconds.

Chapter 4: Experimental Results and Discussion

4.1 Influence of Cutting Tool Design on Cutting Performance

The failure of the carbide milling cutters during hard machining is mostly motivated by severe edge chipping. Excessive cutting force variation throughout the cutting time is an in-process indicator of severe tool wear that can lead to catastrophic tool failure (i.e. edge/shank fracture). Proper cutting edge preparation can be introduced to strengthen the cutting edge by directing the mechanical and thermal cutting loads towards a wider surface area. In turn, the tendency of the cutting edge to micro-chip will be diminished (i.e. effective cutting without breakage). However, cutting edge preparation usually results in higher machining force components when compared to those that resulted from a sharp tool. Therefore, the cutting edge geometry has to be coupled with a tougher coated substrate in order to enhance cutting tool performance against fracture.

Two models of tungsten carbide ball nose end-mills (Mitsubishi C-2MB with three different cutting edge preparations and Mitsubishi C-2SB with un-chamfered cutting edge) were utilized in this set of experimental tests. The cutting tools were coated with experimental nanostructure multilayered coating (TiAlCrN/NbN). The objective of the present investigation is to test the new developed coating and to investigate the influence of cutting edge geometry on tool performance in high speed machining (HSM) of hardened AISI H13 (HRC 54-55). The cutting tests were conducted under the following dry cutting conditions: cutting speed of 300 m/min, feed rate of 0.06 mm/tooth, table feed of 1,146 mm/min, axial and radial depth of cut of 5 and 0.6 mm respectively and pressurized air of 100 PSI (≈ 0.69 MPa) through an open copper tube.

Figure (4.1) shows the development of flank wear along the Mitsubishi C-2MB tool with un-chamfered "Up-sharp" cutting edge. The flank wear developed at very intensive rate during the running-in wear stage. Then it tended to stabilize during the transition between the two stages of tool wear (i.e. running-in and steady-state). However, the appearance of very early edge chipping prevented the rate of flank wear from stabilizing. As a consequence, flank wear progression was accelerated while excessive edge chipping was still developing along the cutting edge causing the coated tool to fail catastrophically by sudden-fracture of the edge and shank.

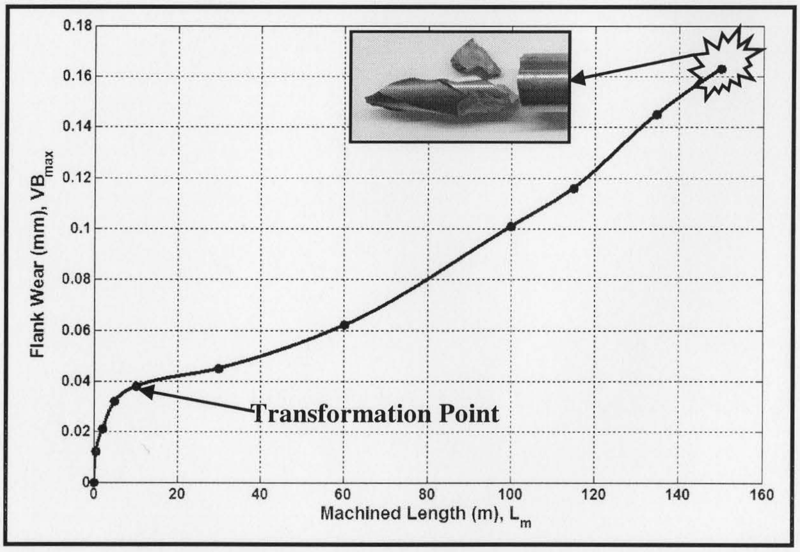

Figure (4.1) Flank wear evolution versus machining length for the un-chamfered cutting edge

Therefore, two facets were designed and applied to new Mitsubishi C-2MB substrates to investigate the influence of chamfered cutting edge preparation on strengthening the cutting edge against fracture. In an additional test, an improved cutting tool design (i.e. Mitsubishi C-2SB with finer grain size, more dense structure, shorter flute length and larger core diameter) was utilized in order to improve tool rigidity.

Facet-A was selected based on tool wear evolution data obtained with un-chamfered cutting edge, as well as the concept of geometrical adaptation of cutting tools, [Banciu, 2005, and Fox-Rabinovich and Totten, 2006]. First, the point of transformation from the running-in wear stage to the steady-state wear stage was located at the curve of flank wear progression; refer to Figure (4.1). The transformation point was found to correspond to a flank wear width of about 0.039 mm. Then the shape of the new un-chamfered cutting edge was extracted to correspond to the shape of natural wear at the specified transformation point, as shown in Figure (4.2). Due to the drastic increase in cutting forces as the chamfer angle increases, the applied chamfer negative angle was kept within 15°-18°. This range was recommended by some researchers in the literature to reduce the negative rake angle effect [Ren and Altintas, 2000, Sikdar et al., 1992 and Zhou et al., 2003]. Accordingly, a chamfer width of 0.15 mm was calculated. Facet-B was designed in accordance with Facet-A except for the doubled chamfer width (i.e. 0.3 mm).

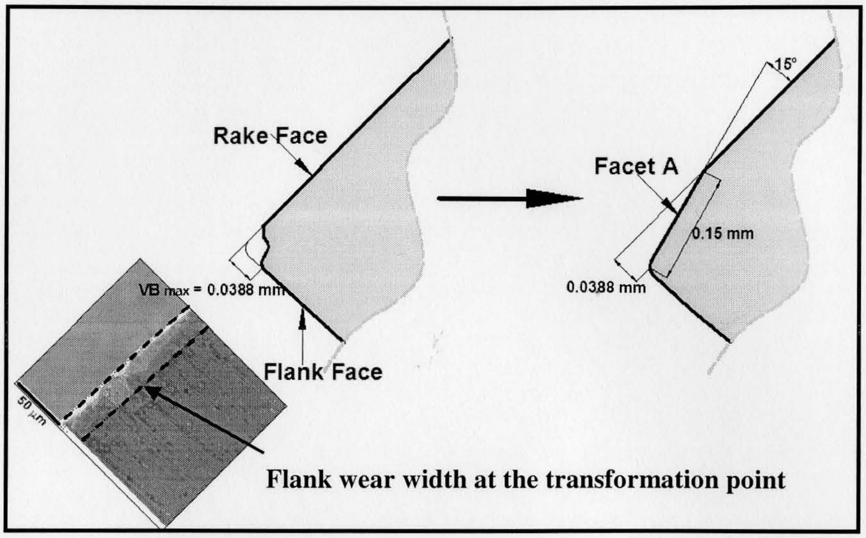

Figure (4.2) Schematic illustration for the extraction of an adaptive cutting edge design

4.1.1 Improved Coating Design

Wear resistance of the nano-straucture multilayered TiAlCrN/NbN tested in this study is influenced by the microstructure of the coating, the deposited metallic-based nitrides and the metallic-based oxide films that are formed. The idea of having about 200 coating layers (≈15 nm each) requires that the grain size be refined down to about 10-12 nm. A fine grain size has a great influence on coating performance. Owing to grain size refinement, more grain boundaries will be involved in the tribo-oxidation process, which results in the formation of more diffusion paths. Consequently, the ability of some coating elements to diffuse to the surface and interact with the oxygen will be enhanced. The formation of metallic-based oxide films which protect and lubricate the tool surface will then be promoted, [Fox-Rabinovich and Totten, 2006].

The multilayered tested TiAlCrN/NbN is based on aluminum-rich TiAlN coatings. Therefore, they exhibit better wear resistance than TiN coatings due to their improved hot hardness, ductility, lubricity and oxidation resistance, which make them ideal for cutting applications, [Fox-Rabinovich and Totten, 2006, Löeffler, 1994, and Stephenson and Agapiou, 1997]. The reason for that is the formation of alumina tribo-films (Al_2O_3-like), on the tool surface, that have better hot hardness, lower coefficient of friction and lower chemical reactivity. Alumina tribo-films also have beneficial heat redistribution at the tool/chip interface due to their lower thermal conductivity (≈ 6.3 W/m-K at 800 °C). Thus, less heat is conducted to the cutting tool surface.

The incorporation of an active element like chromium to the TiAlN-based coating with high aluminum content leads to better cutting tool performance, [Kovalev et al., 2006]. The improved performance of TiAlCrN coatings is attributed to its enhanced oxidation resistance[7]. This class of coatings also has an improved plasticity and lubricity due its lower coefficient of friction up to 1,000 °C, [Fox-Rabinovich et al., 2005, Kovalev et al., 2006 and Ning et al., 2007]. Chromium promotes the beneficial mass transfer and tribo-oxidation during the running-in stage due to its high oxidation diffusivity. Once chromium-oxide is formed on the tool surface, it prevents any further diffusion of oxygen into the underlying material due to its high density (≈ 5220 Kg/m^3). Despite their lower thermodynamic stability when compared to alumina, chromium-oxides have the tendency to dissolve in the alumina films in the later stage of oxidation and to enhance the formation of alumina while suppressing the formation of non-protective titanium-dioxide

[7] TiAlCrN coating exhibited better oxidation resistance up to 1000 °C which is 200 °C higher than that of conventional TiAlN coating, [Yamamoto et al., 2003].

films (i.e. rutile) with lower oxidation resistance, [Fox-Rabinovich and Totten, 2006]. Consequently, $(Al,Cr)_2O_3$ oxide films are formed on the tool surface. These fine-grained complex oxides are thermodynamically stable, which has a beneficial impact on the enhancement of the oxidation resistance of TiAlCrN-based coatings, [Fox-Rabinovich and Totten, 2006].

The incorporation of niobium to nano-structured multilayered (Ti,Al,Cr)N-based coating in the form of transitional metal (Nb)-based nitride[8] resulted in the substantial improvement in cutting performance, as revealed in an earlier study, [Fox-Rabinovich et al., 2008]. Niobium is a heavy element with strong inter-atomic bonds. Thus, higher energy is needed to tribo-diffuse atoms of this element to the outer surface. Consequently, less energy will be left for tool wear progression under severe frictional conditions, [Fox-Rabinovich and Totten, 2006]. Once niobium diffuses to the outer surface, it tends to oxidize in air at approximately 200 °C due to its high affinity with oxygen. Then it acts as a diffusion barrier due to the formation of the very dense niobium-oxide films ($\approx$ 7300 Kg/m^3) on the surface of the tool.

In order to study the influence of the tribological properties of the coating on tool performance, the change in friction coefficient with temperature was monitored. Figure (4.3) shows the variation in coefficient of friction for the TiAlCrN/NbN coating over the tested temperature range. It can be noticed that the lowest range of the coefficients of friction was obtained in the temperature range of 600-1,000 °C. The enhanced friction characteristic of TiAlCrN/NbN was supported by the formation of chemically stable

[8] NbN maintains considerably high hardness at elevated temperature.

crystalline alumina tribo-films with low thermal conductivity on the tool surface. Those films compensate for the thermal and the mechanical loads exerted on the tool during cutting; some of the friction energy will be accumulated and spent in more tribo-oxide generation rather than in wear progression. Thus, more intensive wear due to the adhesion of cutting material to the tool surface can be avoided.

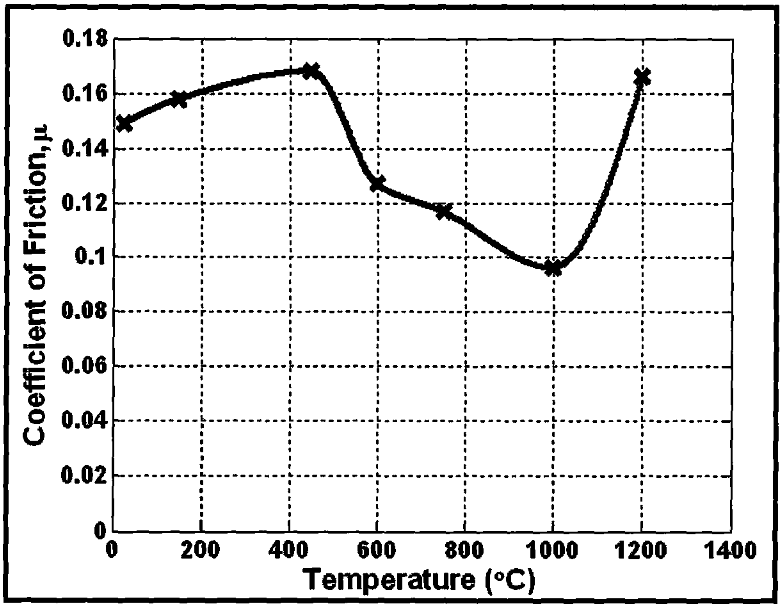

Figure (4.3) Coefficient of friction of TiAlCrN/NbN coating versus temperature

In general, the development of a new coating design like TiAlCrN/NbN coating is an effective way to improve the service life of the coated tools for high speed machining applications of hardened steel due to its improved wear resistance and tribological characteristics. Based on the photoelectron spectra conducted on TiAlCrN/NbN-coated tool surface, all of the coating elements in the metallic-based nitrides were found to be oxidized once the thermal and mechanical loading starts to be exerted on the cutting tool, [Fox-Rabinovich et al., 2008]. The formation of Cr-O-based tribo-films on the tool surface enhances the protective action of the alumina-based films. In addition, the formation of Nb-O-based tribo-films (NbO and Nb_2O_3) on tool surface results in stress relaxation within the friction zone, which in turn leads to less tool surface damage under excessive cutting conditions. The reason for that is the ability of thermally-stable Nb-O-based tribo-films to dissipate energy during friction, [Fox-Rabinovich et al., 2008].

4.1.2 Improved Cutting Edge Geometry

4.1.2.1 Evaluation of Tool Life and Tool Wear Behavior

Flank wear propagation curves for the three cutting tests are shown in Figure (4.4). During the initial wear stage (i.e. the first 3.4 minutes of cutting), the flank wear developed rapidly at the same rate regardless of the cutting edge preparation. During this initial stage, the cutting edge and the coating were almost intact (i.e. unworn surfaces). Therefore, the tools' surfaces experienced very similar diffusion and chemical reactions with the oxygen present in the air.

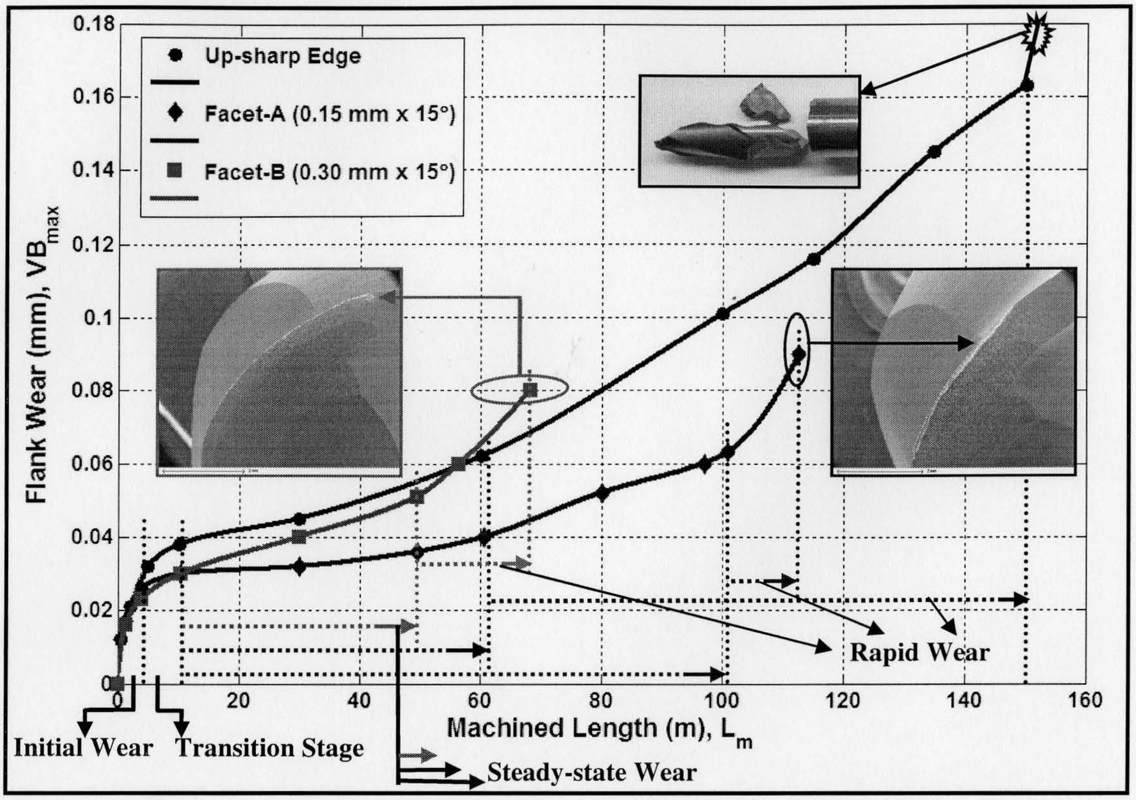

Figure (4.4) Effect of cutting edge geometry on flank wear progression

As a consequence, the adaptive behavior of the coating was triggered, resulting in the formation of similar thin protective layers on the friction surfaces (i.e. tribo-films). However, the stability and strength of these tribo-films varied in accordance to the tribological aspects at the interface between the coated-tool and the workpiece surface. This is attributed to the difference in the chip forming criteria and the cutting temperatures associated with the different cutting edge preparations, as will be discussed shortly. Accordingly, the ability of these tribo-films to regenerate during the transition stage started to deviate, resulting in different coating performances.

During the post-running in stage (i.e. steady-state wear), the performance of the surface layers is mostly affected by the thin films formed on the surface during the running-in stage (i.e. initial wear). In addition, the degree of surface damage at the nano/micro-level during the transition stage was found to have tremendous influence on the overall trend of flank wear progression. It can be noticed in Figure (4.4) that the flank wear rate for the case of Facet-A tends to form the most clearly-defined steady-state wear with the most stable wear rate and consequently the least flank wear intensity, while Facet-B experienced the most rapid flank wear progression.

The improved stabilization in the flank wear propagation is generally attributed to the improved coating adaptability due to the applied adaptive geometry. Accordingly, the appearance of the very early edge chipping was diminished for the case with the chamfered cutting edges. By avoiding very early edge chipping, the formation of stable oxides on tool surfaces will not be interrupted due to the fact that less substrate material was exposed. As a consequence, the tendency of the tool surface to form weak oxides such as cobalt-oxide will be diminished during the very early stage of tool wear.

The detrimental effect of cobalt-oxide on the tool surface is attributed to the tendency of this oxide to flake off very quickly by rubbing, which has a negative effect on the tool binder (i.e. exposes the base metal and weakens the tool matrix). In [Fox-Rabinovich and Totten, 2006], the limiting energy accumulation capacities[9] for some refractory compounds were listed. The cobalt-oxide (CoO) showed the least value of the

[9] Higher value of limiting energy accumulation capacity results in an improved ability of the formed oxygen-containing tribo-films to effectively absorb and dissipate energy during the tool/workpiece interaction. Therefore, the friction energy will be accumulated and spent on tribo-oxide generation rather than in wear progression, [Fox-Rabinovich and Totten, 2006].

limiting energy accumulation capacity among the listed refractory compounds (≈ 79 KJ/mol at 773 °K and 51 KJ/mol at 1273 °K). While, a compound like titanium-oxide (Ti_2O_3) with high oxygen content has higher limiting energy accumulation capacity of (247 KJ/mol at 773 °K and 173 KJ/mol at 1,273 °K). Therefore, the improved energy accumulation and dissipation of any metallic-based oxide, formed on coated tool surfaces, has a beneficial impact on the oxide protective action under the aggressive cutting conditions tested.

Figures (4.5 to 4.8) show the SEM and EDS analyses conducted on the rake and flank faces of the two tools tested. No analysis was performed on the un-chamfered cutting edge due to the catastrophic failure of the cutting part of the tool. It can be noticed in Figures (4.5 and 4.7) that unworn Facet-A experienced more edge line irregularities when compared to those of unworn Facet-B. This is also supported by the scarcity of elements like tungsten (W) along the coated cutting edge line of Facet-B; refer to the EDS analyses in Figures (4.5 to 4.8). These irregularities act as tool surface defects and negatively affect the adherence and concentration of coating within the defected zone of the tool surface. As a consequence, Facet-B exhibited better resistance against chipping (regardless of the difference in cutting lengths and its accelerated flank wear rate) when compared to Facet-A; refer to the worn rake faces in Figure (4.5 and 4.7).

Despite the diversity in the severity of tool surface damage along the three cutting-edge micro geometries, the activated wear mechanisms were the same. First, an abrasion wear mechanism was initiated due to the interaction between abrasive hard grains or inclusions, such as carbide inclusion in steel and the coated tool surface. This interaction resulted in abrasive rubbing between the coating layer and the work-material during the chip forming process and after. Then the cutting mechanical and thermal loads started to increase due to the existence of friction and rubbing zones. The heat generated within this thermally active cutting environment enhanced the diffusivity of all the coating and work-material elements. Consequently, the protective action of the self-adaptive coating was initiated by the generation of protective oxide films (e.g. Al-O-based films) along the interface. These tribo-films act as barriers against the loads exerted on the surface during oxidation; refer to the EDS analyses in (4.5 to 4.8).

Meanwhile, the thermal loads generated at the tool-work interface enhanced the adhesion wear mechanism. The frictional surface layers then started to undergo severe plastic deformation (i.e. island-like seizure formation); refer to the worn flank and rake faces in Figures (4.7 and 4.8). The seizure formation refers to the intensive seizure of the workpiece material that forms on the tool surface and results in unfavorable frictional conditions. These conditions can be controlled by the improved coating characteristics (e.g. lubricity, plasticity and heat accumulation or dissipation). Once deeper damage of the surface layers of the coating occurs, an exposure of tool surface will result. This exposure is usually in the form of separate areas of micro-delamination within the coating layer; refer to the worn flank and rake faces in Figure (4.6 and 4.7).

Owing to the increased thermal and mechanical loads, these types of localized areas started to merge into a continuous band of exposed substrate by completely peeling off the coating. Similar observations on micro-delamination areas were revealed in the study conducted using coated carbide tools in dry turning of AISI 1045 steel, [Lim et al., 1999]. Then the exposed carbide substrate started to undergo thermal cyclic loading only (i.e. without the improved fatigue resistance of multi-layered coating). As a result, thermal fatigue micro-cracks started to initiate and propagate perpendicularly to the cutting edge, as shown in Figure (4.5). Once the size of these cracks reached a certain limit, excessive edge chipping continued to dominate along the cutting edge.

Finally, deeper surface damage started to appear on the tool surfaces especially due to severe damage of the surface layers. The severe damage involved the following mechanisms: deterioration of stable oxide-films, severe coating delamination and extensive exposure of substrate material. The severe damage resulted in unstable wear modes and eventually in accelerated flank wear progression. This was the case with Facet-B with a 0.3 mm chamfered cutting edge. The increase in the chamfer width resulted in larger radial cutting forces and excessive heat generation within the cutting zone. Consequently, the surface-adaptation of the coatings was restrained (despite less chipping being developed along the cutting edge). Therefore, this cutting test was stopped prematurely in order to avoid any unexpected catastrophic damage to the cutting tool or the workpiece.

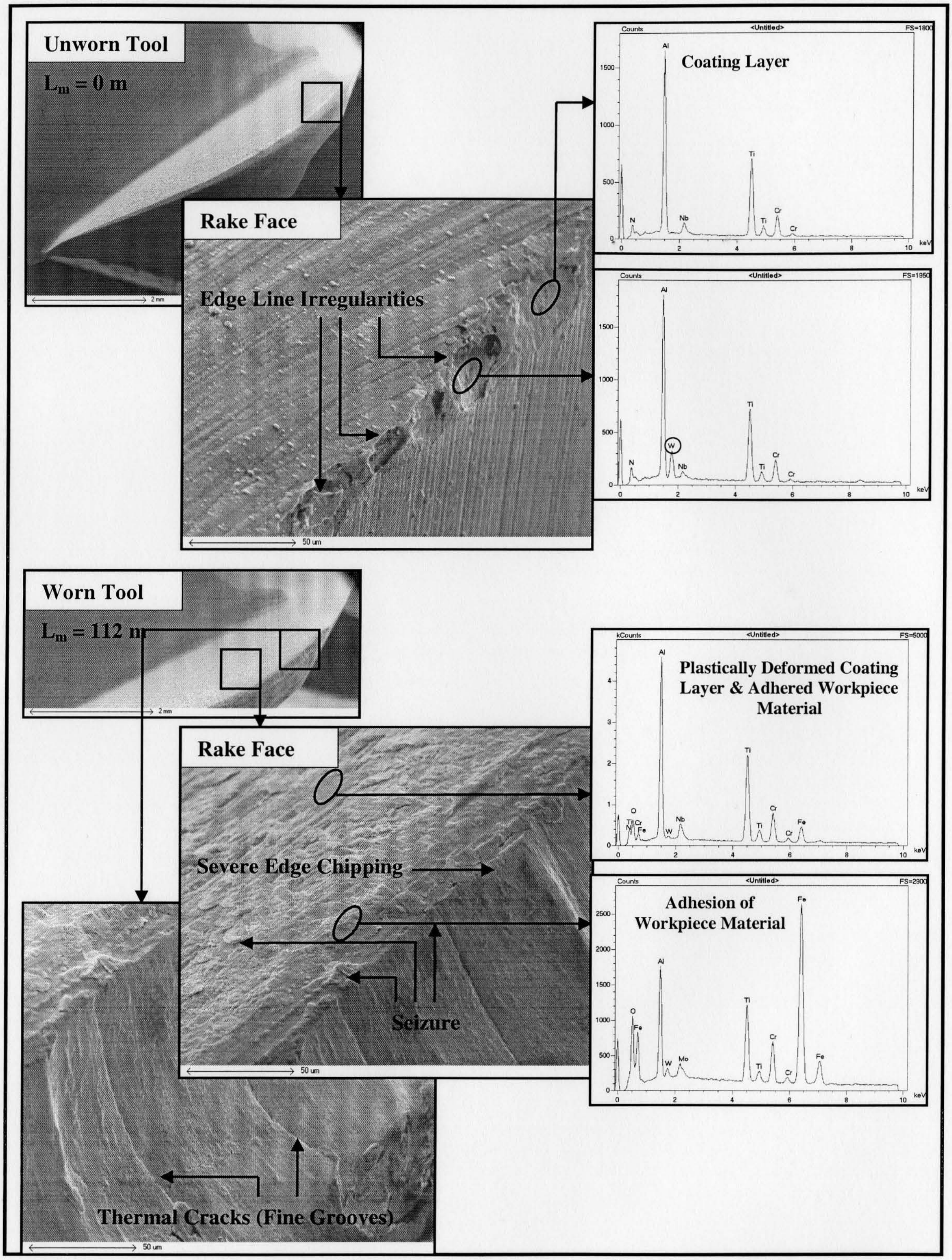

Figure (4.5) SEM images with EDS spectra showing unworn and worn rake sides of a TiAlCrN/NbN coated ball nose end-mill with (0.15 mm x15°) chamfered cutting edge

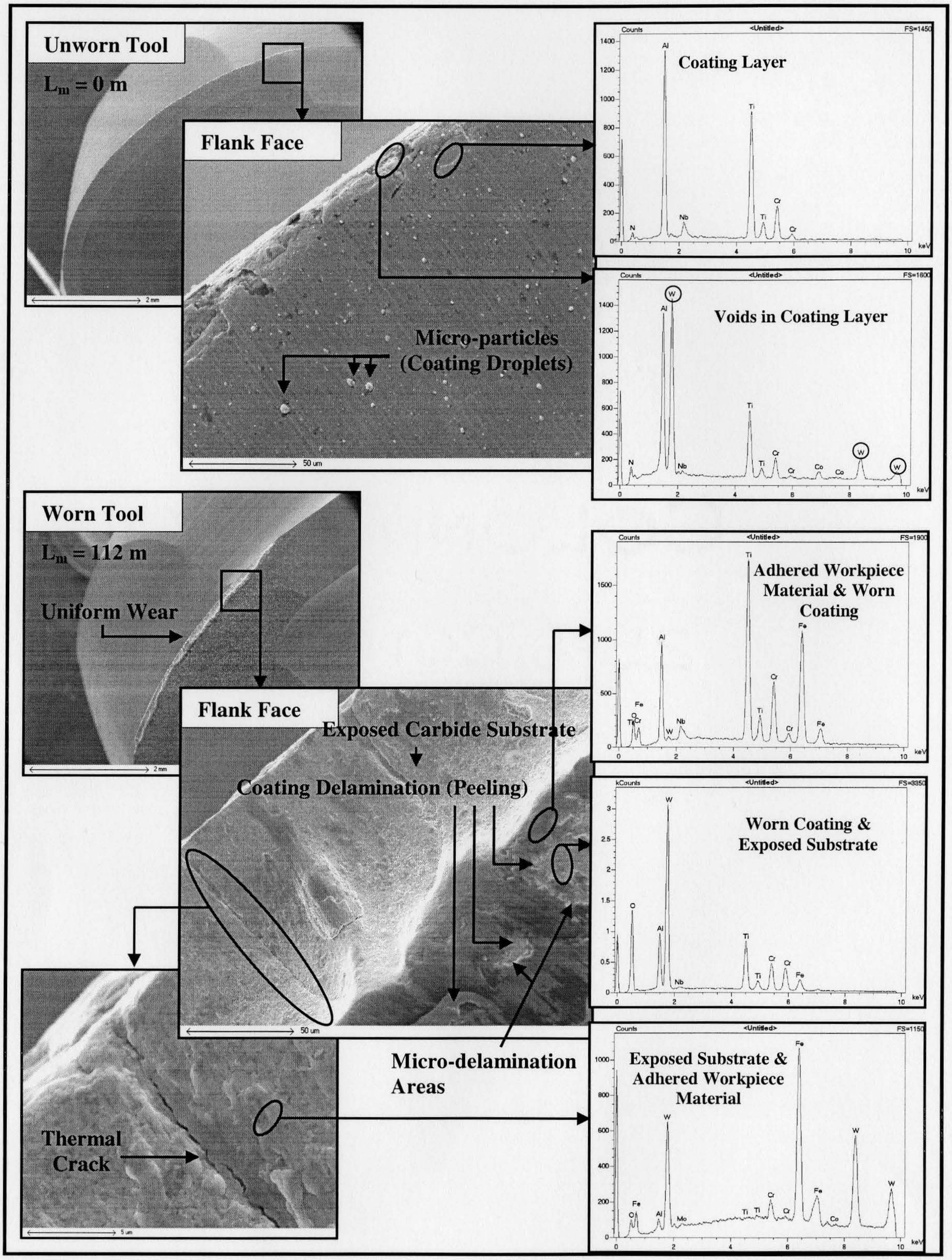

Figure (4.6) SEM images with EDS spectra showing unworn and worn flank sides of a TiAlCrN/NbN ball nose end-mill with (0.15 mm x15°) chamfered cutting edge

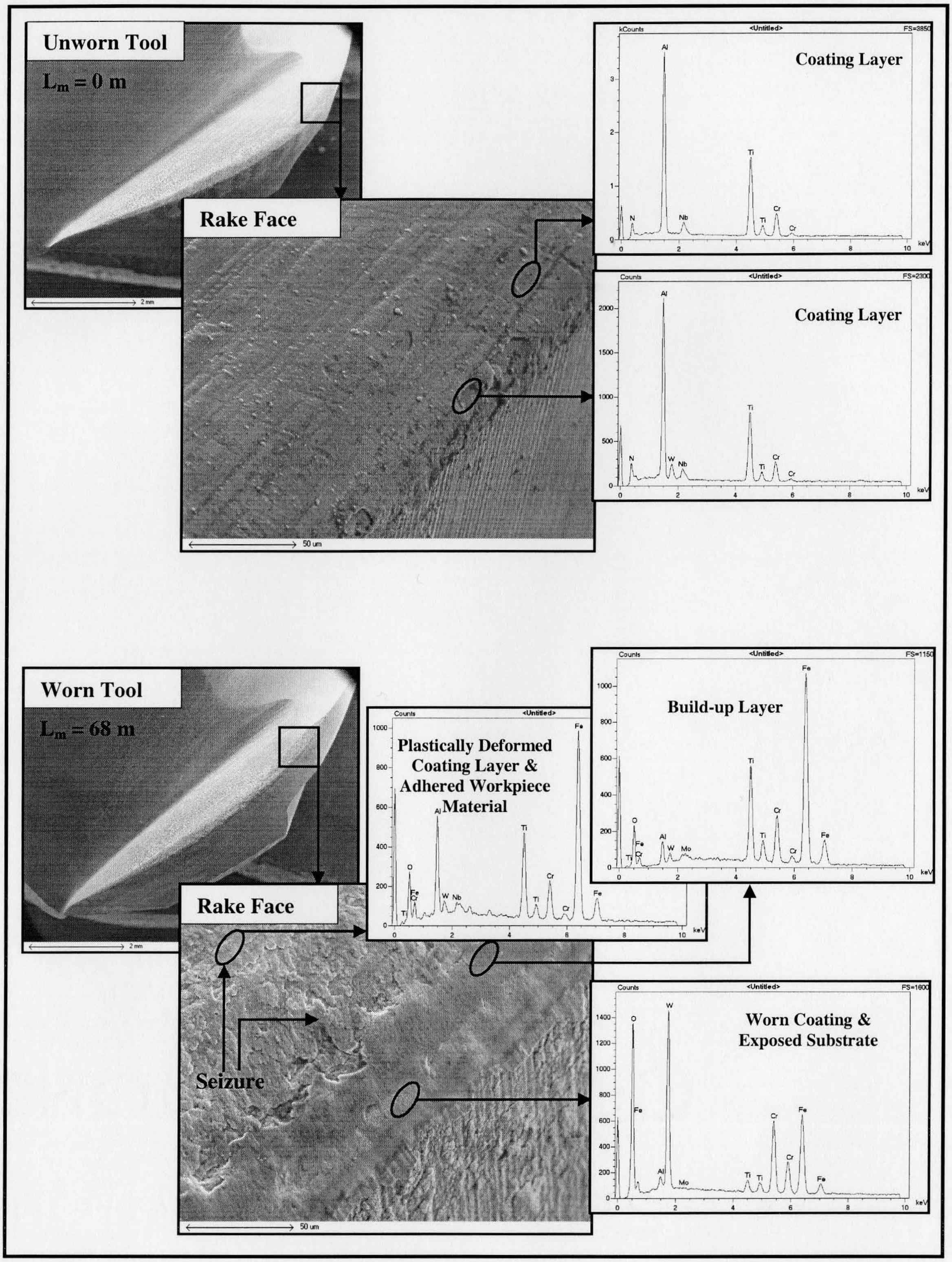

Figure (4.7) SEM images with EDS spectra showing unworn and worn rake sides of a TiAlCrN/NbN coated ball nose end-mill with (0.3 mm x15°) chamfered cutting edge

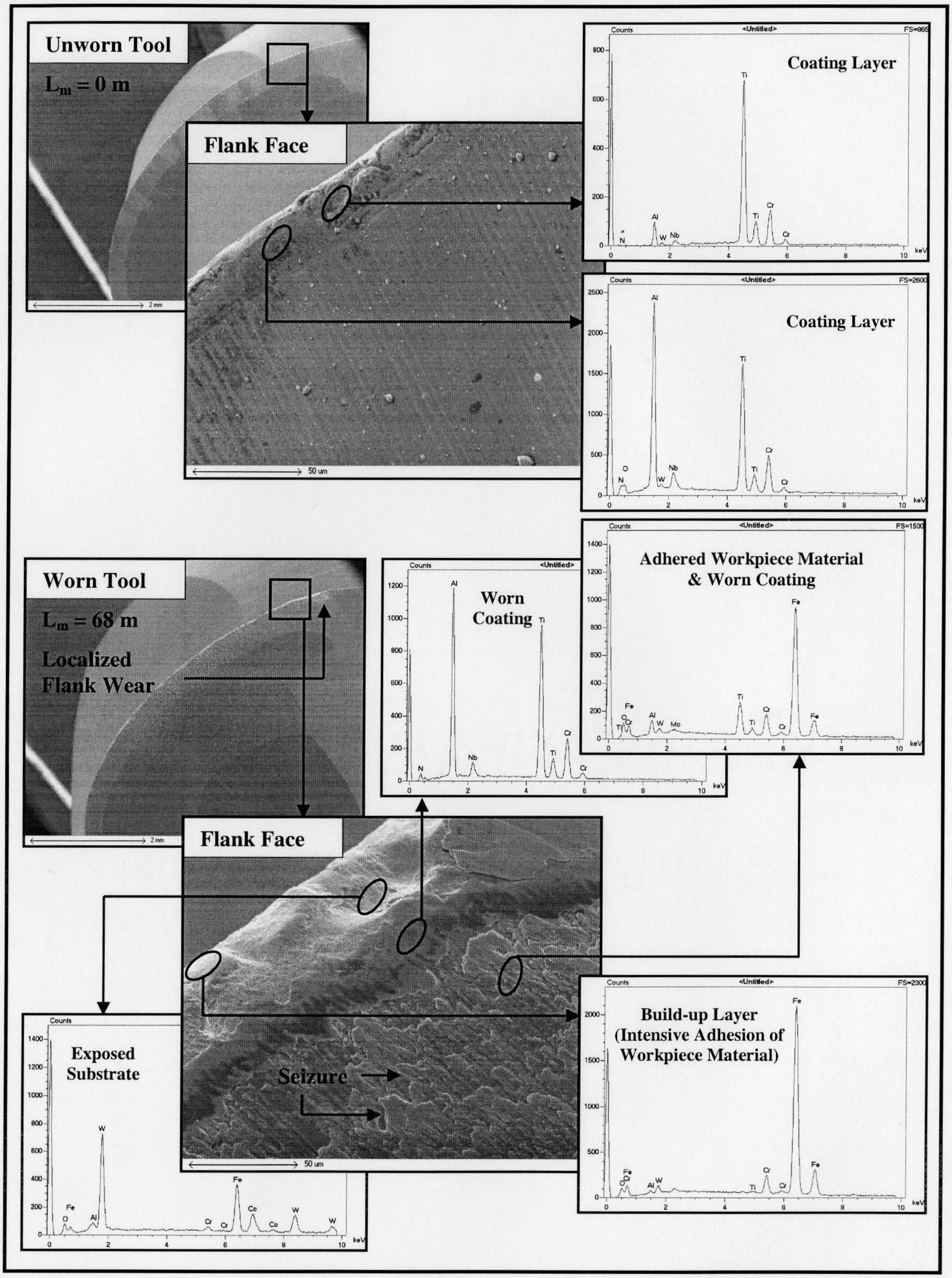

Figure (4.8) SEM images with EDS spectra showing unworn and worn flank sides of a TiAlCrN/NbN coated ball nose end-mill with (0.3 mm x15°) chamfered cutting edge

The excessive mechanical loading also resulted in the breakage of the tool shank in the case of Facet-A. Despite its minimal flank wear rate, the negative-rake angle effect resulted in an excessive increase in the cutting force components to the level which caused the end-mill shank to shear-off without affecting the cutting edge line. The strength of the applied adaptive geometry seemed to prevent the catastrophic brittle-fracture of the cutting edge. The brittle-fracture can be an entry or exit failure. This was not the case with un-chamfered cutting edge (i.e. zero rake angle), where the tool failed catastrophically by massive breakage of the cutting edge due to the excessive tensile loading exerting across the carbide grains. Since the milling strategy utilized is down milling (i.e. zero-chip thickness at the exit and zero-exit angle), it is more likely that the tool failure is of an entry failure[10]. Therefore, further numerical studies are still needed to reveal the root cause of the cutting tool failure during high speed machining of hardened materials.

As shown, for applications of milling hardened steels at high cutting speeds, the improved coating design and the adaptive edge micro-geometry have to be coupled with a tougher carbide grade with an ultra-fine grain size to enhance the performance of the cutting tool against brittle fracture.

[10] Entry failure occurs when the initial contact between the tool and the workpiece occurs very close to the cutting edge line. The entry failure causes catastrophic failure of the edge line. This happens when the maximum tensile stress that the tool can withstand is exceeded. The negative rake angle causes the initial contact to move to a certain point on the rake face away from the cutting edge line.

4.1.2.2 Cutting Forces and FFT Analysis

The three measured components of cutting forces (F_x, F_y and F_z) are plotted versus the machined length in Figure (4.9). Refer to Figure (2.6) for the force directions and the dynamometer coordinate system. It can be observed that the large axial depth of cut and the increased hardness of workpiece material (HRC 54-55) resulted in relatively higher magnitudes of cutting forces than those usually obtained during high speed machining of hardened steels. Similar observation was also obtained in [Urbanski et al., 2000].

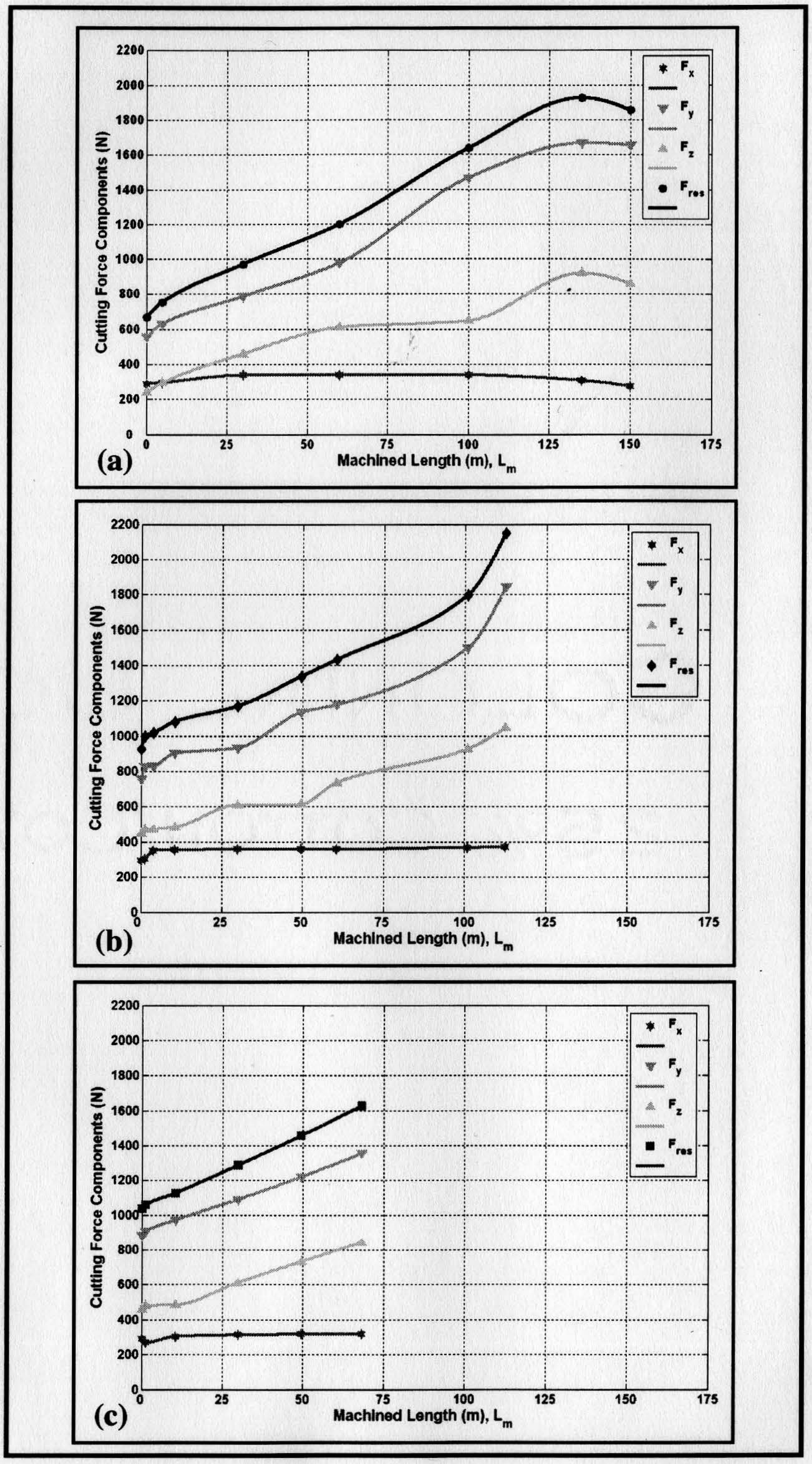

Figure (4.9) The Variation of cutting force components: (a) unchamfered edge; (b) Facet-A (0.15 mm x 15°C) and (c) Facet-B (0.3 mm x 15°C)

Excessive variation of cutting forces in (Y and Z) directions was dominant throughout the cutting time regardless of the cutting edge micro-geometry. A correlation can be observed between the trend of each cutting force component and the trend of flank wear evolution for the three tested edge geometries; refer to Table (4.1). The F_y component was the most dominant and the most correlated to flank wear among the three force components. The excessive variation of cutting forces is mainly attributed to the flank wear progression and the contribution of the ploughing force component. This is due to the fact that cutting with a blunter edge imposes more pressure and more friction on the interface between the flank land and the work-material. The sensitivity of those particular force components to the flank wear progression is related to the geometry of the ball nose end mill that results in larger split components of radial and axial forces[11] in both the Y and Z directions.

Edge Micro-geometry / Force Component	Un-chamfered Edge	Facet-A	Facet-B
F_x	-0.150	0.975	0.964
F_y	0.767	0.968	0.946
F_z	0.760	0.971	0.946

Table (4.1) Correlation coefficients of flank wear and cutting force components

[11] The Axial force is usually more sensitive to the nose ploughing and the cutting edge flank friction, [Fontaine et al., 2006, and Wang, and Zheng, 2003]

Figure (4.10) shows the effect of cutting edge micro-geometry on the resultant force component. It is obvious that providing the cutting edge with chamfered facets resulted in a slight increase in the magnitude of the cutting forces. This increase was related to the negative rake angle effect and eventually resulted in more friction within the secondary deformation zone. Therefore, the cutting action in this case featured the mechanism described in [El-Wardany et al., 1996] as "shearing and pushing off the metal by the tool". A reduction in the cutting force was observed prior to the end of tool life in the case of the un-chamfered cutting edge. The unexpected reduction in the measured cutting force as the tool wear deteriorated can be attributed to the loss of contact between the tool and the workpiece at some cutting points along the cutting edge line. This is usually due to severe cutting edge fragmentation. Similar observations were reported in [Almeida et al., 2005, Dumitrescu, 1998 and El-Wardany et al., 1996].

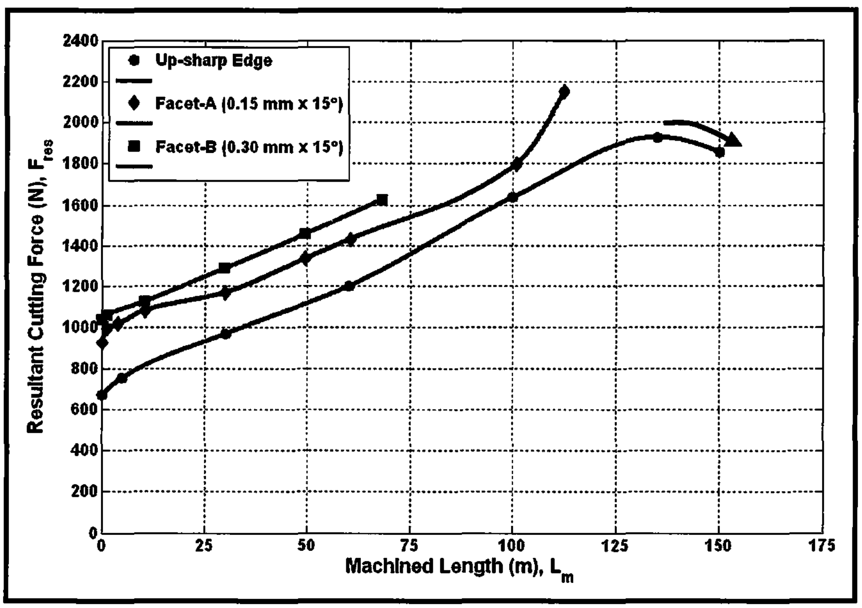

Figure (4.10) Effect of cutting edge geometry on the resultant cutting force

Since the force in the Y-direction was the most sensitive component to flank wear evolution, the experimental frequency responses of F_y were investigated to identify the nature of the vibrations induced during cutting. The experimental Fast-Fourier-Transforms (FFT) are shown in Figure (4.11). These force spectra indicate that all the cutting tools had significant peaks at the fundamental cutting frequency and at the subsequent harmonic frequencies. There are five main peaks spaced apart by a period equivalent to the tooth passing frequency of approximately 318 Hz. Figure (4.11) presents also the influence of flank wear on the cutting harmonics. An increase in the amplitudes of the DC component of the cutting force and the main peaks due to flank wear progression can be observed regardless of the cutting edge micro-geometry. This is mainly attributed to the additional frictional energy that was dissipated due to flank wear evolution, [Toh, 2004].

In addition, several side peaks with lower magnitudes and higher-frequency components (higher than the dynamometer natural frequency response) were detected at larger flank widths; refer to Figures (4.11.a and 4.11.b). Since these side peaks are used for the purpose of comparative monitoring, the influence of the dynamometers natural frequency response can be neglected due to the fact that this effect will be almost constant during the machining as long as the cutting conditions are unchanged, [Lee et al., 1989]. These peaks are more likely to be "hints of chatter frequency" developed while the system was in transition stability, [Suh et al., 2002]. An evidence of these higher-frequency modes can be observed in the case of Facet-A; refer to the FFT spectrum for F_z in Figure (4.11.b). It is obvious that the substantial increase in the cutting force prior to the machined length of 112 m (i.e. prior to the shank fracture) was accompanied by some excited vibrations. These vibrations can be used to interpret the premature tool-failure.

In order to calculate the frequencies associated with the oscillations arising from the tool-clamping system, the tool holding system was approximated as a clamped-free beam and a longitudinal rod; refer to Appendix A for frequency modes. The calculations returned a beam natural frequency of about 4,410 Hz and a longitudinal rod natural frequency of 86 KHz. Owing to the limitations on the data acquisition system and on the dynamometer natural frequency response, it was difficult to decide precisely whether those higher modes of vibrations were being excited or not during cutting. Similarly, the frequencies associated with the chip segmentation could not be recorded using the available data acquisition system due to the increased chip velocities attained under the applied cutting conditions. Therefore, other techniques such as acoustic/noise emission should be considered in the future for better detection of any vibrations that might be induced during cutting due to chip segmentation, chatter or severe tool wear (i.e. severe edge chipping or tool fracture).

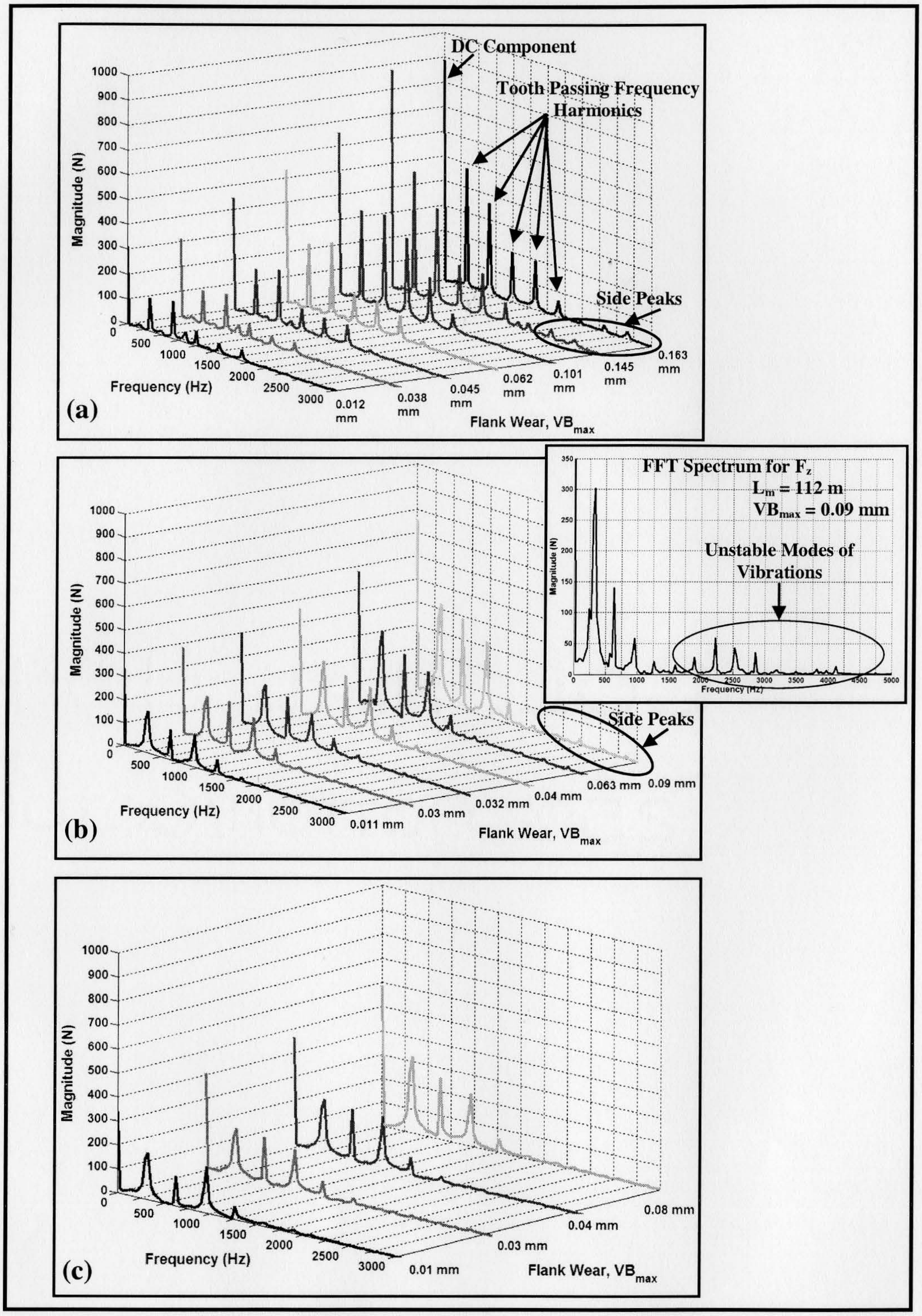

Figure (4.11) Frequency spectrum for the measured forces: (a) F_y, un-chamfered edge; (b) F_y and F_z, Facet-A (0.15 mm x 15°C) and (c) $F_{y,}$ Facet-B (0.3 mm x 15°C1)

4.1.2.3 Evaluation of Surface Roughness

Figure (4.12) shows the variation in the average surface roughness over the machined length along the pick-direction. It can be observed that irrespective of the edge geometry, the obtained surface finish was generally influenced by flank wear progression. An increased surface roughness was obtained as the tool wear started to develop on the flank face due to the rubbing induced during the formation of pick-interval scallops. The induced vibration effects also seemed to have an influence on the obtained surface roughness. The force acting in the axial direction (F_z) was the most correlated to the surface roughness among the three force components. Similar observation was reported in [Mativenga et al., 2003]. The increase in the chamfer width resulted in slightly higher surface roughness due to the corresponding increase in the cutting forces. The sculptured surface finish for these two cutting tests was comparable and within the range of ($R_a \approx 0.5$- 2.3 μm) as tool wear deteriorated (the variation is not shown). This range is within the range usually required for the die and mould industry, [Axinte and Dewes, 2002 and Elbestawi et al., 1997].

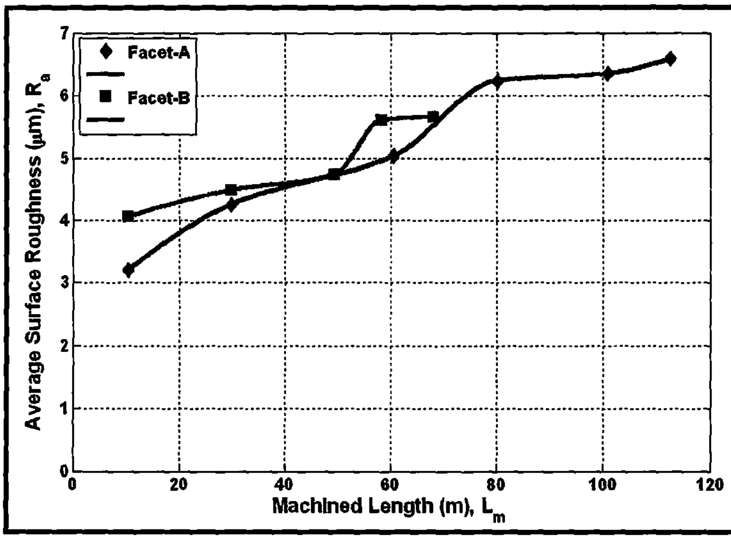

Figure (4.12) Effect of cutting edge geometry on machined surface roughness

4.1.2.4 Chip Configurations

<u>Chip Color</u>

The chip analyses proposed in [Fox-Rabinovich et al, 2006, Ning et al., 2001, Ning et al., 2007, Toh, 2005, Venkatesh et al., 1993, and Yeo and Ong, 2000] were adopted in order to estimate the chip surface temperature based on the chip color. The estimated chip-surface temperatures with the corresponding cutting edge preparation and machined length are listed in Table (4.2). It can be noticed that the chip colors are mostly ranging from dark brown with medium violet red to dark blue as tool wear develops.

Chip characteristics / Edge prep. and Machined length (*m*)		Chip color	Estimated chip-surface temperature (°C)
Un-chamfered	0.26	Dark golden brown and medium violet red	860-920
	30	Violet red, dark blue and dark golden brown	900-920
	60	Blue and medium violet red	920-960
	100	Dark blue and medium violet red	960-1,000
Facet-A	0.26	Dark golden brown and dark blue	860-920
	30	Dark blue and medium violet red	920-960
	60	Dark blue and medium violet red	960-1,000
	100	Blue-green, light grey (*silver*) and dark blue	1,100-1,200
Facet-B	0.26	Medium violet red and dark blue	920-960
	30	Dark blue and medium violet red	960-1,000
	60	Dark blue and trace of medium violet red	1,000-1,100

Table (4.2) Estimated chip-surface temperature as a function of cutting edge geometry

Chip Shape and Morphology

Figure (4.13) presents SEM images taken for the inside and backside surfaces of the chips. These chips were collected during the first few minutes of the cutting tests to ensure that the cutting edge is almost intact. It is obvious that the chips obtained using different cutting edge preparations experienced different curling intensity. This is attributed to the different temperatures and frictional conditions associated with the different edge geometries. The heat generated during the cutting resulted in a temperature gradient within the chip thickness due to the difference between the inside and the backside surface temperatures. Hence, the chips tend to have different curling intensity with different contact lengths between the chip and the tool. The contribution of friction to the chip flow criterion is also important.

At the early stage of cutting, the cutting edge is still intact. Consequently, the temperature becomes the dominant factor affecting the flow stress within the chip surface layer which is in contact with the tool rake surface. The higher the temperature, the lower the flow stress (i.e. less resistance to plastic deformation in the secondary deformation zone), which in turn enhanced the frictional conditions by causing intensive chip curling with less contact length; refer to Figure (4.13.a).

Providing the cutting edge with a very large chamfered facet resulted in more cutting pressure due to the negative rake angle effect. Consequently, higher mechanical loadings were generated within the cutting zone. More intense sticking and negative frictional conditions were then activated. Accordingly, the friction force component started to significantly increase. This caused more resistance against the plastic deformation in the secondary deformation zone. Hence, the friction factor started to dominate and resulted in wider chips with less curling and an increased tool-chip contact length; refer to Figure (4.13.c).

Chip edge serrations or chip breaks were also more dominant with chamfered cutting edges due to the more intensive stresses applied on the working material during cutting; refer to Figure (4.13.b and 4.13.c). These edge serrations are more likely to form on the trailing side of the chips. The trailing side corresponds to the zero uncut-chip thickness in down milling. The stress concentration that developed around this zone of zero-chip thickness resulted in inhomogeneous strain and inhomogeneous loading distributions along the chip width, [Kishawy, 1998]. Unlike in turning, these chip edge serrations do not yield any tool wear in milling due to the nature of the cutting action that relatively eases chip control.

Moreover, the surface morphology of the backside of the chips showed dependency on the frictional conditions for the three tested cutting edge geometries. The chips produced by Facet-B exhibited rough surface texture with compression marks; refer to Figure (4.13.c). The compression marks were caused by the intensive pressure applied on the workpiece material during the deformation. The chips produced by Facet-A exhibited a relatively smoother surface texture; refer to Figure (4.13.b). The smoother surface texture is an indication of the improved surface adaptability[12] and heat redistribution along the tool-work interface. This surface adaptability was previously reflected on the improved flank wear behavior of this adaptive cutting edge geometry. Similar results were also reported in [Fox-Rabinovich and Totten, 2006].

[12] The improved surface adaptability is supported by the reduction in the coating coefficient of friction between 600-1,000 °C; refer to Figure (4.3).

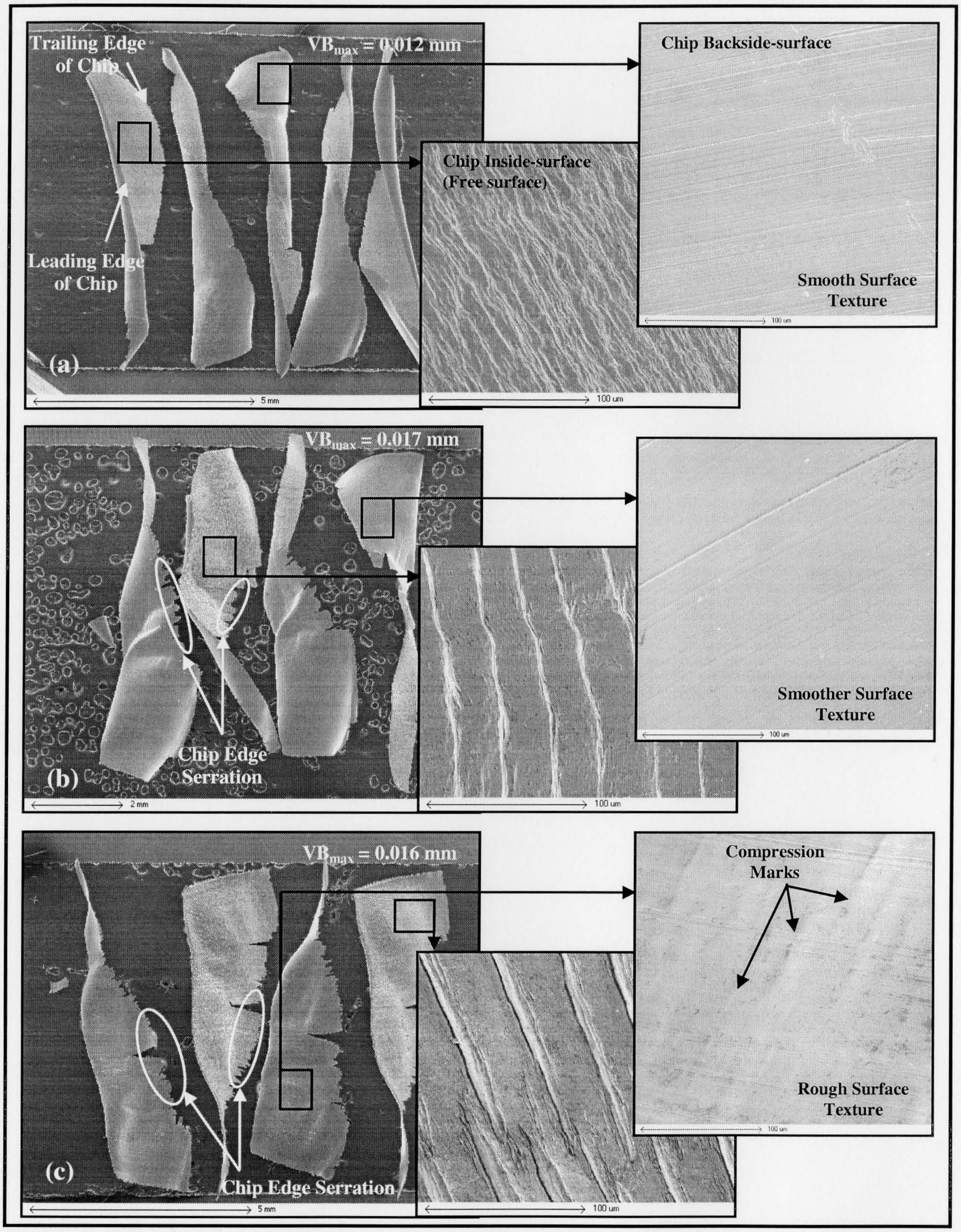

Figure (4.13) SEM images showing bright and dull surfaces of the chips collected at a machined length of 0.26 m: (a) un-chamfered edge; (b) Facet-A (0.15 mm x 15°C) and (c) Facet-B (0.3 mm x 15°C)

The chips produced by worn tools showed similar dependency on thermal and frictional conditions; refer to Figure (4.14). The chips exhibited more brittleness as tool wear deteriorated due to the effect of thermal shocks. The thermal shocks were activated as cutting temperature increased and thus more heat was transferred into the chips.

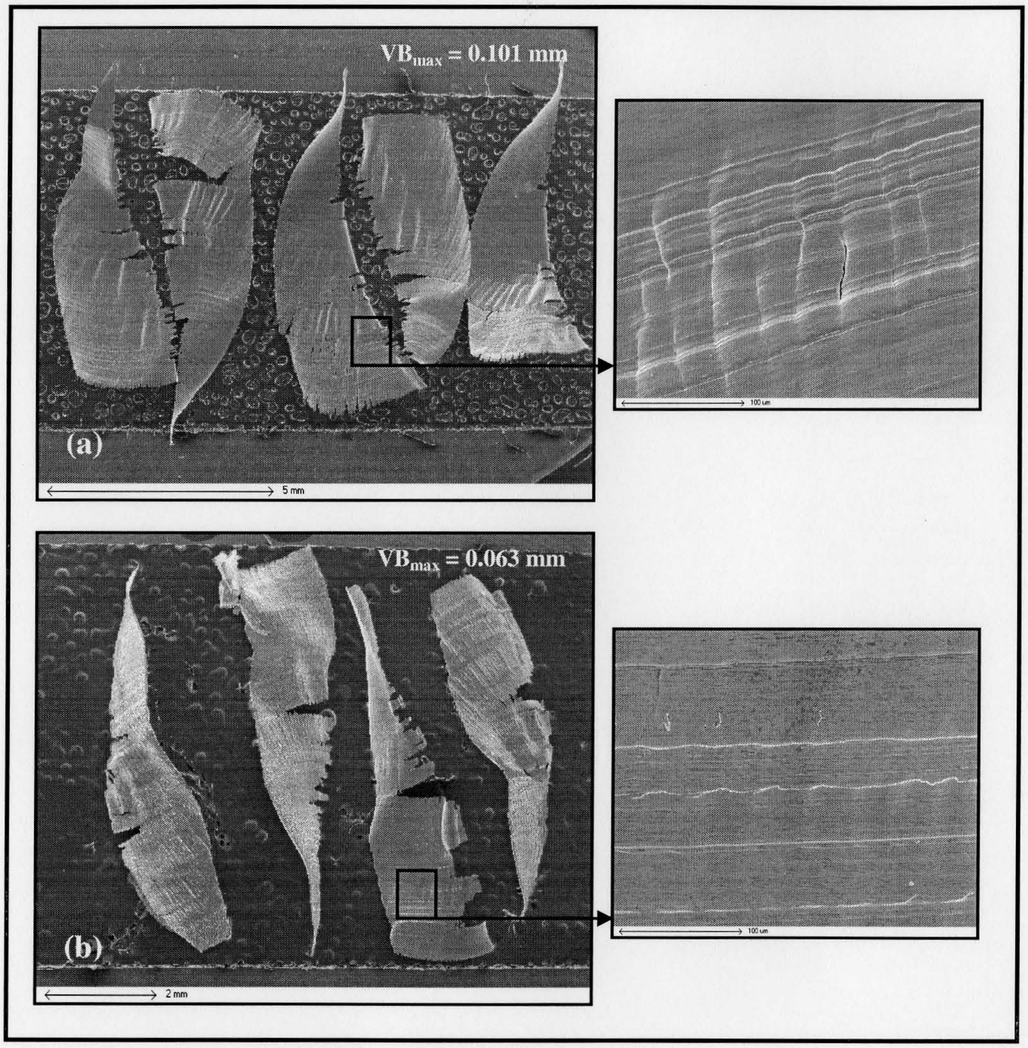

Figure (4.14) SEM images showing bright and dull surfaces of the chips collected at a machined length of 100 m: (a) un-chamfered edge and (b) Facet-A (0.15 mm x 15°C)

More investigations were conducted in order to study the chip morphology by examining the cross sections of the chips. During the very early stage of tool wear, it has been observed that continuous chips with an average thickness of about 20 μm were produced using the un-chamfered cutting edge while chamfered cutting edges resulted in the formation of segmental chips; refer to Figure (4.15). It is of interest to mention that the 20 μm chip thickness was considered a transitional chip thickness between continuous chips and segmental chips when cutting hardened steel, [Toenshoff et al., 2000]. The material plastic flow was also evident in almost all the cross sections of the chips. All the chips experienced large cutting ratios (i.e. larger than one). This was also supported by the studies presented in [Nakayama el al., 1988, Shaw, 2005, and Shaw and Vyas, 1998] in which the cutting ratio exceeded one, when cutting hardened steel using tools with zero or negative rake angles. At the early stage of cutting, increasing the chamfer width did not have any significant influence on the mechanism of chip segmentation.

According to the study conducted in [Ng and Aspinwall, 2002], the morphology of the segmental chips obtained in this investigation can be classified into two different types: "inhomogeneous deformed segmental chips" and "shear localized chips". For the former, the inhomogeneous deformation within the entire chip, exhibits highly deformed zones between the segments and along the chip/tool contact surface, while the core of the segment is barely deformed; refer to Figures (4.15.b and 4.15.c).

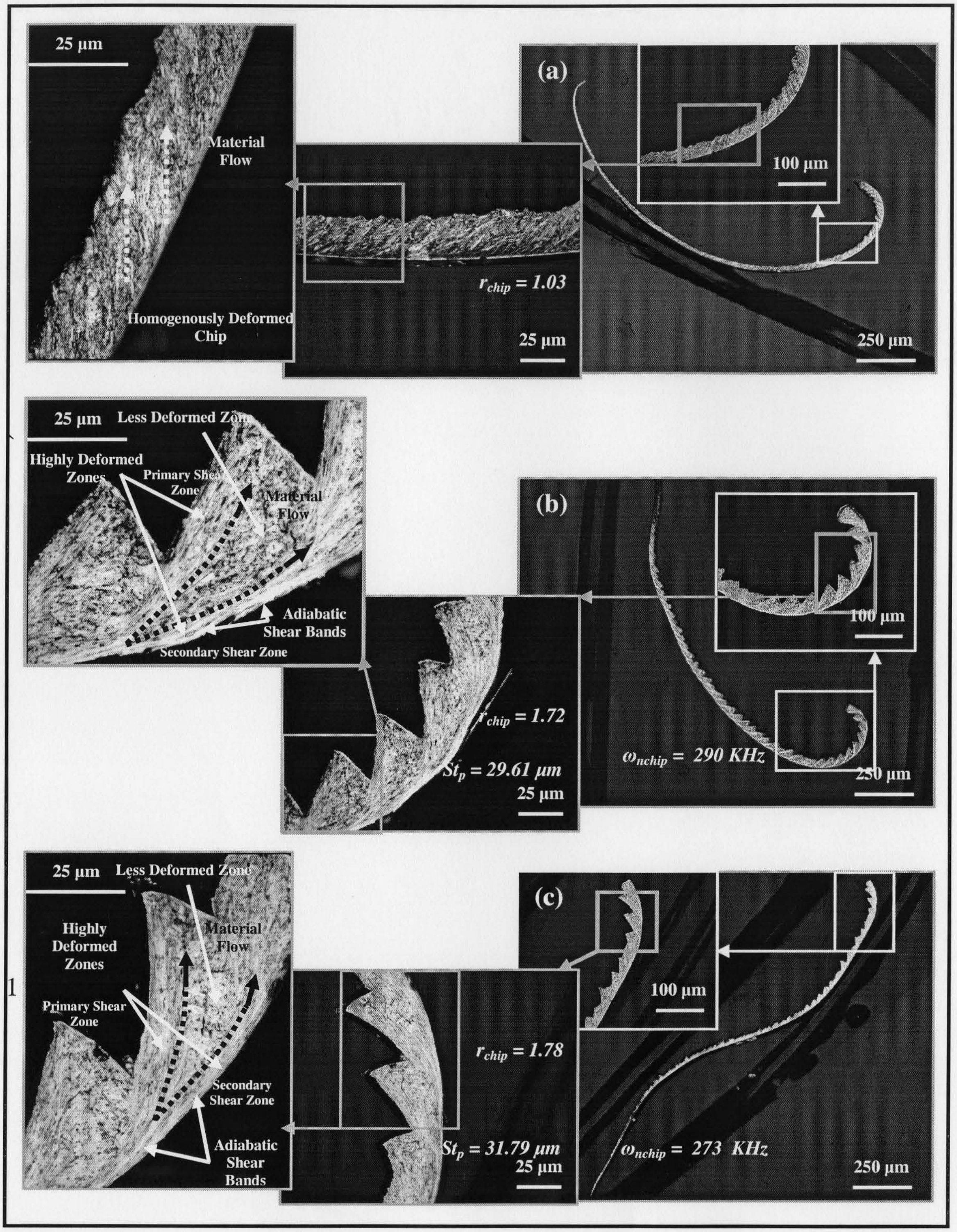

Figure (4.15) Optical microscopic images showing the effect of edge geometry on chip morphology at 0.26 m machined length: (a) un-chamfered edge; (b) Facet-A and (c) Facet-B

As shown in Figure (4.16), the most clearly defined shear localized chips were produced by the un-chamfered cutting edge. The two chamfered edges resulted in the formation of inhomogeneous deformed segmental chips with larger localized plastic deformation zones. This is attributed to the increase in the mechanical and thermal loadings due to the negative rake angle effect. As a consequence, a larger volume of the material underwent severe plastic deformation, which imposed more resistance against any further propagation of the micro-cracks within the chip thickness. Therefore, the effective rake angle of the tool seems to have an influence on the morphology of the chip segmentation. In addition, increasing the chamfer width yielded chips with uneven segmentation due to the higher strain and pressure imposed on the work-material (particularly with a worn tool). This behavior is similar to that which is caused by a cutting edge with an excessive level of bluntness.

It is evident that the adiabatic shear bands which initiated within the primary shear zone and extended to the free surface were not dominant in all the segmented chips produced during this set of experimental tests; refer to the cross sections of the chips in Figure (4.16). It was observed that some shear bands were initiated at the tool tip but they did not propagate sufficiently to the free surface so as to cause catastrophic thermoplastic instability. The formation of these bands casts doubt on the adiabatic shear theory as the only theory that accounts for the formation of segmented chips; refer to the magnified image in Figure (4.16). The thermal-based analysis seems to account for the initiation of adiabatic shear bands within the lower region of the primary shear zone, while the failure within the upper region of the primary shear zone occurred in accordance to the cyclic crack propagation theory. Similar observations were revealed by other researchers in the literature [Barry and Byrne, 2002, Ning et al., 2007, Shaw, 2005, and Shaw and Vyas, 1993].

The effect of tool wear on the chip morphology was also investigated. Figure (4.16) shows the variation in chip morphology for the three tested geometries over the obtained cutting length. As the tool wear deteriorated, more mechanical loads were imposed within the chip thickness which increased the compressive stresses acting on the shear plane and hence increased resistance against crack propagation at the chip free surface. Therefore, the worn tools yielded segmented chips with a lower frequency of segmentation. Any variation in the segmentation pattern within the entire chip can be attributed to the in-homogeneity within the work-material that leads to different cracking patterns, [Shaw, 2005]. It was also observed that the adaptive geometry (i.e. Facet-A) resulted in the least segmentation frequency. By decreasing the tendency of the chip to segment, the fatigue loading exerted on the cutting edge, due to the stress fluctuation, will also be decreased once this type of chip starts to form.

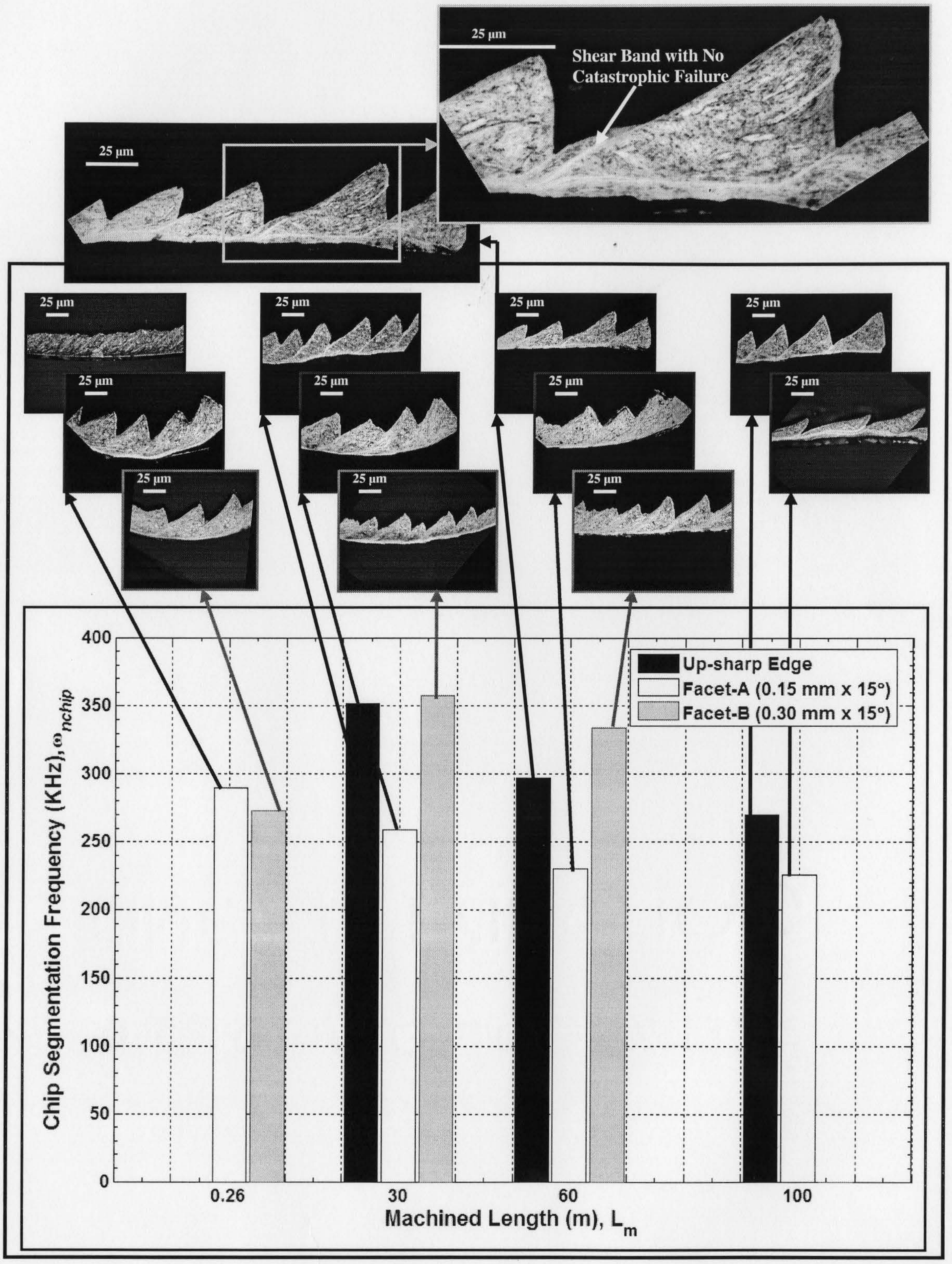

Fig (4.16) Progression in chip morphology and chip segmentation frequency over the length of cut

4.1.3 Improved Cutting Tool Design

<u>**Evaluation of Tool Life and Tool Wear Behavior**</u>

The improved design of the Mitsubishi C-2SB substrate had a beneficial influence on coated tool performance. The shorter flute length and the larger core diameter improved the tool rigidity which beneficially improved the stability of the cutting action. Consequently, the coating stability was enhanced due to the more stable interaction between the tool and the work-material during the chip forming and flowing processes. This improved the ability of the tribo-films to regenerate more gradually during the initial and the steady-state stages of tool wear; refer to Figure (4.17).

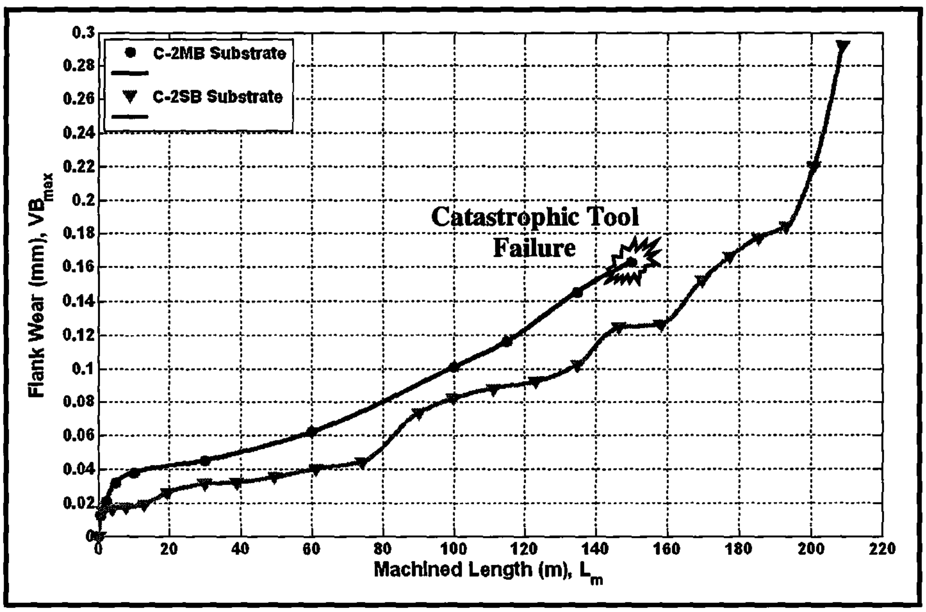

Figure (4.17) Effect of substrate design on flank wear progression

The harder substrate material (HV 1950-2000) also resulted in better abrasion wear resistance with less edge chipping particularly during the rapid wear stage. In addition, the improved toughness resulted in more predictable tool wear by avoiding any catastrophic brittle fracture of the cutting tool. This was not the case with the other substrate when the tool failed catastrophically by edge and shank sudden fracture.

Figure (4.18) shows the SEM images of the rake and flank faces of the C-2SB coated tool at the end of the cutting test. The EDS analysis conducted on the tool surface revealed that; the typical wear pattern on coated carbide tools during HSM of hardened steels can be divided into two main regions. The first region was referred to before as an island-like seizure formation, where the work-material tends to stick and harden to the tool surface as a result of surface plastic deformation. The second region is where the real damage to the tool surface occurred. The damage of surface layers can be classified into two surface zones: namely, the shallow zone and the deeper zone. The former zone yielded worn coating layers with less resistance to attrition and to catastrophic modes of tool surface failure due to severe plastic deformation at the frictional surface while, the latter zone is where the substrate started to participate in the deformation action after the coating layers had been completely delaminated. Build-up layers were also observed very close to the point on the cutting edge line that corresponds to the maximum cutting speed.

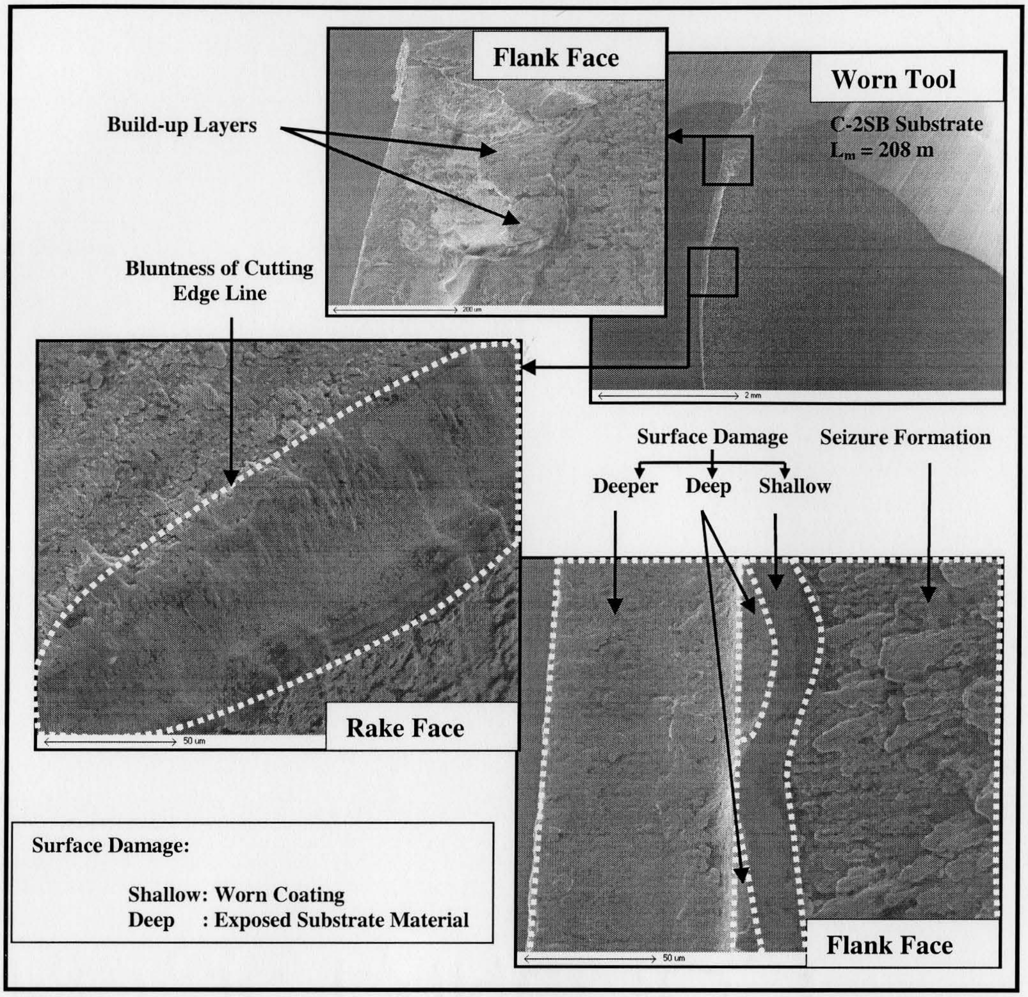

Figure (4.18) SEM images showing the typical wear patterns on rake and flank sides of coated carbide ball end-mill in HSM of hardened steels

Cutting Forces

The variation of cutting forces was dominant throughout the cutting time. Less excessive variation was observed in the case of the improved substrate design (C-2SB). This is due to the lower intensity of flank wear and edge chipping; refer to Figure (4.19).

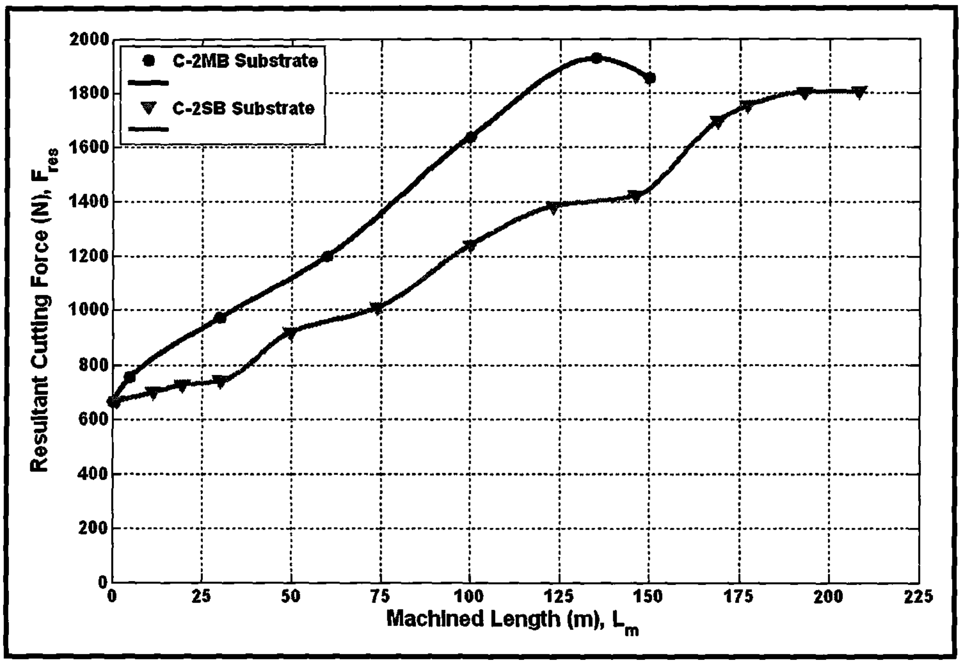

Figure (4.19) The effect of substrate design on the resultant force component

Chip shape and morphology

Figure (4.20) presents the SEM and Optical microscopic images taken for the surfaces and cross sections of the chips at different machined lengths. Up to a machined length of 100 m, the chips produced by the two substrates showed similar curling intensity due to the similar temperature distribution through the chip thickness.

The chip segmentation was evident in all the chips collected throughout the two cutting tests. Using different substrate designs had no significant influence on the initiation mechanism of the segmented chips. However, the tool wear and the friction along the chip-tool interface had an impact on the chip formation homogeneity. The tool wear that developed caused cutting edge bluntness. Consequently, an inhomogeneous strain is enforced on the machined surface and the chip is formed with uneven serration, less segmentation frequency and thicker white layers (within the secondary shear zone). The severe frictional conditions along the chip-tool interface negatively affected the material plastic flow. This then resulted in more brittleness and less ductility within the deformed material and eventually in deeper crack propagation between each segment; refer to the difference in the chip segmentation pattern obtained at the machined length of 100 m in Figure (4.20). The severe frictional conditions in the case of C-2MB substrate resulted in a highly segmented chip pattern.

As the tool wear deteriorated, the cutting pressure increased leading to chips with more uneven serration on the free surface and "ears" on the backside of the chips; refer to the chip morphology at 200 m cutting length in Figure (4.20). This type of inverted (i.e. curled-back) chip morphology has a detrimental effect on the tool rake face due to the following reasons:

- The diffusion wear mechanism occurs under conditions of high transformation temperature and increased chip speed (particularly when the cutting ratio exceeds one);
- The abrasive interaction between the hard white layers formed around each segment and the tool surface. This might lead to spalling and pitting of the tool rake surface.

Therefore, efficient techniques for cooling and forced chip evacuation are mandatory for this type of metal cutting applications, as will be discussed shortly.

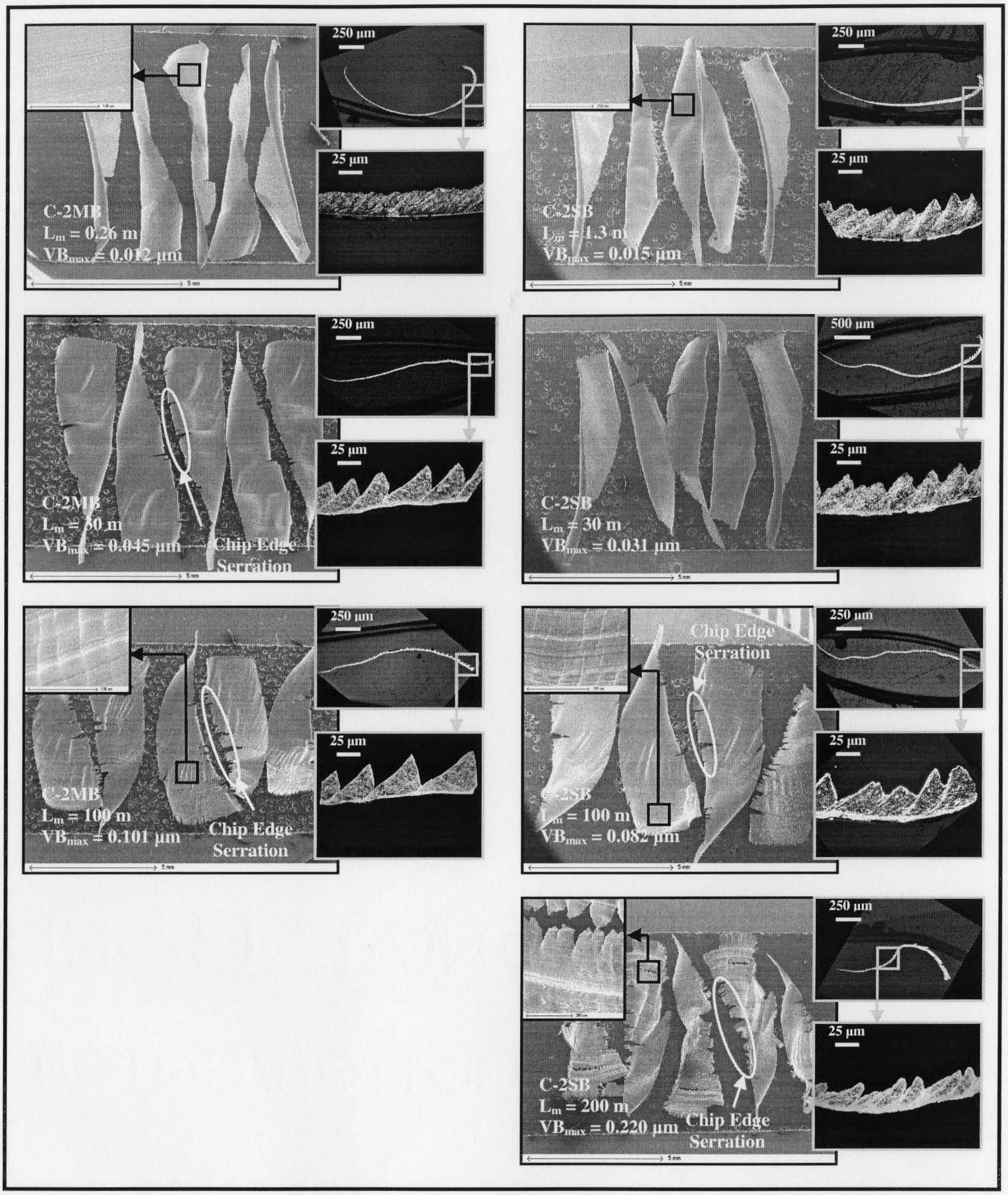

Figure (4.20) SEM and Optical microscopic images showing the evolution in chip morphology over the length of cut for chips produced using two different substrate designs

4.2 Testing of Hard PVD Coatings under Different Dry Cooling and MQL Cutting Environments, and Cutting Speeds

Despite the vast development of hard coatings with improved tribological behavior and surface adaptability, using coated carbide tools for dry high speed milling of hardened steels (above 55 HRC) is still limited to certain range of cutting speeds (200 to 300 m/min). This is due to excessive heating of the cutting edge, intensive seizure formation and eventually severe edge chipping. Accordingly, the improved cutting tool design has to be coupled with a suitable cutting environment in order to improve cutting performance.

The objective is to assess the cutting performance of TiAlCrN/NbN PVD coated carbide tools under different strategies of air cooling, in order to develop a feasible approach for effective cooling and sufficient air flow. The best air cooling strategies was then selected for further investigation; the influence of dry and MQL cutting conditions was evaluated in terms of the cutting performance. The experimental coating was also tested at different cutting speeds to investigate the coating behavior and to identify the limitations in the operational cutting speeds. In addition, the feasibility of improving tool life by post-treatment polishing of coating surfaces was investigated. Testing of a different class of commercially available PVD Supernitride-HSN^2 was conducted for a comparative study.

4.2.1 Influence of Dry Cutting Environment on Coated Tool Performance

Owing to its improved design, the TiAlCrN/NbN coated carbide tools (Mitsubishi C-2SB ball nose end-mills) were utilized in this set of experimental tests. The cutting tests were conducted under the following dry cutting conditions: maximum cutting speed of 350 m/min, feed rate of 0.06 mm/tooth, table feed of 1,337 mm/min, axial and radial depth of cut of 5 and 0.6 mm respectively. The cutting tests were performed under different settings of dry cooling for chip evacuation and cooling purposes. The stream of air was directed to the cutting zone using four different techniques:

- An open copper tube at volumetric flow-rate of almost 15.5E-3 m^3/sec and at room temperature of almost 22 °C;
- A vortex tube at volumetric flow-rate of almost 11.3E-3 m^3/sec and at chilled temperature of almost -15 °C;
- Different vortex tube setting at volumetric flow-rate of almost 15.1E-3 m^3/sec and at chilled temperature of almost -5 °C;
- A super air nozzle at volumetric flow-rate of almost 18.3 E-3 m^3/sec and at room temperature of almost 22 °C.

In all of these settings, the air blast was initially driven to the cutting zone by pressurized air of 100 PSI (≈ 0.69 MPa). The stream of air was directed toward the tool rake face.

4.2.1.1 Evaluation of Tool Life and Tool Wear Behavior

Flank wear propagation curves for the four tested settings of dry cooling are shown in Figure (4.21). The different dry cooling settings had a comparable impact on flank wear during the first or initial stage of tool wear due to the relevant adaptive behavior of the coating. Once the frictional heat starts accelerating along the contact zones, the two chilled-air settings were found to reduce the rate of flank wear during the post-running stage due to better heat dissipation and cooling efficiency. The higher chilled-air flow setting, despite its lower temperature drop, yielded slightly longer tool life than that of the lower chilled-air flow setting.

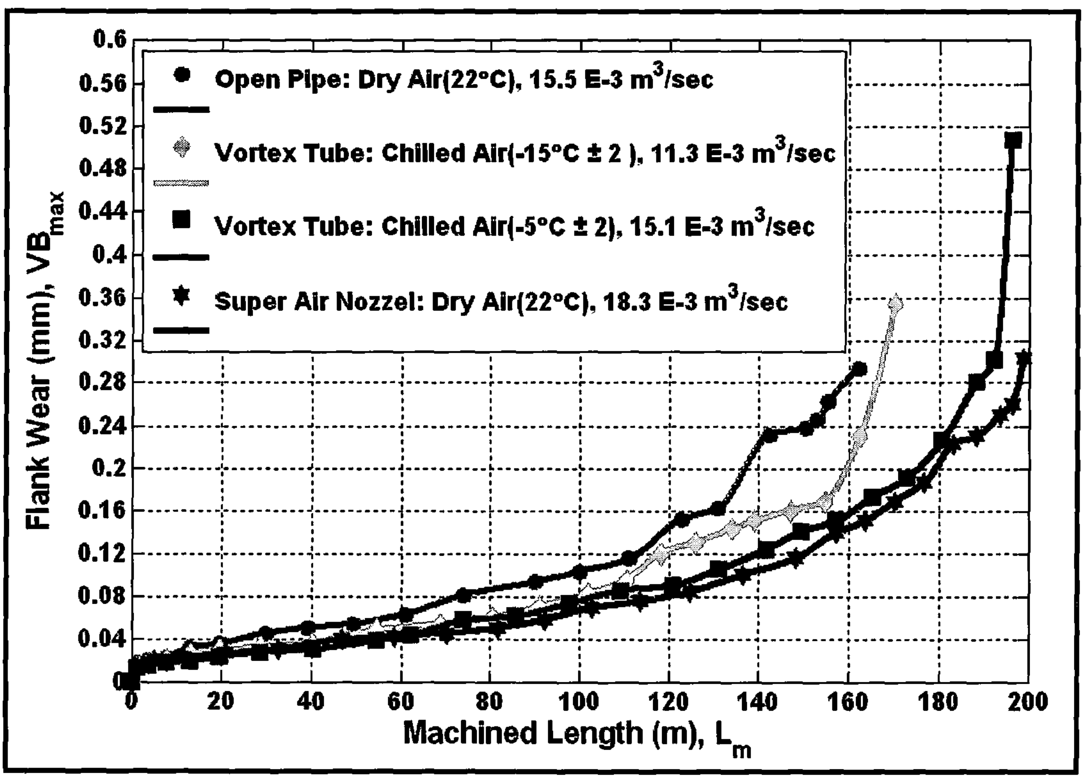

Figure (4.21) Effects of different dry cooling conditions on flank wear progression

This indicates that for the present cutting application the maximum-flow settings for the dry cooling environment can give a higher cooling efficiency than the minimum-temperature settings. This is due to the latter's lower heat transfer coefficient. In the same way, the super-air nozzle gave the lowest flank wear rate and the longest tool life among all tested dry cooling strategies. Similar observations were revealed in [Liu and Kevin Chou, 2007], where experimental and numerical studies were conducted to evaluate the machining of hypereutectic Al-Si alloys (A390) using the vortex-tube cooling in a dry cooling environment. The analytically estimated heat convection coefficients showed significant difference when two different minimum-temperature and maximum-flow settings were employed. The results also showed that the higher maximum-flow setting results in higher heat-flux induced into the tool, which affected the cooling capacity along the tool-chip contact zone.

The evaluation of the wear patterns developed along the rake and the flank faces of the cutting tools revealed that using chilled-air as a cutting environment resulted in severe damage to the rake faces; refer to Figures (4.22 and 4.23). The room-temperature-air-flow, ejected by the super-air nozzle, yielded a lower flank wear rate and thus there was less damage to the rake face. The previously reviewed results in [Liu and Kevin Chou, 2007] can be adopted to describe the relationship between the air flow rate and the heat-flux induced into the tool rake-face. The higher heat-flux induced into the tool rake-face, associated with the higher air flow rates, can beneficially protect the rake-face during interrupted cutting by maintaining sufficient heat dissipation without activating the onset of thermal shocks.

Adhesion, fatigue and abrasion wear mechanisms are the typical wear mechanisms activated during high-speed milling of hardened steel. Owing to the small value of tool immersion inside the workpiece and to the high cutting speed of 350 m/min, each cutting tooth is engaged in cutting (i.e. heating-up period) for about 0.419 ms followed by non-cutting period (i.e. cooling-off period) of about 2.28 ms. Therefore, the heat input into the coated tool during the heating-up periods activates the diffusion of the elements along the contact zones followed by adhesion and eventually abrasive interaction along the frictional surfaces. Meanwhile, the thermal cycling activates the fatigue wear during the transition between the cutting and non-cutting periods.

It can be observed that a combination of the aforementioned wear mechanisms were encountered on the rake face when chilled-air was employed in the cutting environment; refer to Figures (4.22.b and 4.22.c). The existence of severely damaged areas along these rake faces indicates an intensive thermal fatigue followed by abrasive interaction along the chip-tool interface. This is where rapid coating delamination was followed by wider and deeper areas of exposed substrate material. These areas exhibited valley-like pitting of the tool rake surface. This damage intensified the negative impact of the thermal cyclic loadings during the interrupted cutting action under chilled-air cooling conditions.

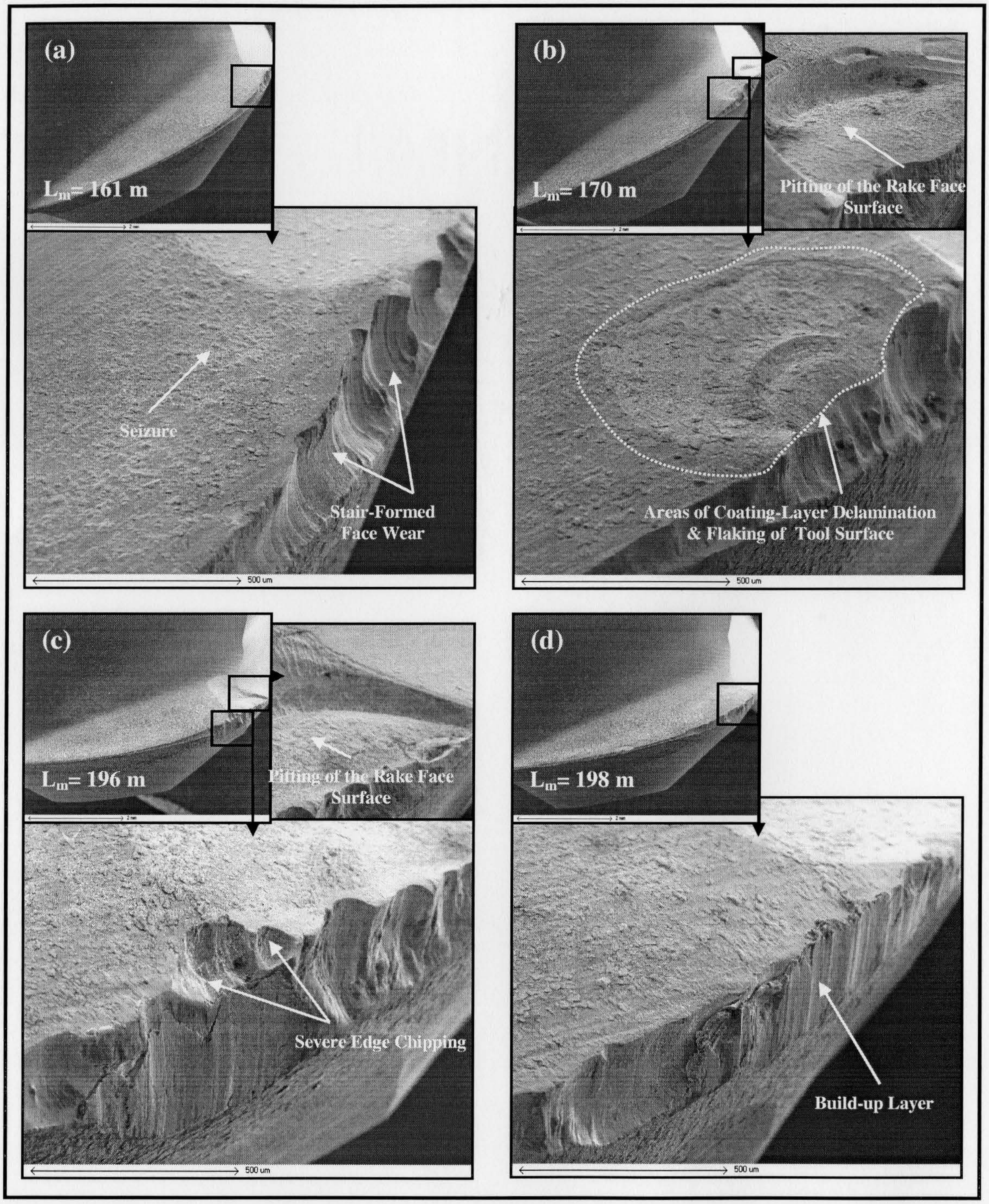

Figure (4.22) SEM images with EDS analysis showing worn rake sides of coated tools under different dry cooling conditions: (a) Dry air (22 ºC, 15.5E-3 m^3/sec), (b) Chilled air (-15 ºC ± 2, 11.3E-3 m^3/sec), (c) Chilled air (-5 ºC ± 2, 15.1E-3 m^3/sec) and (d) Dry air (22 ºC, 18.3E-3 m^3/sec)

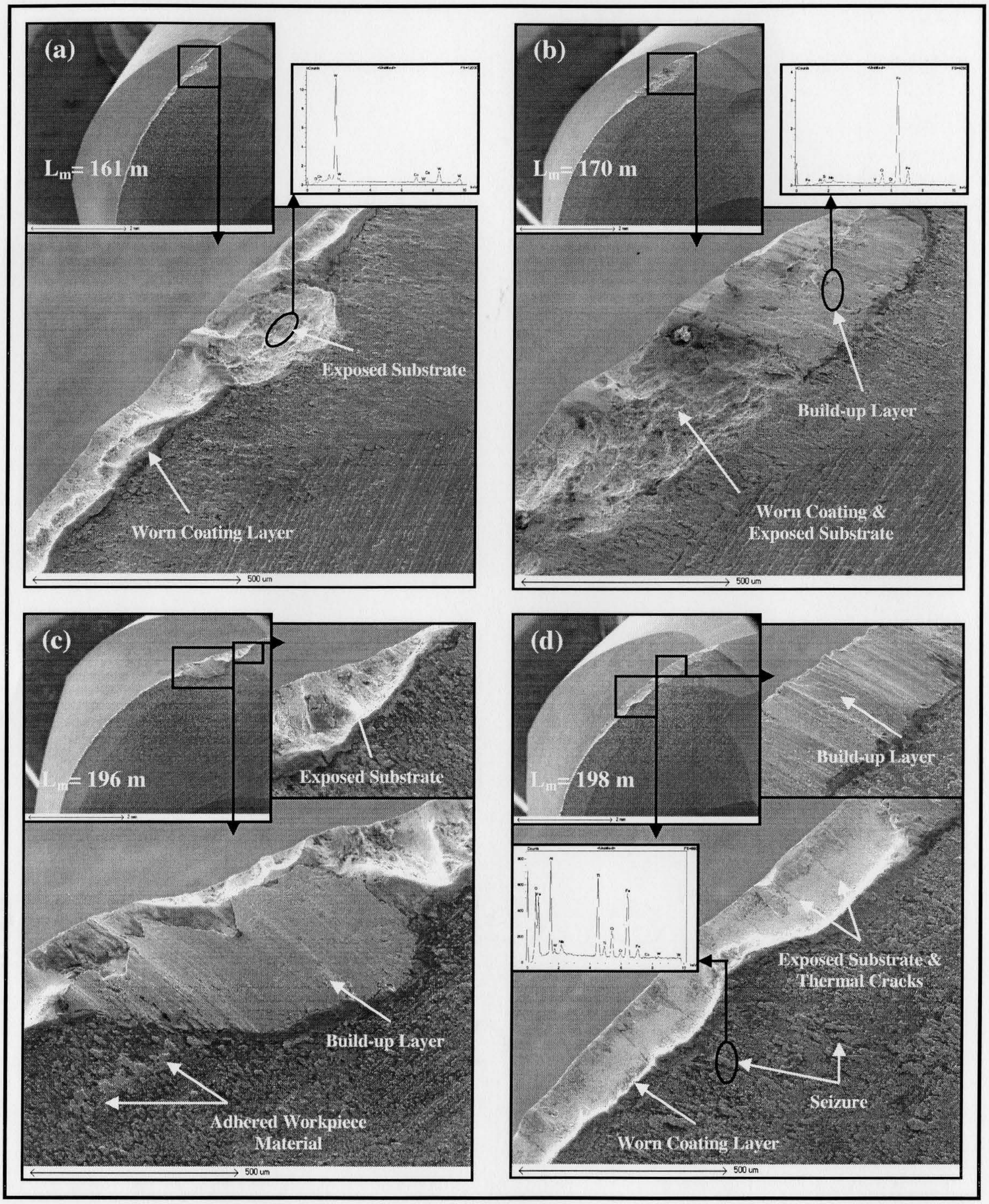

Figure (4.23) SEM images with EDS analysis showing worn flank sides of coated tools under different dry cooling conditions: (a) Dry air (22 ºC,15.5E-3 m^3/sec), (b) Chilled air (-15 ºC ± 2, 11.3E-3 m^3/sec), (c) Chilled air (-5 ºC ± 2, 15.1E-3 m^3/sec) and (d) Dry air (22 ºC, 18.3E-3 m^3/sec)

EDS elemental mapping was performed to show the distribution of elements over two rake surfaces for two different dry cooling settings; refer to Figure (4.24). The increase in the volume of air-flow could not provide any distinct reduction into the adhesion of workpiece material to the tool rake surface. Oxidation of all coating elements can be observed. This indicates the ability of these elements to self-diffuse to the surface and thus interact with the oxygen from the cutting environment. The elements then form protective metallic-based oxide films (e.g. $(Al,Cr)_2O_3$ complex films and Nb-O films). As previously discussed, these oxide-films are beneficial to the enhancement of oxidation and diffusion resistance of coating layers.

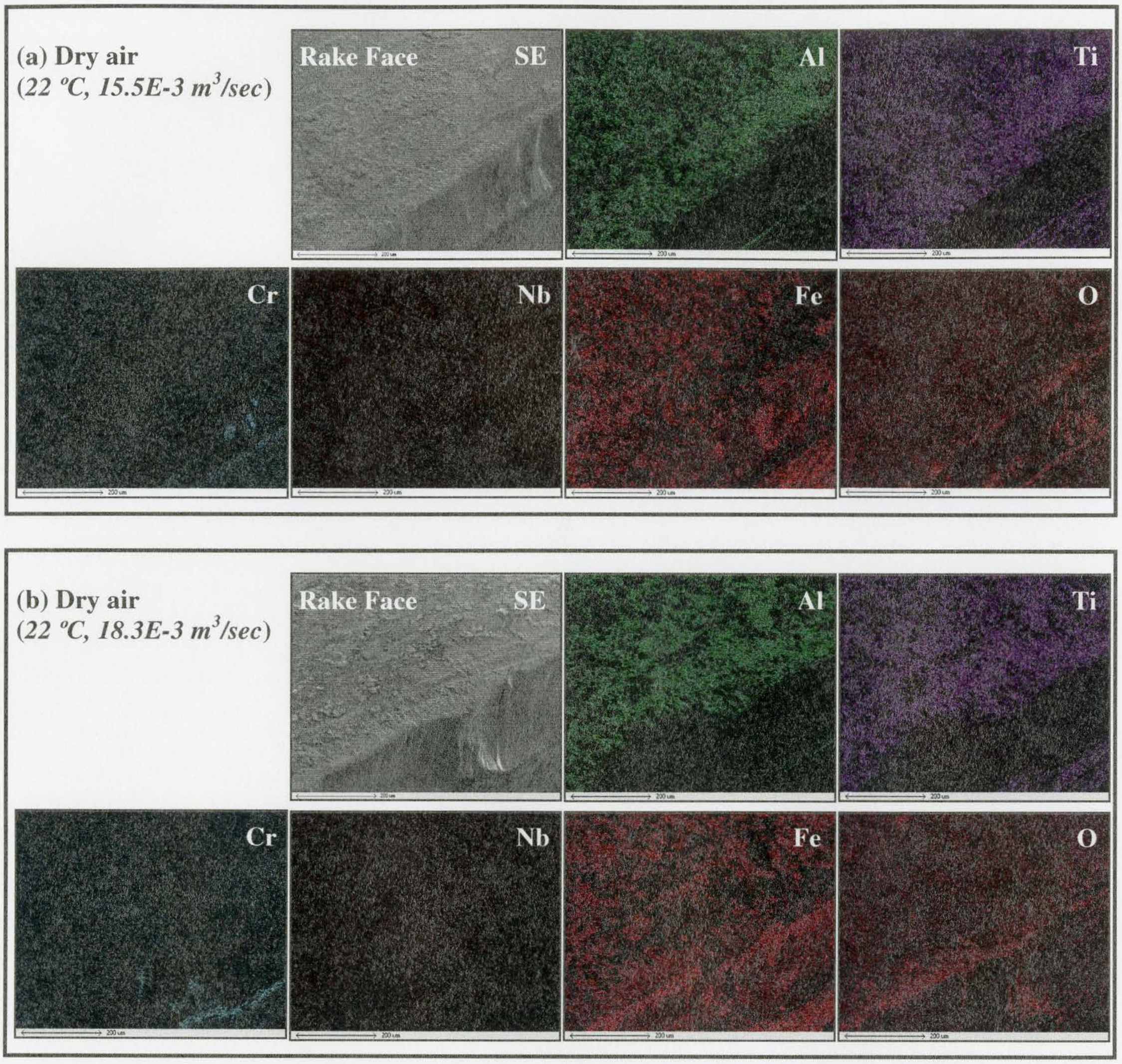

Figure (4.24) SEM images with elemental mapping showing worn rake sides of coated tools under two different dry cutting environments

In conclusion, the cooling setting of the dry air blow-off environment proved to be secondary when compared to the air-flow setting for the cutting application presented in this study. A well-controlled air flow is very important for this type of hard cutting application where relatively abrasive and hard chips are produced.

4.2.1.2 Cutting Forces

The variation of cutting forces in the (X, Y and Z) directions was dominant throughout the cutting time regardless of the employed cutting environment; refer to Figure (4.25). A correlation was found between the variation of each cutting force component and the evolution of flank wear. The increase in the cutting force components was mainly attributed to the additional pressure and frictional energy, imposed and dissipated along the interface between the flank land and the work-material. F_x and F_y cutting force variations showed strong correlation to flank wear evolution with correlation coefficients of 0.975 and 0.945 when dry-air was blown-off at 15.5E-3 and 18.3E-3 m^3/sec respectively. F_z and F_y showed the strongest correlation to flank wear evolution with correlation coefficients of 0.960 and 0.967 when chilled-air was blown-off at 11.3E-3 and 15.1E-3 m^3/sec respectively.

In addition, the types of tool wear developed on the rake face and along the cutting edge line had an influence on the trend of the cutting force components particularly when chilled-air was utilized. The force in the x-direction fluctuated throughout the cutting time with a sudden drop prior to the end of tool life; refer to Figures (4.25.b and 4.25.c). This is attributed to the fact that the developed wear patterns along the rake face, when chilled-air was utilized, changed the effective rake angle which altered the mechanics of cutting. The unexpected reduction in any measured cutting force component prior to the end of tool life is mainly due to the loss of contact between the tool and the workpiece at some cutting points. This is where severe edge chipping and stair-formed face wear are developed along the cutting edge line. Similar observations were reported in [Almeida el al., 2005, Dumitrescu, 1998 and El-Wardany et al., 1996].

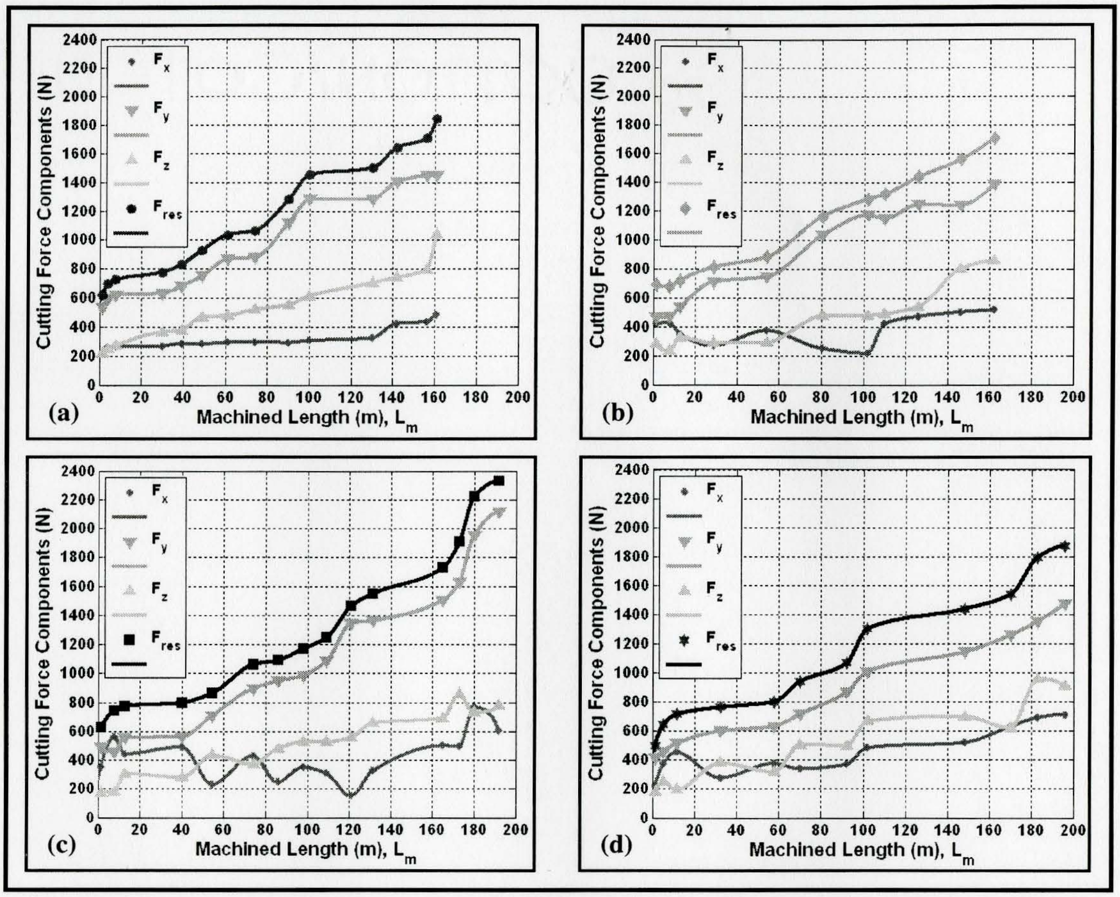

Figure (4.25) The Variation of cutting force components versus the machined length for different dry cooling conditions: (a) Dry air (22 ºC, 15.5E-3 m^3/sec), (b) Chilled air (-15 ºC ± 2, 11.3E-3 m^3/sec), (c) Chilled air (-5 ºC ± 2, 15.1E-3 m^3/sec) and (d) Dry air (22 ºC, 18.3E-3 m^3/sec)

Figure (4.26) shows the effect of different dry cooling conditions on the resultant force component. No distinctive difference was observed in the magnitude and the trend of the resultant force components. However, the resultant cutting force was lower when the super-air nozzle was used, which indicates the beneficial impact of having lower flank wear on the stresses imposed on the cutting edge and consequently on the overall tool life.

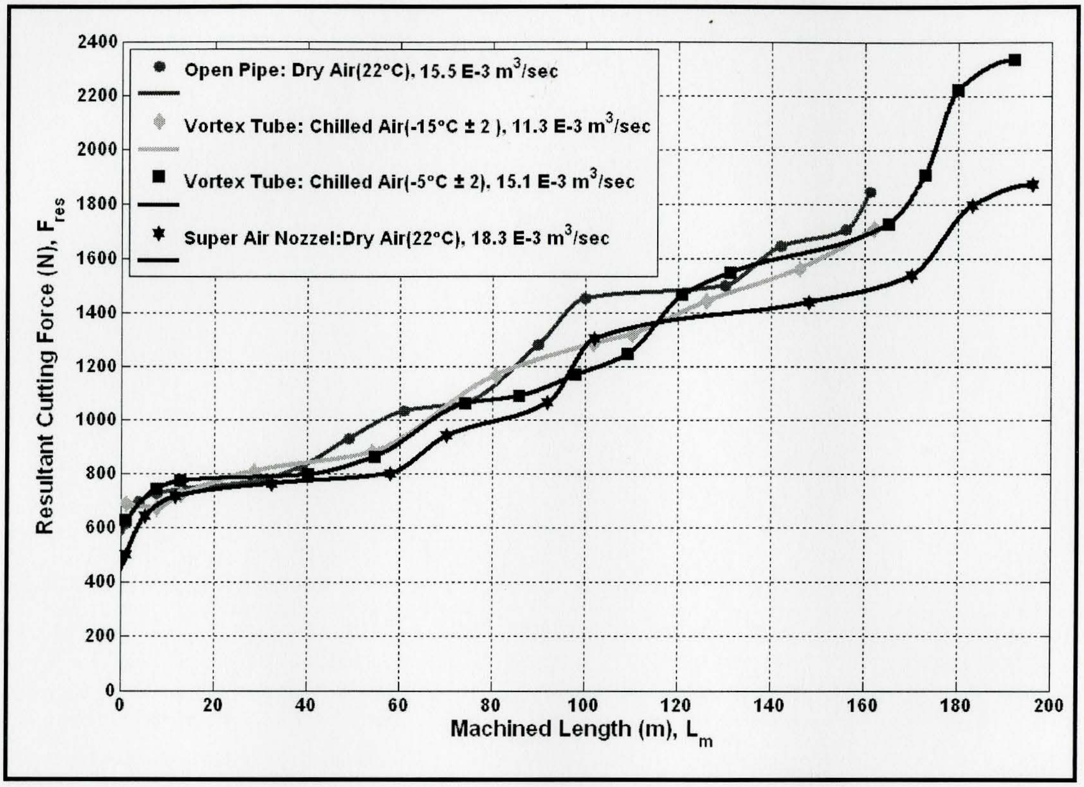

Figure (4.26) Effects of different dry cooling conditions on the resultant cutting forces

In general, the fluctuation in the trend of any measured cutting force component throughout the cutting time is related to the interaction of the following factors:

- The bluntness-status of the cutting edge accounts for the increase in the resultant cutting force due to the contribution of the ploughing force component;

- The frictional energy dissipated along the interface between the flank land and the work-material accounts for the increase in the resultant cutting force;
- The damage along both the cutting edge line and the rake face accounts for the reduction in the resultant cutting force. For the former, the reduction is due to the loss of contact between the tool and the work-material due to severe edge chipping. For the latter, the reduction is related to the lower level of force needed to shear the material due to the lower effective rake angle with a corresponding increase in the shear angle;
- The heat generated during flank wear evolution accounts for the reduction of the cutting force due to the higher thermal loading with a corresponding reduction in the yield strength of the work-material, [Wang and Liu, 1999];
- The improved tribological behavior of the coating accounts for the reduction in the cutting force due to the formation of lubricious oxide-films on the coated tool surface, [Ning et al., 2007].

4.2.1.3 Evaluation of Surface Roughness

Figure (4.27) shows the variation in the average surface roughness over the machined length for the three tested dry cooling settings. It can be observed that the deterioration in surface finish was mostly influenced by the flank wear progression and the variation in cutting forces. This is due to the presence of possible vibration effects and to the corresponding rubbing and intensive material deformation induced during the formation of the pick-interval scallops. Therefore, the surface obtained, when the super-air nozzle was utilized, exhibited the lowest average surface roughness. Strong correlations were found between the variations of the F_y and F_z cutting force components and the average surface roughness for all of the tested cutting environments.

Fluctuations in surface roughness were obtained at some cutting lengths, particularly at the beginning of cutting and prior to the end of tool life; refer to Figure (4.27). The fluctuations are attributed to the balance between three competing factors: namely, the tribological behavior of the coating, the tool wear pattern developed along the flank land and the amount of heat induced into the workpiece during cutting with a corresponding fluctuation in the cutting force components, particularly the one measured along the axial or z-direction. Therefore, surface roughness could be misleading, if it is used solely in the assessment of cutting tool performance; a similar conclusion was made in [Elbestawi et al., 1997].

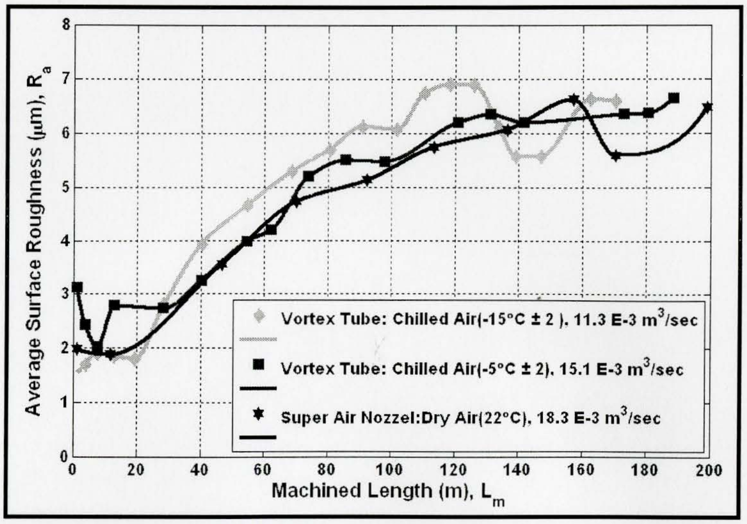

Figure (4.27) Effects of different dry cooling conditions on machined surface roughness

4.2.1.4 Chip Configurations

Chip Shape and Morphology

Figure (4.28) presents SEM images taken for the inside and backside of the chips at different machined lengths for the four tested cutting environments. The chips exhibited comparable shapes and surface textures. The influence of tool wear on the shape of chips was the same regardless of the utilized cutting environment. The chips first formed with relatively intense curling, smoother backside and fewer edge serrations. Then chips started showing a combination of flat and curly profiles with a slightly rough backside-surface and intensive edge serration due to more intensive cutting stresses. As tool wear deteriorated, very brittle and rough chips started forming and curling back with intensive cracking and compression marks.

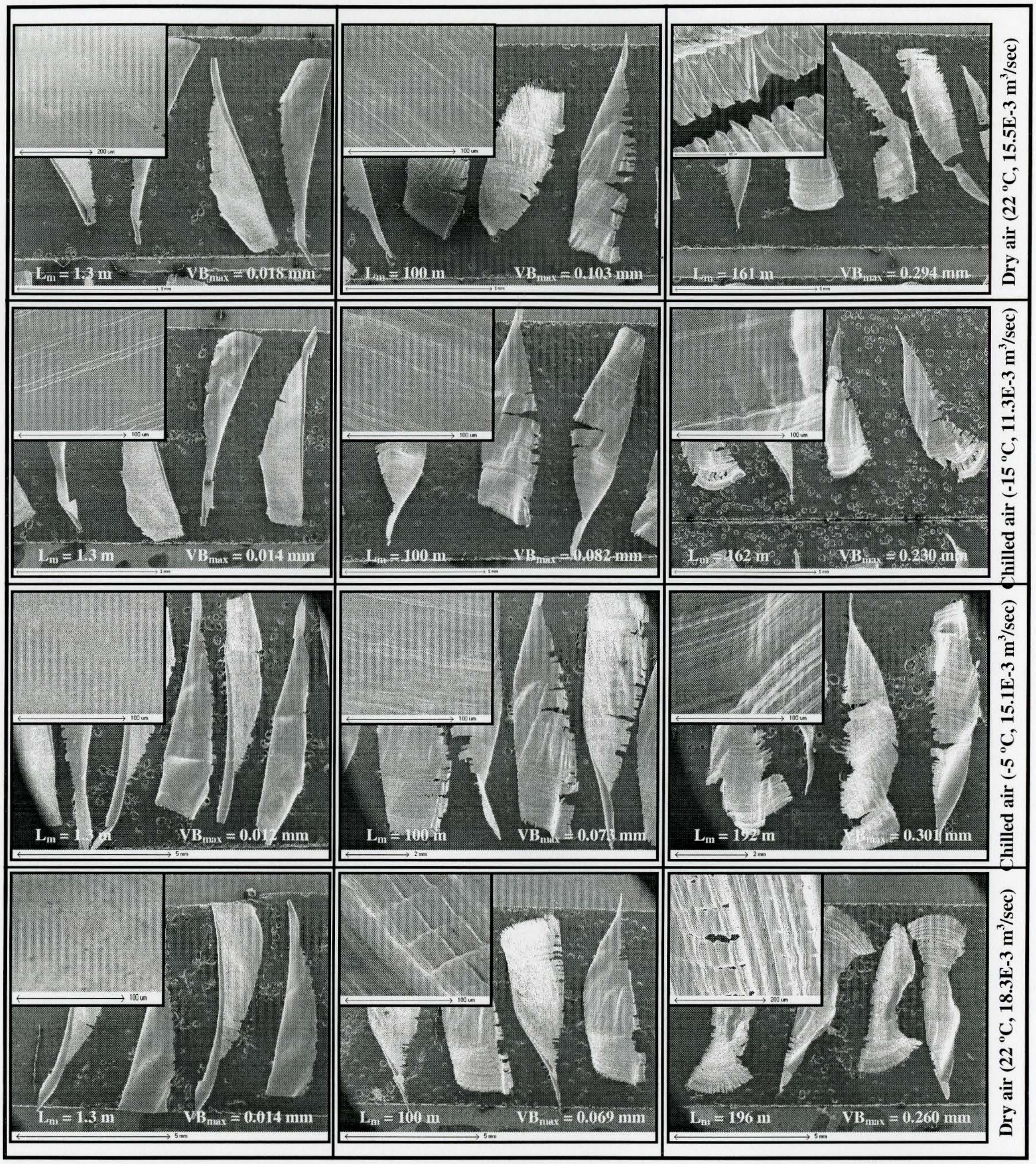

Figure (4.28) Effects of different dry cooling conditions on chip shape at different machined lengths

Chip segmentation was evident under all cutting environments tested in this experimental set. Using different dry cooling environments had no significant influence on the initiation mechanism of the segmented chips. However, the tool wear and the friction along the chip-tool interface had an impact on the chip formation homogeneity. The chips experienced inhomogeneous morphologies at the beginning of cutting due to the non-uniform temperature distribution within the chip thickness; refer to Figure (4.29).

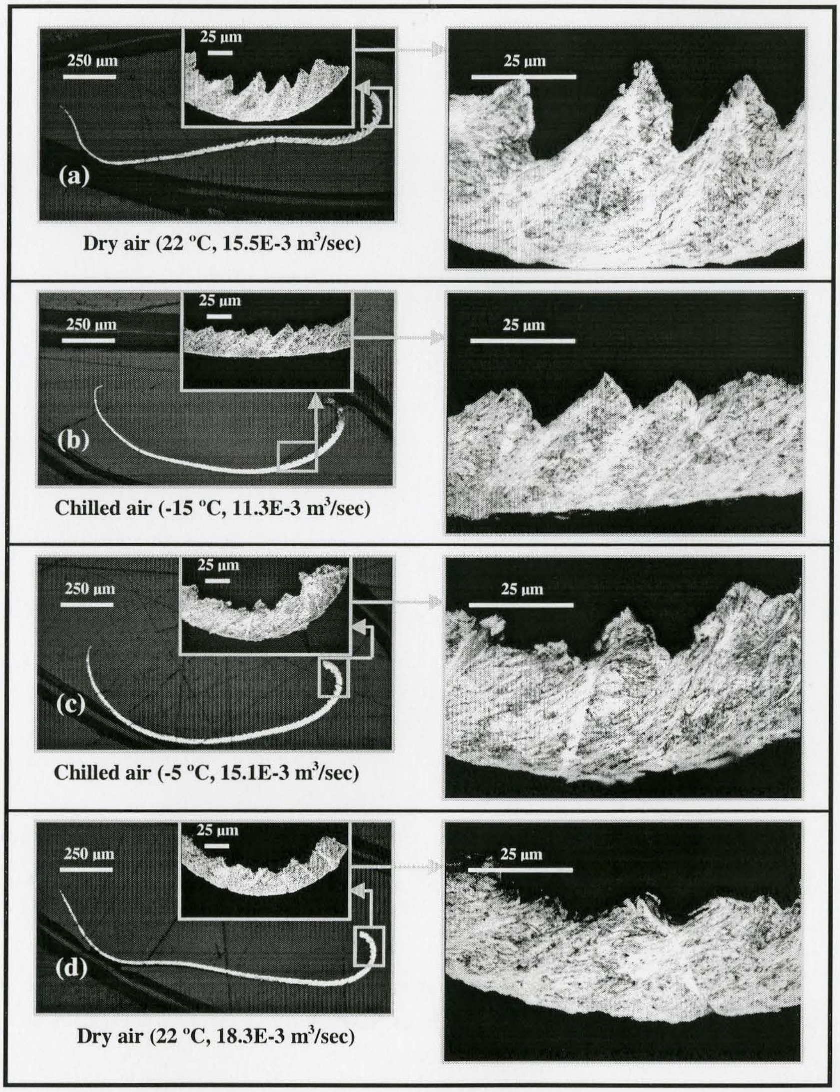

Figure (4.29) Optical microscopic images showing the effects of different dry cooling conditions on chip morphology at 1.3 m machined length

4.2.2 Influence of MQL Cutting Environment on Coated Tool Performance

This set of the experimental tests was conducted under the following cutting conditions: maximum cutting speed of 400 m/min, feed rate of 0.06 mm/tooth, table feed of 1,528 mm/min, axial and radial depth of cut of 5 and 0.6 mm respectively. Two cutting environments were utilized in this experimental set. The cutting tests were first performed by using dry pressurized air as a cutting environment. A stream of pressurized air (100 PSI) was directed to the cutting zone through a super air nozzle. In order to investigate the influence of mist lubrication on coated tool performance, another cutting test was then performed using MQL as a cutting environment. An oil-mist applicator (Accu-Lube Precision Applicator) was operated to dispense a controlled amount of (Accu-Lube LB-2000) oil at 30 ml/hr by using a stream of pressurized air (80 PSI).

<u>**Evaluation of Tool Life and Tool Wear Behavior**</u>

Flank wear propagation curves for the two tested cutting environments are shown in Figure (4.30). The dry and MQL cutting environments resulted in a comparable flank wear progression during the first two stages of tool wear. During the rapid wear stage, using pressurized air as a cutting environment yielded slightly longer tool life and a lower flank wear rate as compared to those obtained under an oil-mist cutting environment. This is mainly related to the extensive amount of heat generated during this last stage of tool wear which intensified the stresses exerted on the cutting edge due to thermal shocks. MQL has the ability to carry the heat out of the cutting zone by convection to the pressurized air flow and through the evaporation of the small oil droplets. Therefore, utilizing an oil-mist as a cutting environment activated the onset of thermal shocks more rapidly. For high-speed milling applications, stresses due to thermal shocks are more likely to exceed the transverse rupture strength of the tool material, [Barnett-Ritcey, 2004]. This was reflected not only on the progressive flank wear but also on the severe surface damage encountered on the rake face.

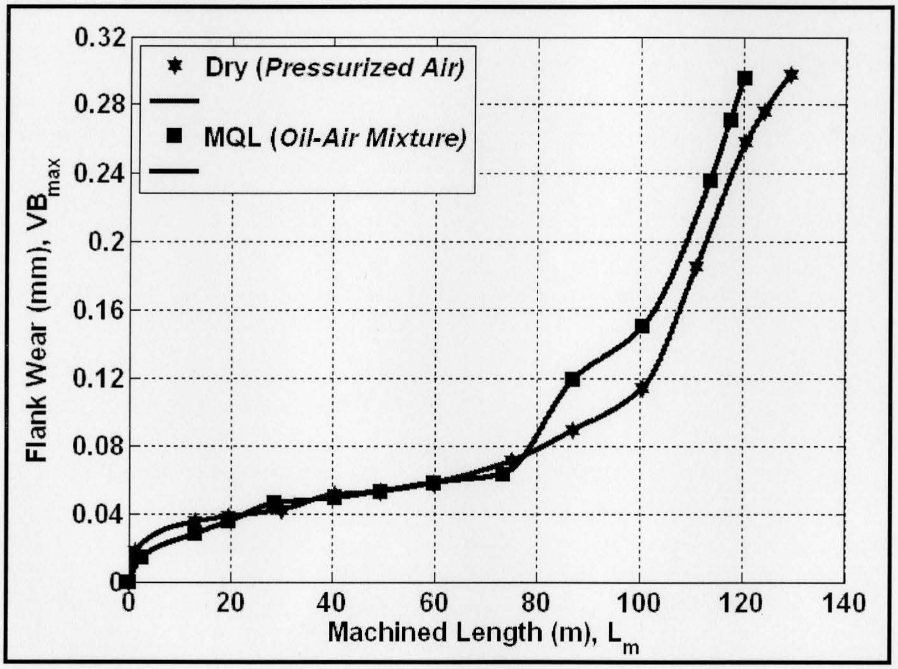

Figure (4.30) Effect of cutting environment on flank wear progression

The evaluation of the wear patterns developed along the rake faces of the cutting tools revealed that the tool surface damage under MQL was more severe as compared to the damage encountered under a dry air cutting environment; refer to Figure (4.31).

Figure (4.31) shows areas exhibited valley-like pitting of the tool rake surface. Intensive seizure formation can be observed on the tool rake and flank surfaces under dry air cutting conditions. The beneficial tribological effect of mist lubrication is also obvious; the formation of these metallic bonds at the tool-work interface was interrupted under MQL cutting conditions due to the existence of lubricating films between the two mating surfaces. However, the early activation of a thermal fatigue mechanism under MQL cutting conditions seemed to suppress the beneficial lubricious effect on both the flank and rake surfaces of the tool.

Closer examination of the cutting tools throughout each cutting test showed that under MQL cutting conditions, areas of micro-chipping and flaking started to appear very early at 13 m cutting length (i.e. cutting time of 8 minutes) along the cutting edge and the rake surface respectively. This early loss of tool fragments assisted flank wear progression and offset the tribological effectiveness of mist lubrication. Therefore, both cutting tools showed similar flank wear behavior under the cutting speed tested in this study.

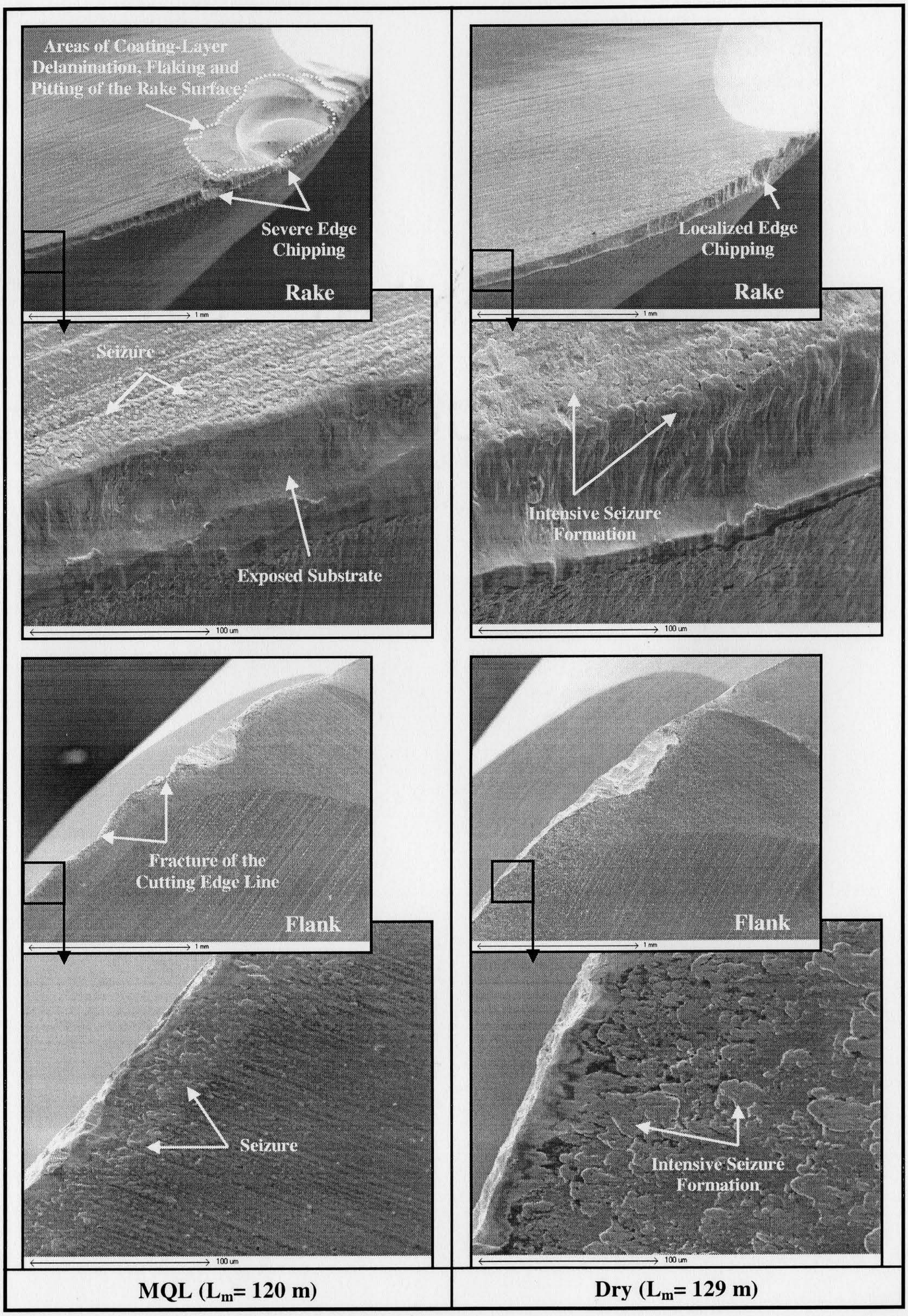

Figure (4.31) SEM images with EDS analysis showing worn rake and flank sides of coated tools under different cutting environments

Evaluation of Cutting Forces and Surface Roughness

The variation of cutting force components is presented in Figures (4.32.a and 4.32.b). The resultant cutting forces for dry cutting were slightly lower than those for MQL; refer to Figure (4.32.c). The variation was partially correlated to the flank wear progression. Utilizing MQL as a cutting environment did not lead to any distinguishable improvement in the surface finish; refer to Figure (4.32.d). Strong correlations were found between the trend of certain cutting force components and the trend of the average surface roughness which can be used to interpret the slight discrepancy in the surface finish obtained.

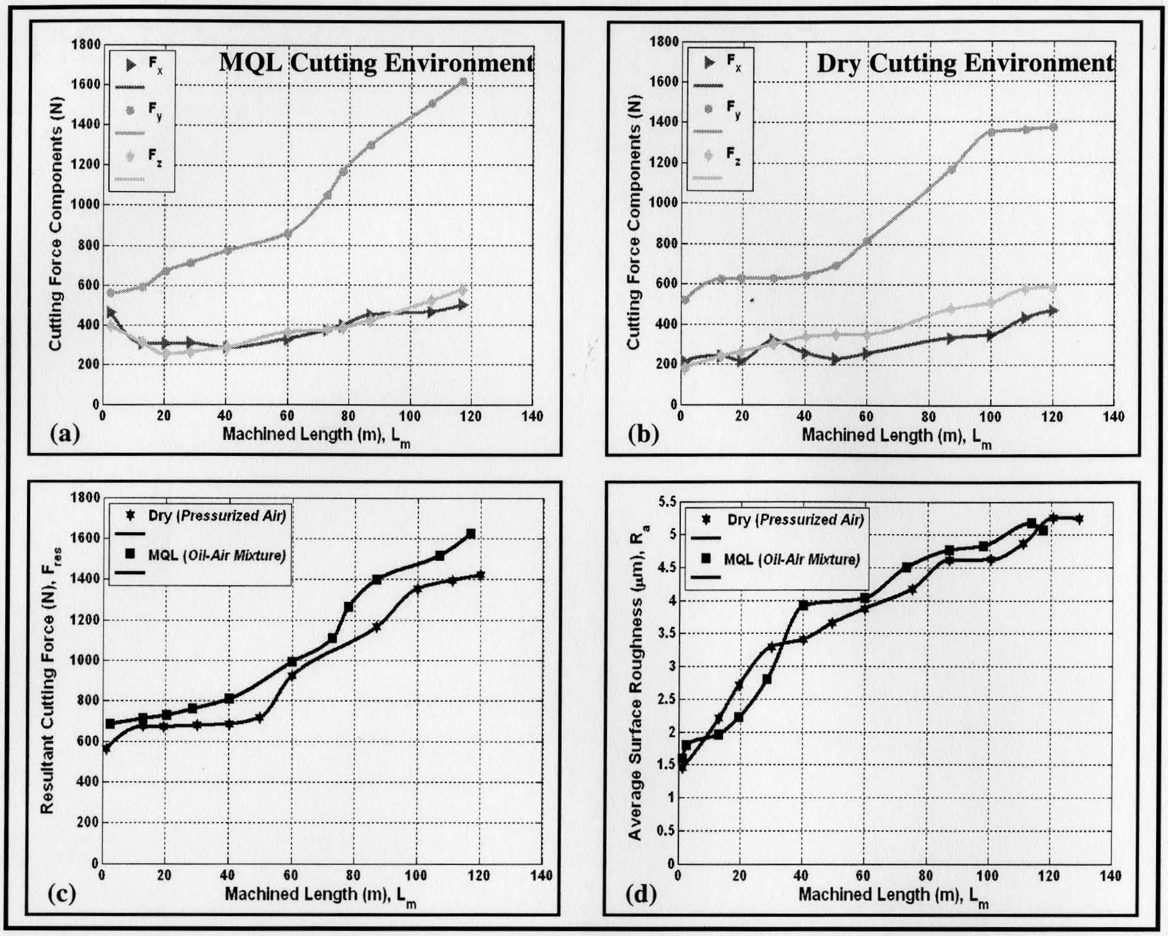

Figure (4.32) Effect of cutting environment on: (a, b) Cutting force components; (c) Resultant cutting forces and (d) Average surface roughness

Chip Configurations

Figure (4.33) presents SEM images taken for the inside and backside surfaces of the chips. The chips obtained under dry cutting conditions showed less brittleness and a smoother surface morphology, despite the less effective lubrication, as compared to those obtained under MQL conditions. This behavior became even more evident prior to the end of tool life. This indicates that the temperature factor was more dominant than the friction factor during the material deformation. Therefore, the working material exhibited larger plastic deformation and less thermal shocking under the dry-air cutting environment. In general, the dry-air cutting environment seemed to not only favor the wear behavior of the cutting tool but also the deformation behavior of the working material under the cutting speed tested in this study.

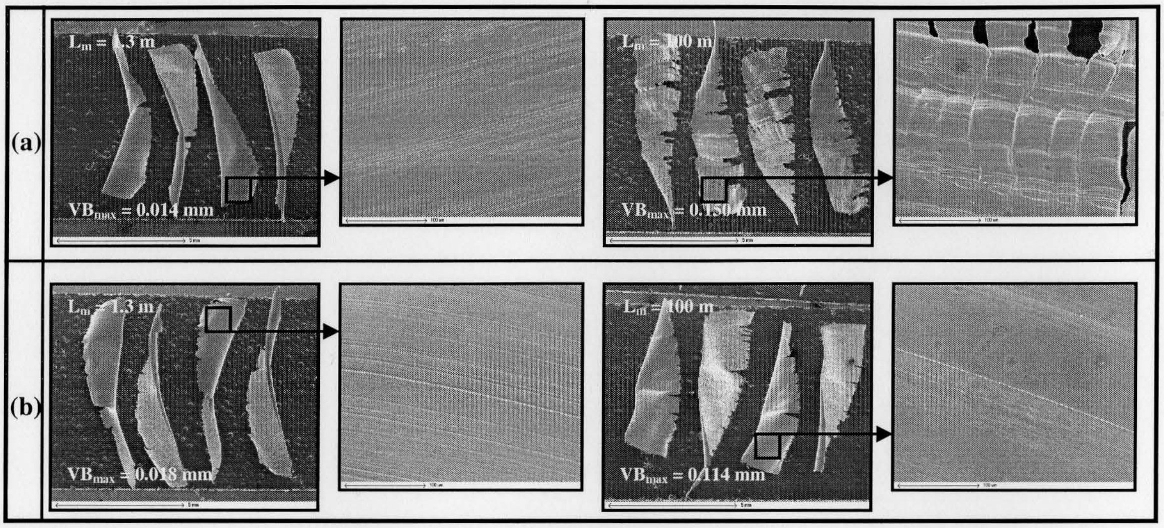

Figure (4.33) Effect of cutting environment on chip shape (a) MQL (b) Dry

4.2.3 Influence of Cutting Speed on Coated Tool Performance

Three different cutting speeds were utilized in this set of experimental tests. The objective was to test the newly developed TiAlCrN/NbN coating under different cutting speeds. The high speed machining of hardened steel AISI H13 (HRC 54-55) was conducted under the following three dry cutting conditions: maximum cutting speeds of 300, 350 and 400 m/min with corresponding table feeds of 1,146, 1,337 and 1,528 mm/min; feed rate of 0.06 mm/tooth; axial and radial depth of cut of 5 and 0.6 mm respectively; and pressurized air of 100 PSI (≈ 0.69 MPa) through an open copper tube.

4.2.3.1 Evaluation of Tool Life and Tool Wear Behavior

Flank wear propagation curves for the three tested cutting speeds are shown in Figure (4.34). The flank wear evolution revealed that at the tested range of cutting speeds, higher cutting speed was always accompanied by shorter tool life regardless of the variation in the tool wear behavior. For instance, the highest tested cutting speed (400 m/min) resulted in a slightly lower flank wear rate than the one obtained at (350 m/min) up to a machined length of 80 m. Then the flank wear started to develop rapidly in an unpredictable fashion resulting in the shortest tool life. Even though the reduction in flank wear rate was insignificant, it still suggests the existence of certain ranges of higher cutting speeds that can favor the behavior of working material under very high strain rates. This can result in an improvement in tool wear behavior and tool life, especially with the vast development of coated carbide tools for high speed machining applications.

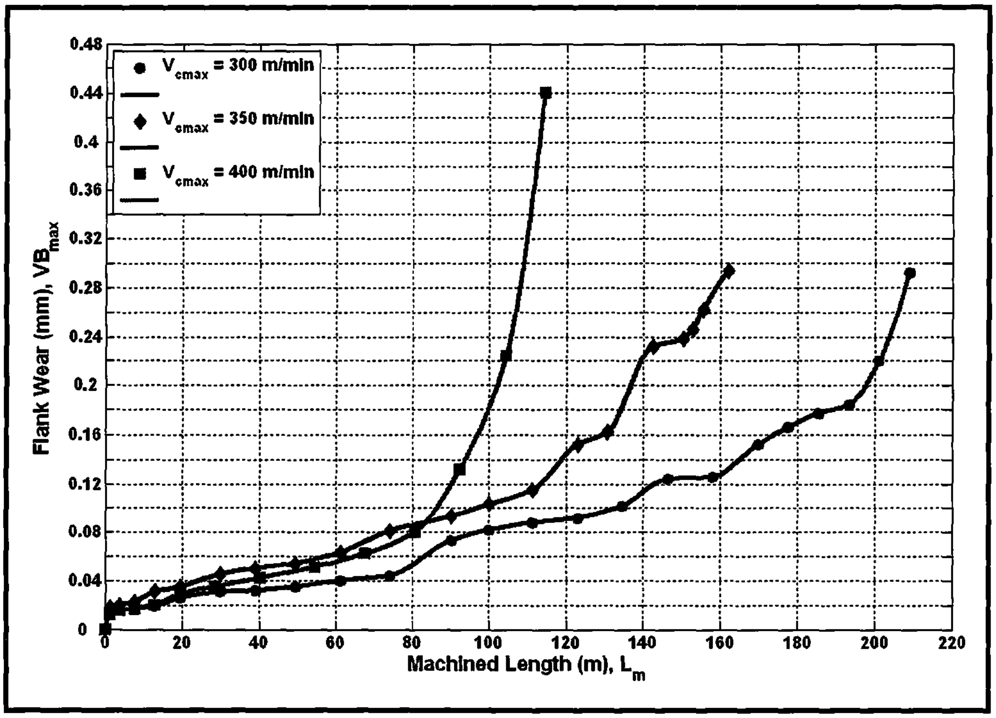

Figure (4.34) Effect of cutting speed on flank wear progression

The evaluation of the wear patterns developed along the rake and the flank faces of the cutting tools revealed that the maximum flank wear tended to be more localized around the highest contact point[13] between the tool and the workpiece as cutting speed was increased; refer to Figure (4.35). A relatively uniform flank wear developed along the cutting edge at a cutting speed of 300 m/min. Figures (4.35.b and 4.35.f) show areas on flank land completely covered by layers of adhered workpiece material. This indicates an intensive seizure formation followed by an intimate contact between the tool

[13] Point of maximum cutting speed and maximum axial depth of cut.

and workpiece material at these specified areas. Regardless of the tested cutting speed, all cutting tools first experienced edge chipping localized at certain areas along the cutting edge. These areas then merged into a continuous band resulting in the deterioration of the cutting edge line.

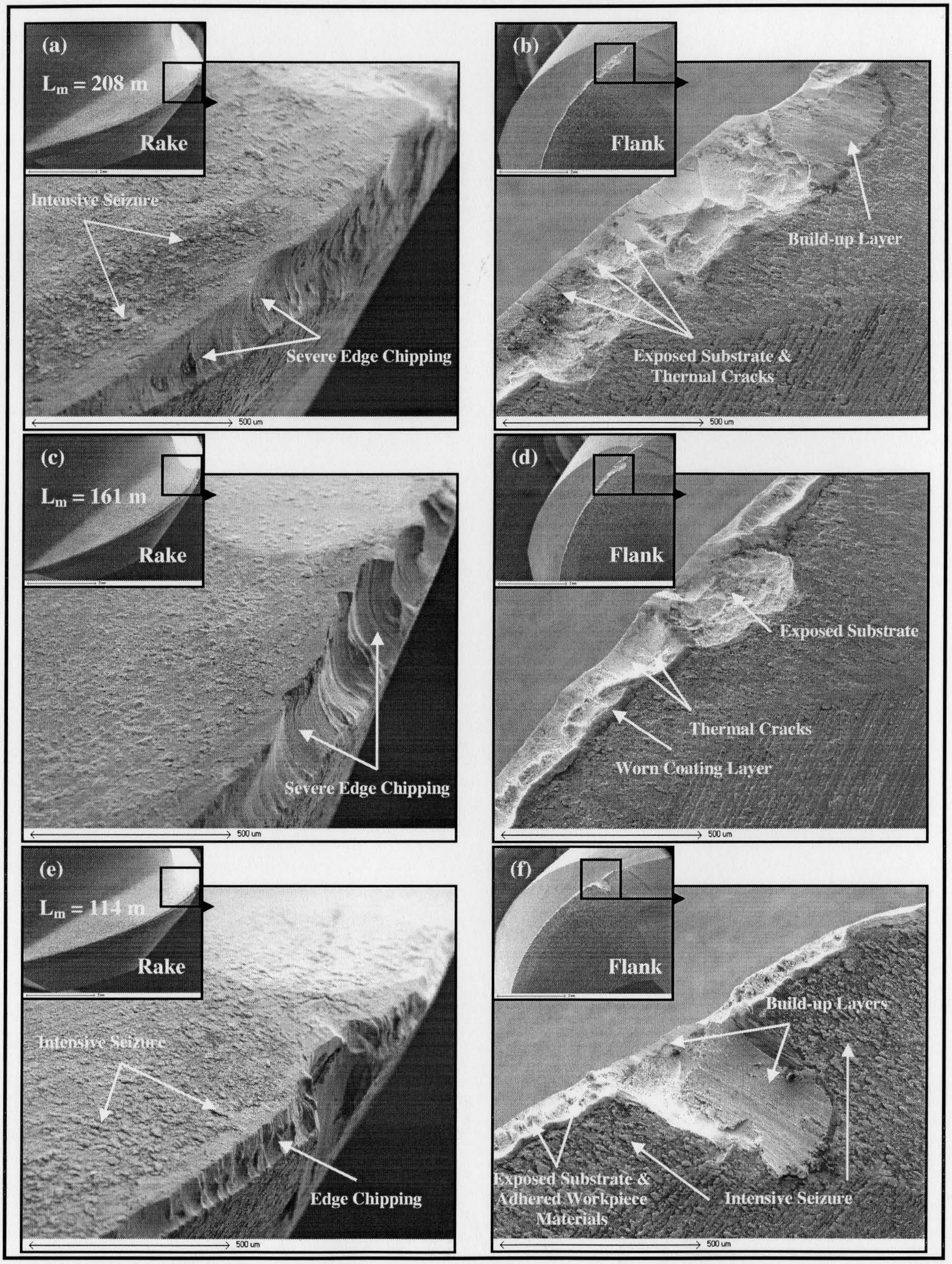

Figure (4.35) SEM images with EDS analysis showing worn rake and flank sides of coated tools at different cutting speeds: (a, b) 300, (c, d) 350 and (e, f) 400 m/min

Closer evaluation of the wear patterns that developed on the cutting tools revealed that the intensity of micro-cracks was reduced with the increase in cutting speed (bearing in mind the difference in the tool wear evolution and the cutting lengths). Tool wear was initiated by intensive adhesion due to higher cutting temperatures generated at higher cutting speeds. This was followed by an abrasion wear mechanism and then diffusion and oxidation wear mechanisms (oxidation of carbide occurs at ≈ 700 °C) with a corresponding pull-out of tool fragments. Fewer thermal micro-cracks developed on the worn tool surfaces at the highest cutting speed. This indicates that thermal fatigue cracking did not strongly contribute to the tool wear progression. This is due to a rapid cutting action (≈ 0.367 ms) in conjunction with a rapid plastic material flow. Consequently, less heat flowed into the tool and eventually delayed the onset of thermal shock.

Therefore, the accelerated wear evolution at higher cutting speeds can be partially attributed to an intensified abrasion and attrition between the tool and the burrs formed along the outer leading edge of the workpiece[14] (i.e. around the highest point of engagement between the tool and the workpiece). These areas of accelerated wear were also reported in [De Melo et al., 2006, Ducros et al., 2003 and Trent and Wright, 2000]. Optimized cutting kinematics and cutter path strategies can be utilized to diminish the formation of burrs during milling, [Byrne et al., 2003].

[14] Visual inspection of the workpiece revealed the formation of debris of hardened steel along the outer leading edge of the machined surface.

4.2.3.2 Cutting Forces and FFT Analysis

The variation in cutting force components at different cutting speeds is presented in Figures (4.36.a, 4.36.b and 4.36.c). The variation is certainly correlated to tool wear behavior. No dramatic drop in the resultant cutting force was detected as cutting speed increased; refer to Figure (4.36.d). However, the highest cutting speed resulted in a slightly lower resultant cutting force up to a machined length of 60 m. The differences detected can be related to the behavior of the working material at higher cutting speed (i.e. thermally-reduced yield strength of AISI H13). The higher speed resulted in more heat flowing within the shear zone and a corresponding increase in shear angle and reduction in shear flow stress, particularly with a hard workpiece material, [Ng and Aspinwall, 2002].

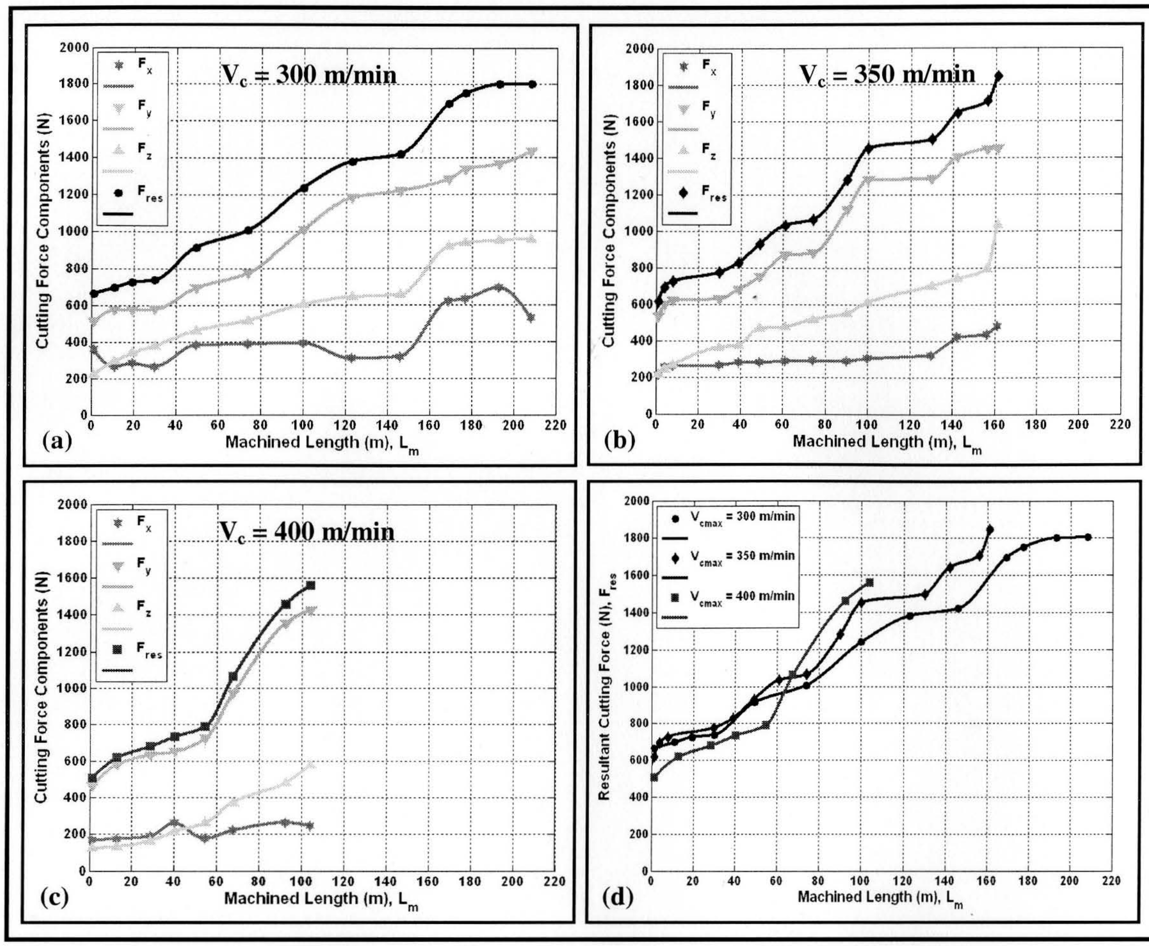

Figure (4.36) Effect of cutting speed on cutting force components

The experimental frequency response of the cutting force components were investigated to identify the nature of vibrations induced during cutting. The Fast-Fourier-Transforms (FFT) for the three tested cutting speeds are shown in Figure (4.37). At the tested range of cutting speeds, the cutting process showed chatter-free dynamic behavior throughout cutting. The force spectra indicate that significant peaks were excited at the fundamental cutting frequency and its subsequent harmonics; refer to Figure (4.37. b). At 300, 350 and 400 m/min, there are five, six and seven main peaks spaced apart by three periods equivalent to the tooth passing frequencies of approximately 318, 371 and 424 Hz respectively.

The spindle frequency (corresponding to the cutter or tool run-out 5-7 μm) became more distinguishable as cutting speed increased, particularly from the measured F_x and F_z cutting force spectra; refer to Figures (4.37.a and 4.37.c). Despite the peaks lower amplitudes, the cutter run-out should be kept within a lower range (≈ 2-3 μm) for better cutting performance. This is due to the significant influence of cutter run-out on the dynamic stability of a chatter-free cutting process and consequently on the machined surface quality obtained [Liu and Cheng, 2005].

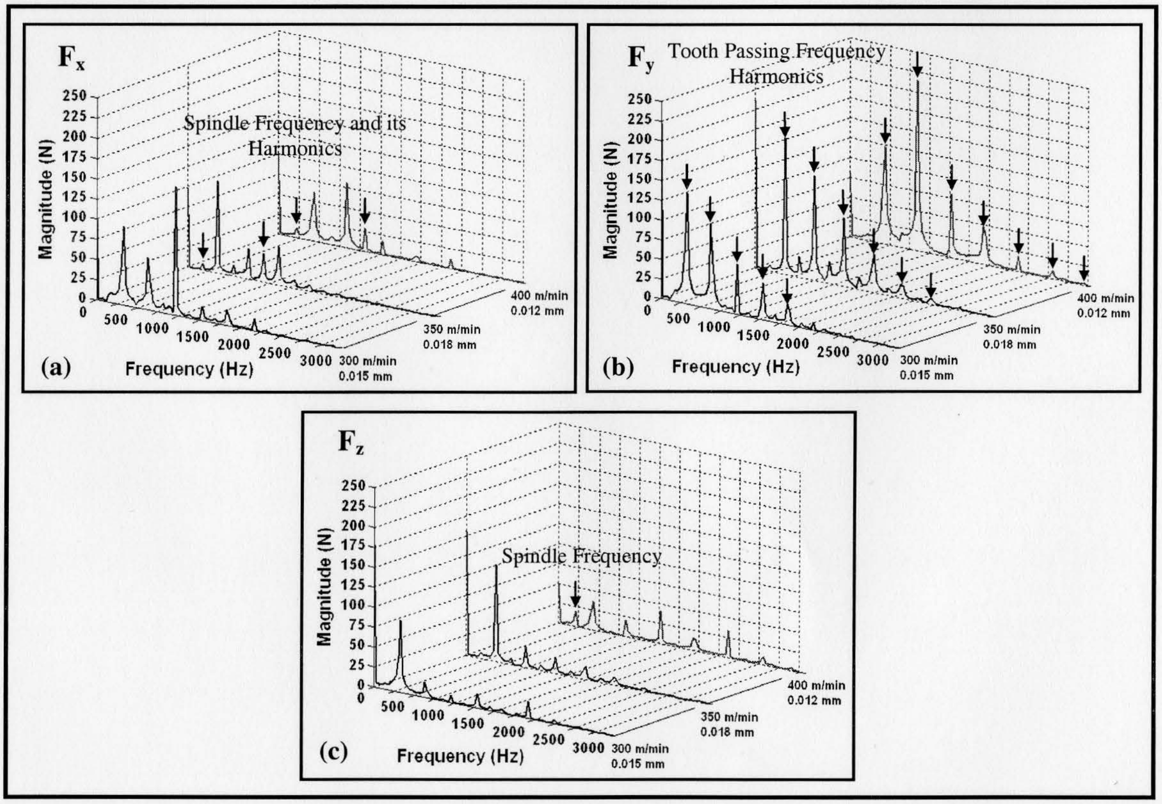

Figure (4.37) The variations in frequency spectra for the measured cutting force components with the corresponding values of cutting speed and flank wear

4.2.3.3 Evaluation of Surface Roughness

Figure (4.38) shows the variation in average surface roughness over the machined length for two different cutting speeds. At the higher cutting speed (400 m/min), the average surface roughness (corresponding to the formation of pick-interval scallops on the machined surface) was almost the same throughout the cutting test. The increase in roughness as a result of flank wear evolution and tool run-out was compensated by the decrease in cutting forces which favored the steadiness of surface roughness. Under the tested range of cutting speeds, using a higher cutting speed did not lead to a distinguishable improvement in the surface finish. This is attributed to some extent to the tool-clamping system utilized in this study which had relatively high cutter run-out.

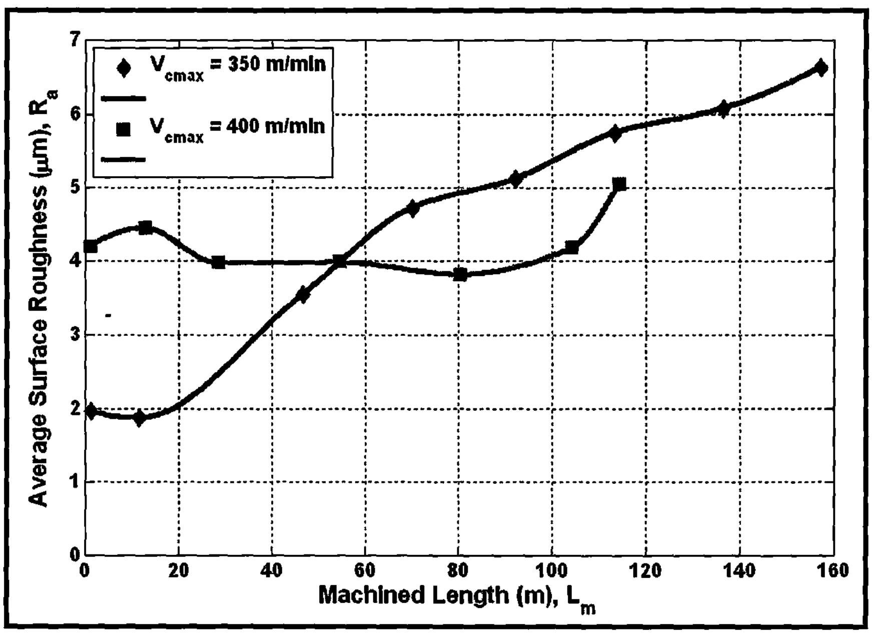

Figure (4.38) Effect of cutting speed on machined surface roughness

4.2.3.4 Chip Configurations

Chip Color and Shape

As the cutting speed increased, both the tool and the chips are subjected to a rapid flow of intensive heat. Different cutting speeds returned chips with different distributions of colors. At a cutting speed of 400 m/min, the chip surface colors changed from (medium violet red and blue) to (green blue and traces of silver) and finally to (light grey-silver and traces of green blue) as tool wear developed. The color distributions indicate that the temperature in the cutting zone exceeded 1200 °C as tool wear deteriorated. Therefore, very brittle chips were produced with intensive cracking and rough surface textures; refer to Figure (4.39). However, the influence of tool wear on the shape of the chips was more dominant than that of increasing cutting speed. Closer examination of the rake faces revealed that the tool-chip contact length reduced as cutting speed increased.

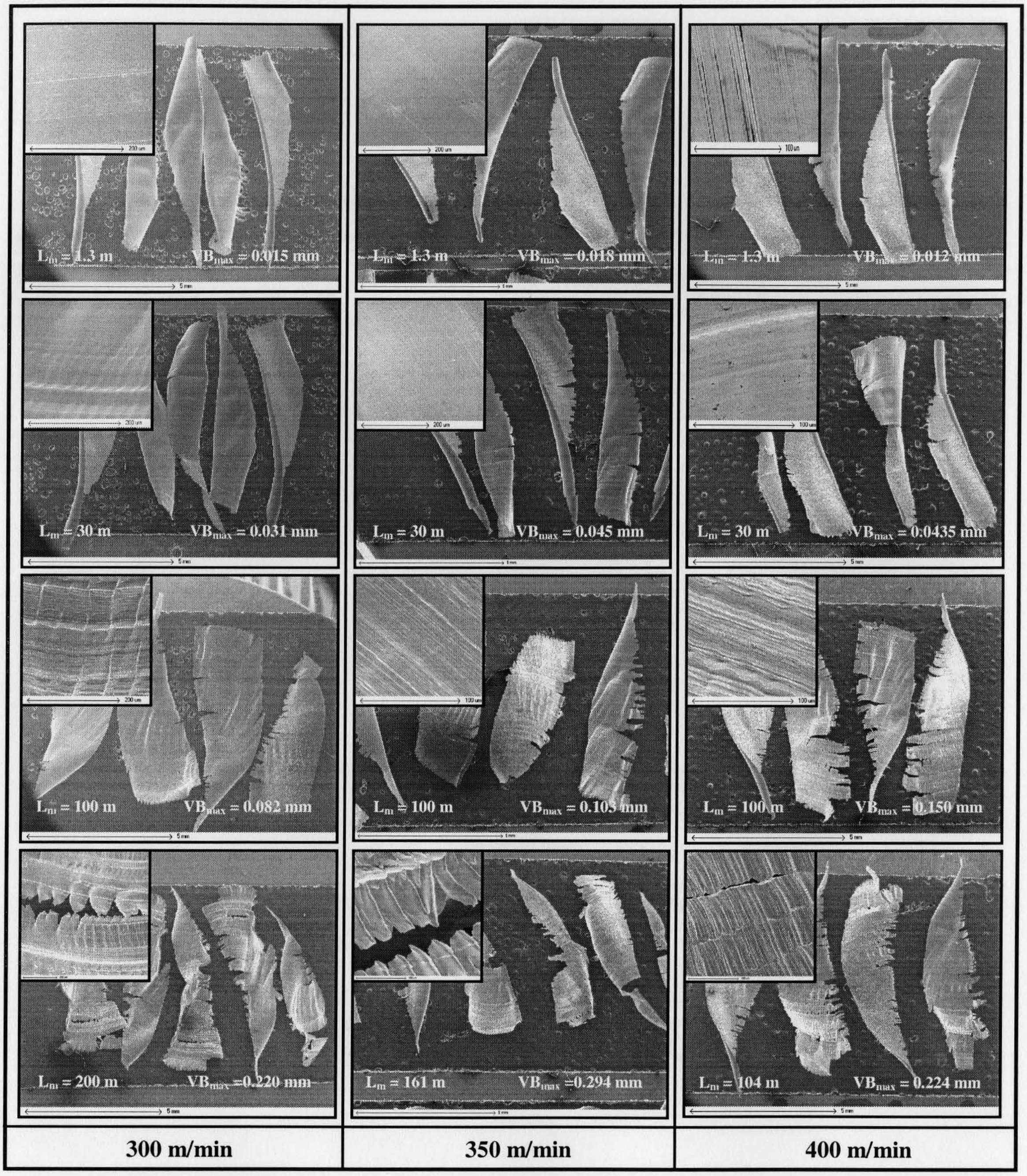

Figure (4.39) SEM images showing the effect of cutting speed on chip shape at different machined lengths

Chip Morphology

Figure (4.40), shows the morphology of the chips collected at different cutting speeds and different machined lengths. Chip segmentation was evident for all the tested cutting speeds. As expected, thinner chips were obtained as cutting speed increased. This correlates to the reported increase in shear angle as cutting speed increases [Kishawy and Becze, 2002, and Ng and Aspinwall, 2002]. At the beginning of cut (1.3 m), the average chip thicknesses of 31.25, 23.5 and 22.8 μm were obtained corresponding to cutting speeds of 300, 350 and 400 m/min respectively. The reduction in chip thickness has an influence on the detected reduction in the resultant cutting forces as the cutting speed increased.

As cutting speed increased, shear localized chips were produced with thicker white layers formed along the chip/tool contact surface due to the higher concentrated thermal energy developed within the secondary shear zone; refer to the chips produced at the 30 m machined length in Figure (4.40). A similar observation was made in [Poulachon et al., 2007]. As tool wear deteriorated, the chips produced at higher cutting speeds experienced more brittleness and discontinuity under high temperature and high frictional conditions; very deep crack propagation resulted in discontinuous chips. This type of chip, as mentioned previously, is a special type of catastrophic-shear chip with the sheared chip segments being separated. This is an indication that the working-material showed almost no resistance to crack propagation with the failure in the primary shear zone being of a brittle nature rather than ductile.

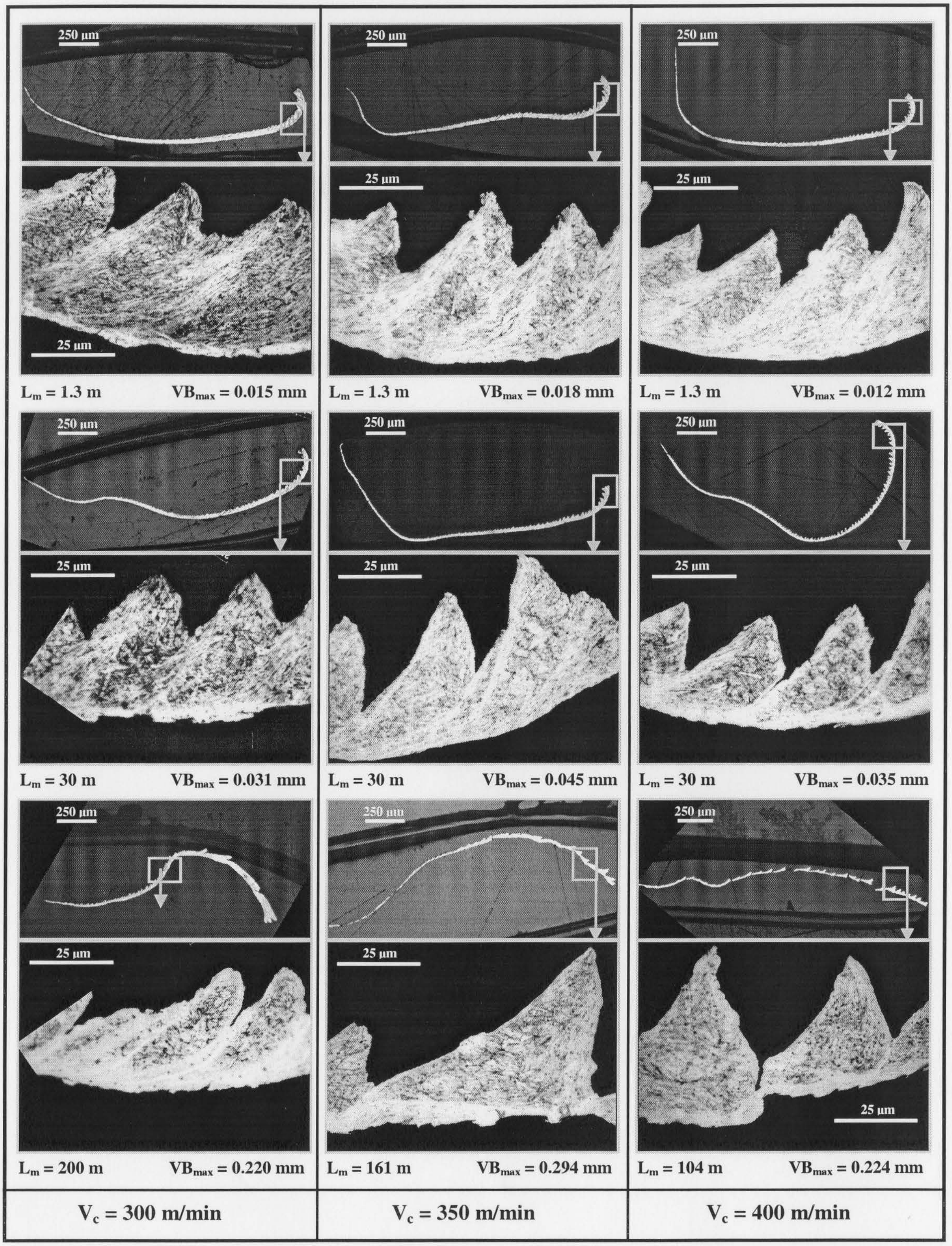

Figure (4.40) Optical microscopic images showing the effect of cutting speed on chip morphology at different machined lengths

4.2.4 Investigation of Cutting Tool Performance Using Different Hard PVD Coatings

4.2.4.1 Influence of Post-surface Treatment on Coated Tool Performance

The objective is to investigate the feasibility of improving the cutting performance of TiAlCrN/NbN coated-carbide tools (Mitsubishi C-2SB) by post-treatment-polishing of their coated-surfaces. The cutting tests were conducted under the following dry cutting conditions: maximum cutting speed of 350 m/min, feed rate of 0.06 mm/tooth, table feed of 1,337 mm/min, axial and radial depth of cut of 5 and 0.6 mm respectively, and pressurized air of 100 PSI (≈ 0.69 MPa) through super-air nozzle.

The coating surfaces of the tool were examined before and after the treatment; refer to Figure (4.41). It can be observed that the polished coating-surface exhibited a smoother texture with an almost droplet-free surface morphology. However, the attrition of "macro-particles" during the surface treatment resulted in the formation of "micro-pores" on the treated surface. These pores or pits formed on the coating surface represent a loss-mechanism[15] of the coating material. Therefore, they might have a detrimental impact on coating performance particularly in dry hard cutting. In addition, closer examination of the cutting tools revealed that there is a scarcity of most of the coating elements Ti, Cr and Nb along the cutting edge line after treatment.

[15] The loss-mechanism can be either in the form of micro-pores or complete delamination of some of the coating layers (≈15 nm/layer in thickness).

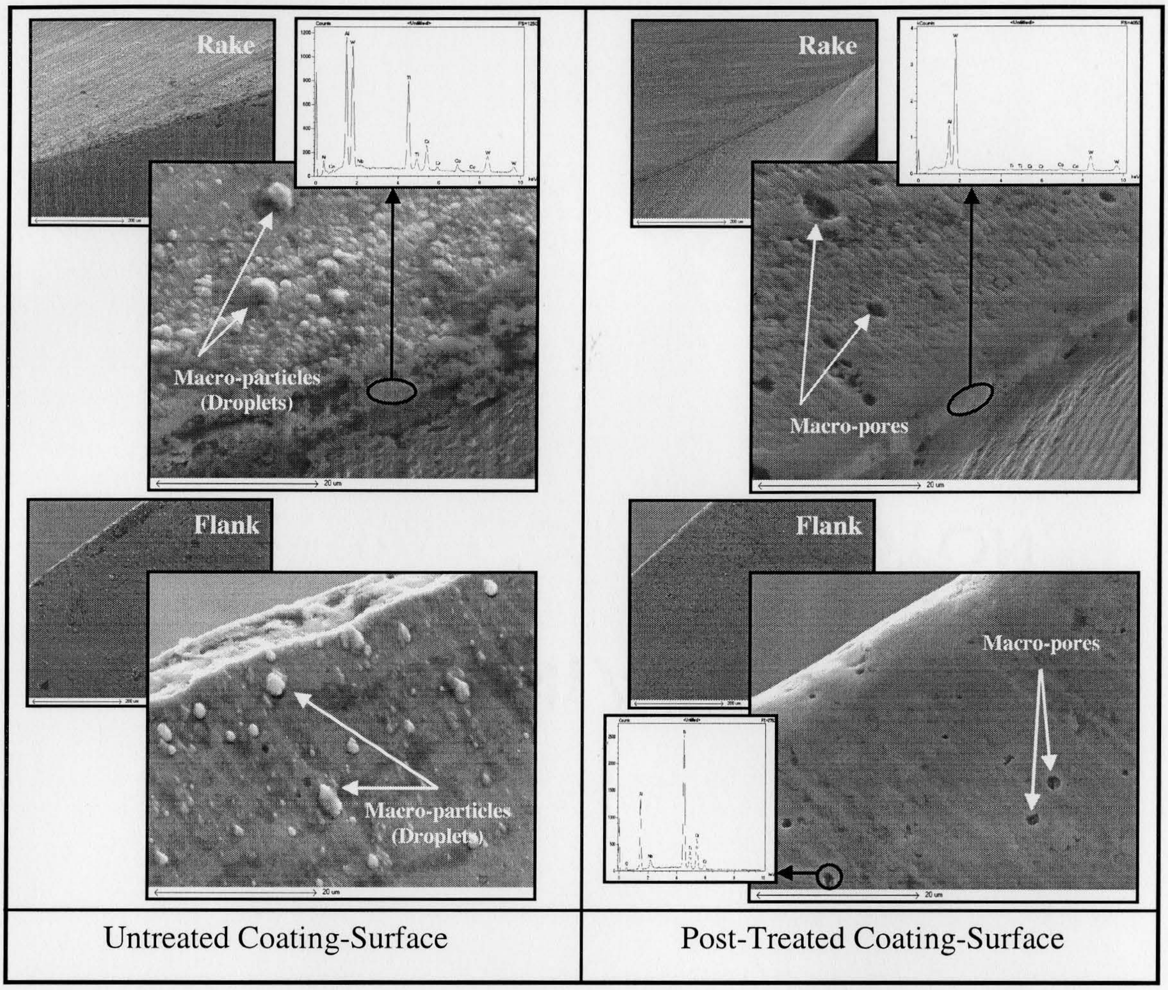

Figure (4.41) SEM images with EDS analysis showing rake and flank sides of unworn (new) TiAlCrN/NbN-coated tools without and with post-treatment

Evaluation of Tool Life and Tool Wear Behavior

Figure (4.42) shows the development of flank wear along the untreated and post-treated coated-tools. The flank wear developed at almost the same rate during the running-in and the post-running in wear stages (i.e. up to a machined length of 113 m). Then both tools started to exhibit different flank wear evolutions. The untreated coated-tool showed more predictable and uniform tool wear behavior and consequently longer tool life, while the treated one experienced an accelerated and localized flank wear progression; refer to the SEM images in Figure (4.42). Despite the smoother surface morphology and the improved tribological characteristics of the post-treated coated-tool, the loss-mechanism of the coating material during the surface-treatment negatively altered the coating adaptability and eventually offset the capabilities of the coating. This observation is in conflict with the study reported in [Endrino et al., 2006], where post-treated AlCrN coated-tool were found to have an improved tool life during end-milling of Austenitic Stainless Steel under wet cutting conditions. They related the longer tool life of the post-treated tool to the ability of the formed micro-pores to carry the coolant during cutting, which enhanced the lubricity. In this case since liquid coolant was not used this beneficial effect of the pores could not be realized.

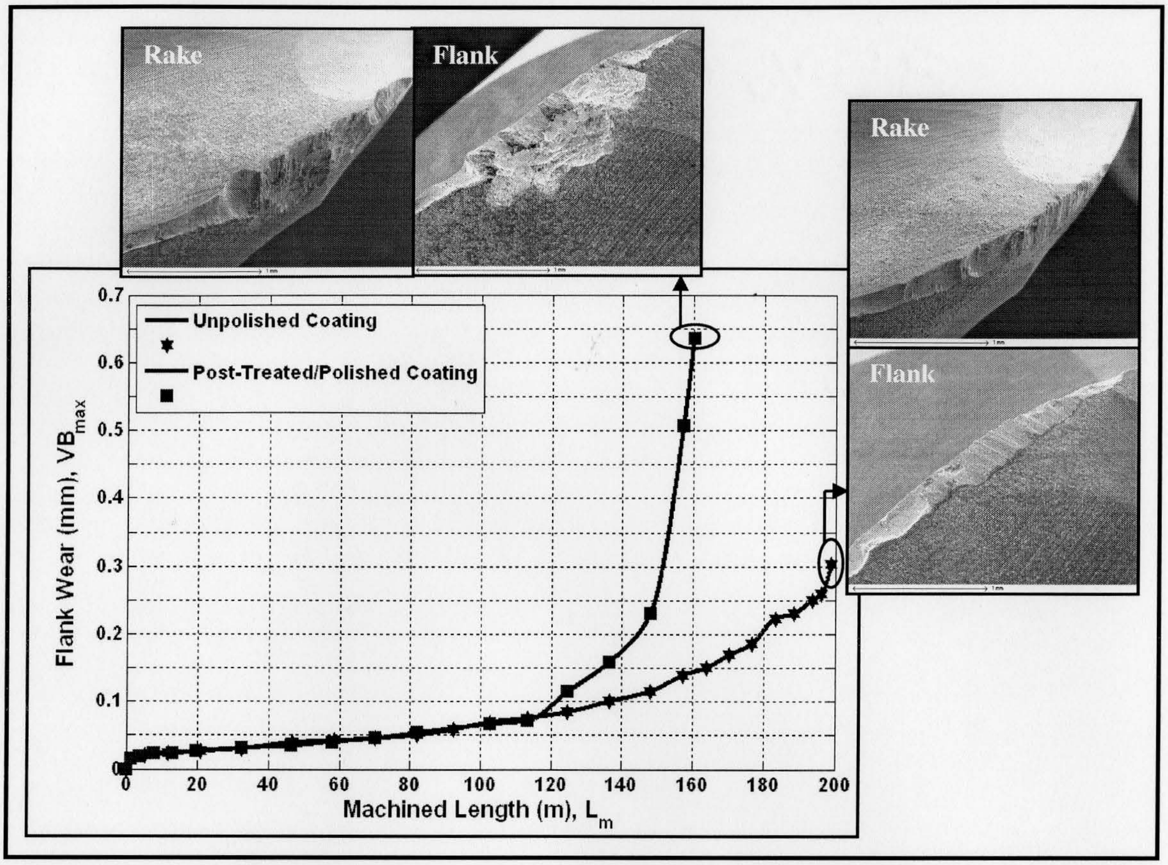

Figure (4.42) Effect of post-treatment of coating surface on flank wear progression and developed tool-wear patterns

Evaluation of Cutting Forces and Surface Roughness

The variation of cutting force components is presented in Figures (4.43.a, 4.43.b and 4.43.c). The variation is correlated to tool wear behavior particularly in the case of untreated coated-tool. There was a sudden increase, then decrease, in all cutting force components prior to the end of the tool life in the case of the treated tool. The sudden increase is correlated with the dissipation of more frictional energy along the interface between the flank land and the work-material with a corresponding increase in the cutting force at the onset of the rapid wear stage (corresponds to a machined length of almost 120 m). On the other hand, the sudden drop is mainly attributed to the tremendous amount of heat that is suddenly starting to generate and accumulate during this rapid wear stage. This amount of heat accounted for the reduction of cutting force due to the higher thermal loading with a corresponding reduction in the yield strength of the work-material. Therefore, the variation in cutting forces is still the most reliable approach for in-process monitoring of tool wear.

Strong correlations were found between the variations of F_y and F_z cutting force components, and the average surface roughness for the untreated and post-treated cutting tools; refer to Figure (4.43.d). The average surface roughness showed the strongest correlation to F_y cutting force variation with correlation coefficients of 0.982 when post-treated coated tool was used. Both tools returned a comparable surface finish. However, the discrepancy in the obtained surface roughness up to a machined length of 60 m can be attributed to the tribological behavior of the untreated coating surface that resulted in more heat to be induced into the workpiece material during cutting. This heat induction relatively eased the material deformation and returned better surface finish.

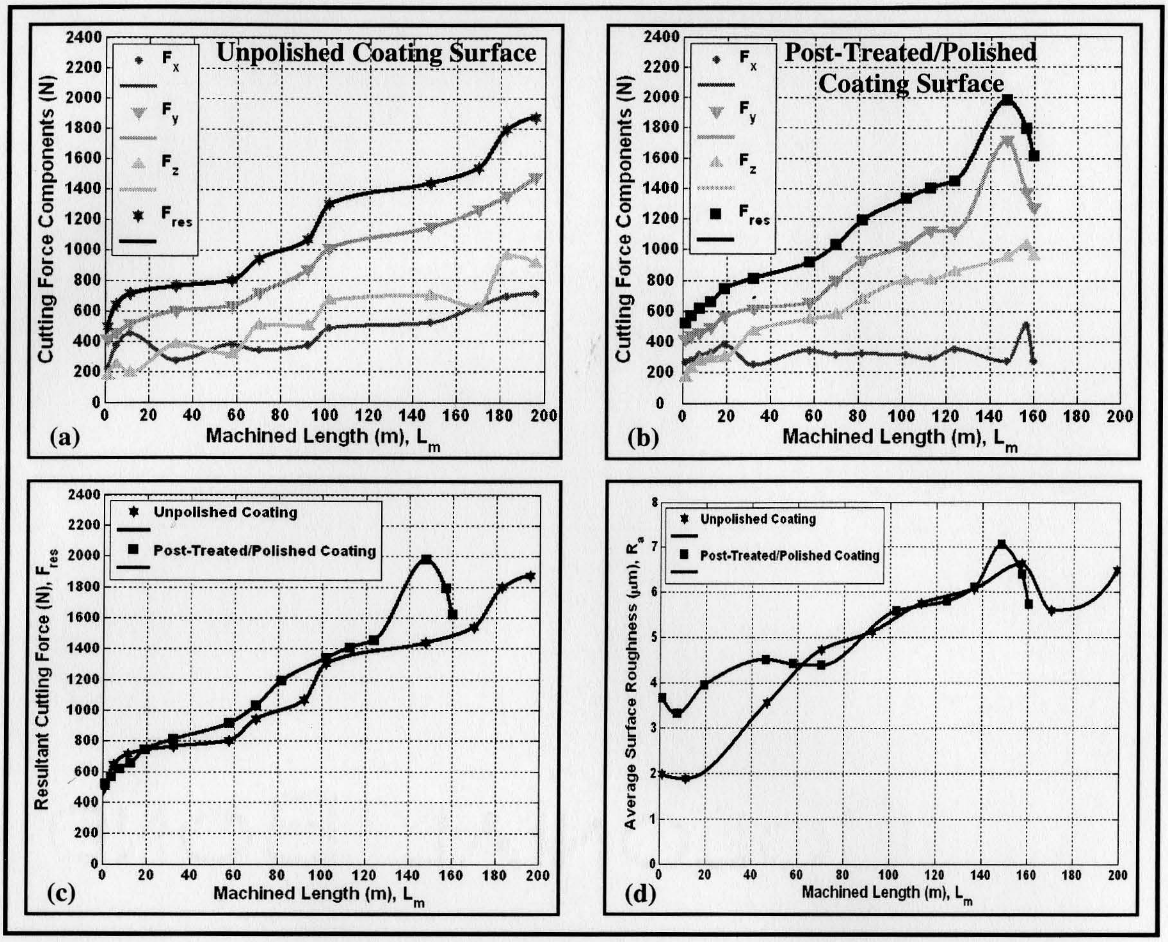

Figure (4.43) Effect of coating surface-treatment on: (a, b) Cutting force components; (c) Resultant cutting forces and (d) Average surface roughness

Chip Configurations

Figure (4.44) presents SEM images taken for the inside and backside surfaces of the chips collected during the two cutting tests. The comparable cutting performance of the two tools resulted in chips having almost the same shapes and surface textures. However, the improved surface roughness of the post-treated coating was obvious at 30 m machined length (corresponds with the onset of coating self-adaptability). In this case, the backside of the chips, produced by the treated-tool, exhibited smoother surface morphology than that of the chips produced by the untreated-tool.

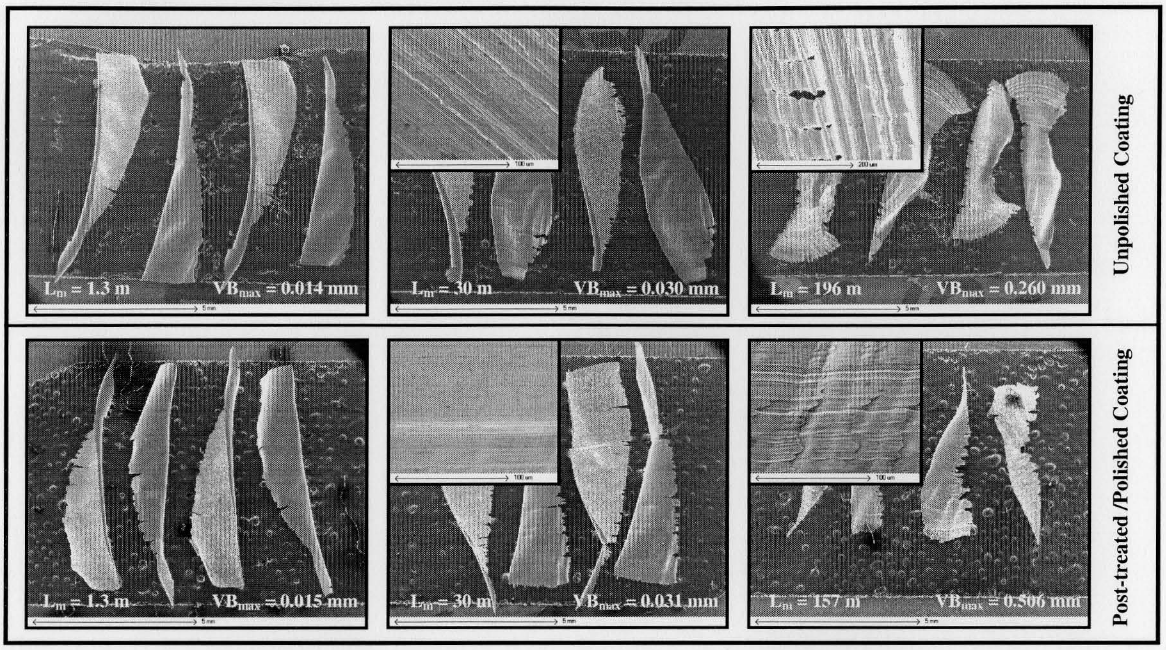

Figure (4.44) Effect of coating surface-treatment on chip shape

4.2.4.2 Evaluation of Super-Nitride Hard-Coating for Hard Cutting Application

Supernitrides (SN) are another class of hard coatings. Owing to their advanced sputtering technology, the coating layers are not only hard with an enhanced oxidation resistance but also chemically stable. This improves the performance of the formed oxide-layers in hard machining, [Erkens, 2007, Erkens et al., 2004, Erkens et al., 2003 and Weinert et al., 2004]. A commercially available AlTiN-based SN-coated-tool was tested under the following dry cutting conditions: machining of hardened AISI H13 (HRC 54-55), cutting speed of 300 m/min, feed rate of 0.06 mm/tooth, table feed of 1,146 mm/min, axial and radial depth of cut of 5 and 0.6 mm respectively, and pressurized air of 100 PSI (≈ 0.69 MPa) through an open copper tube. It was difficult to formulate any comparison between the SN-coating and the nano-multilayered TiAlCrN/NbN due to the difference in design and manufacturing of the substrates used in each case. Figure (4.45) shows the development of flank wear along the SN-coated-tool.

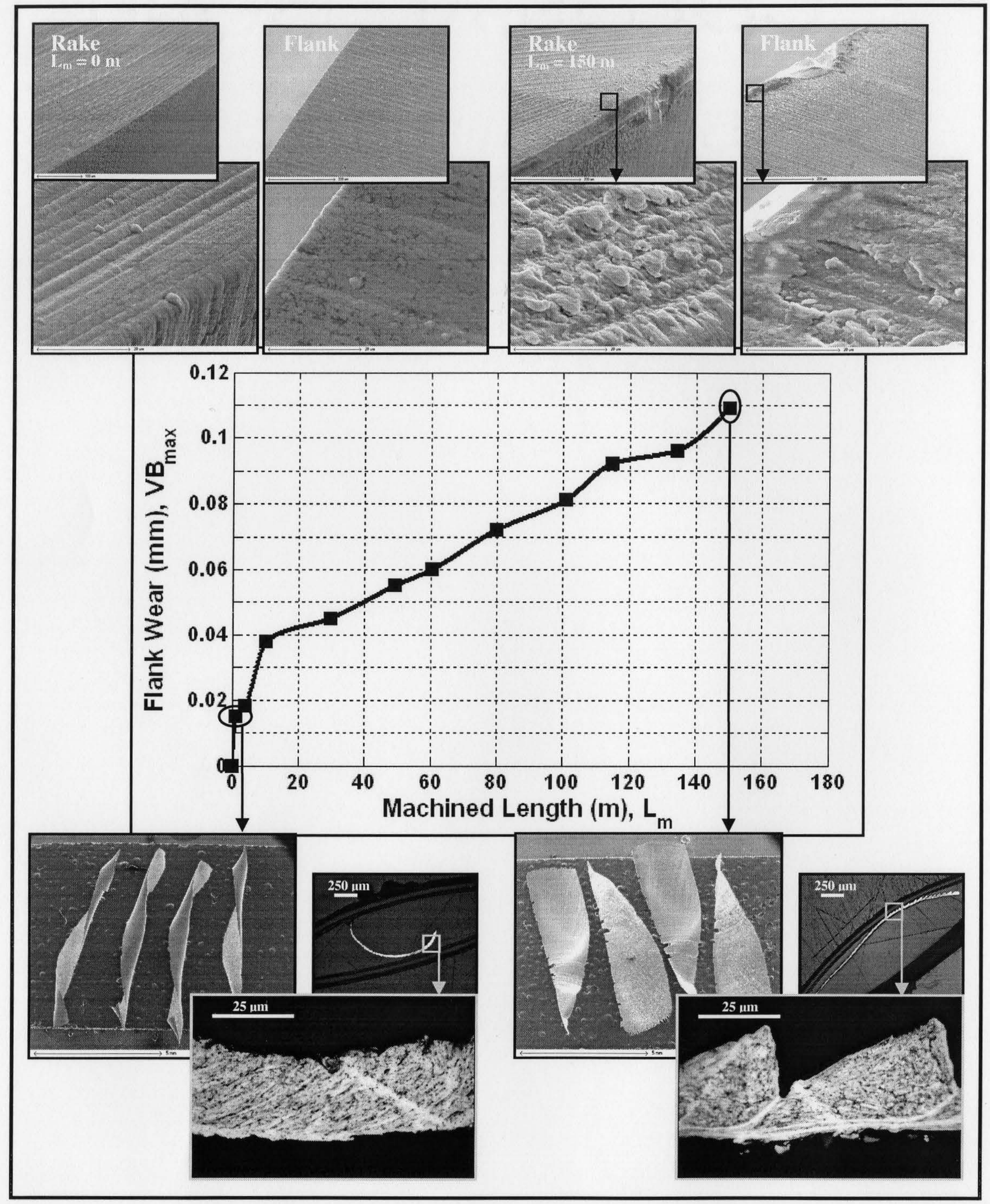

Figure (4.45) Flank wear evolution with the corresponding tool-wear patterns and chip morphology for SN-HSN^2 coated-tool

The enhanced coating surface morphology can be observed; refer to the SEM images of the rake and flank sides of the unworn (i.e. new) tool in Figure (4.45). The smooth and droplet-free coating surface improved the coating performance; small chip-tool contact length (≈ 150 μm) was observed on the rake side of the cutting tool. The chip configurations at the beginning of the cut revealed that golden-brown curly chips with thin chip thickness (≈ 20 μm) and continuous morphology were produced. This is an indication of the improved frictional conditions along the contact zones with a corresponding increase in the shear angle and decrease in the shear force. Closer examination of the cutting edge by the end of the cutting test showed small flank wear patterns scattered along the cutting edge with less chipping intensity. In addition, less seizure formation was encountered on the rake face. The variation of cutting force components is presented in Figure (4.46). The cutting forces exhibited lower magnitudes than those usually obtained under the same cutting parameters. This correlates with the improved coating performance.

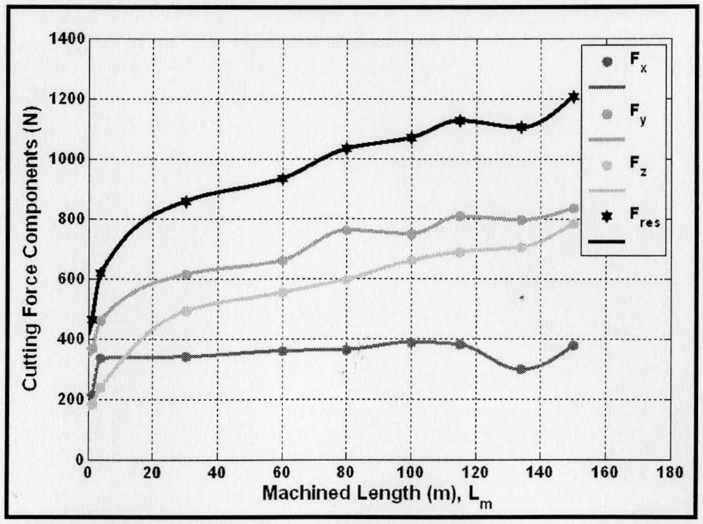

Figure (4.46) The variation of cutting force components versus the machined length for SN-HSN^2 coated-tool

Despite the improved coating performance, the substrate design did not complement the coating that well due to its lower stiffness. The cutting test was aborted when signs of early chatter vibration were observed on the cyclic variation of the cutting force components. Figure (4.47) shows samples of the measured cutting force data with the corresponding FFT spectra. It can be observed that several distinct peaks with higher frequency-components (1,750-3,000 Hz) were excited close to one of the natural frequencies of the cutting tool ($\approx$ 3790 Hz). In addition, chatter marks were imprinted on the machined surface leading to a poor surface finish.

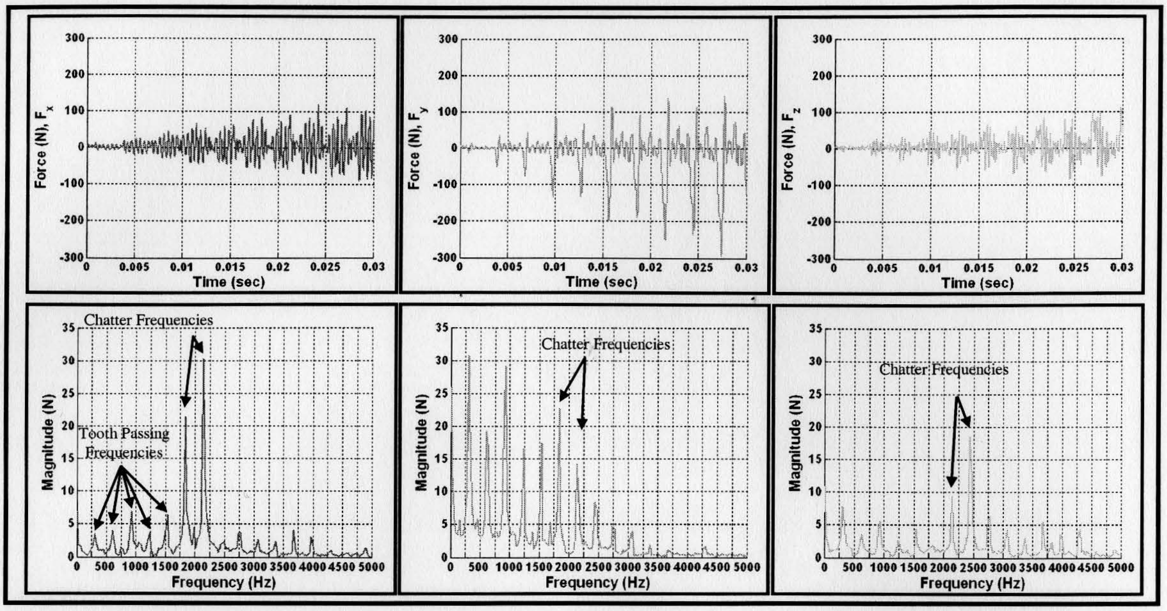

Figure (4.47) Measured components of cutting forces with the corresponding frequency spectra

Chapter 5: Conclusions and Future Work

5.1 Summary and Conclusions

This study attempted to provide a detailed investigation on the cutting performance of coated carbide tools during high speed milling of hardened Die Steel (AISI H13) with a hardness of (HRC 54-55). Three different micro-grain tungsten carbide substrates were employed for the experimental work. The influence of substrate design on the cutting performance was investigated. Two different multi-layered PVD hard coatings were deposited on the cutting tools that were tested in the presented study: namely, experimental Nano-multilayered TiAlCrN/NbN PVD coating and commercially available Supernitride-HSN^2 AlTiN PVD coating. An enhanced design of cutting edge micro-geometry was developed based on the concept of geometrical adaptation. The difference in cutting performance between the adaptive and non-adaptive geometries of the cutting tools was highlighted.

An improved substrate design of ball nose end mills suited for high performance machining was selected for further investigation of TiAlCrN/NbN PVD coating under a higher range of cutting speeds (300-400 m/min). Different dry air cooling strategies and MQL cutting condition were investigated as well. The feasibility of improving the cutting performance of the coated-carbide tools by post-treatment or coating surface polishing was examined. In the presented experimental investigation, the cutting performance was analyzed based on the evaluation of tool life, tool wear behavior and machined surface roughness. In addition, the cutting dynamics were analyzed based on the measured cutting force data and chip configurations. The main findings of the presented work can be summarized as follows:

- Nano- multilayered TiAlCrN/NbN PVD hard coating was found to be suited for hard high-speed-milling applications. Metallurgical design of the coating (i.e. nano-laminated structure) enhanced the formation of metallic-based oxide tribo-films on the tool surface during cutting. The formation of protective oxides such as $(AlCr)_2O_3$ complex tribo-oxides and Niobium-based oxides enhanced the surface-adaptability of the coating. This eventually improved the tool wear resistance under aggressive conditions of diffusion and abrasion tool wear mechanisms. Development of such coating has made it possible for the coated carbide tools to function satisfactorily under a higher range of cutting speeds (300-400 m/min);
- The integrated methodology for the designing of the cutting tool edges helped provide the cutting edge with a strong adaptive micro-geometry, which eventually enhanced the self-adaptability of the coating. However, the chamfered cutting edge preparations resulted in higher magnitudes of the machining forces than those resulting from the un-chamfered cutting edge. This increase in the mechanical loadings was intensified by tool wear evolution and accompanied by some excited vibrations "hints of chatter frequency" and hence premature shank brittle fracture. Therefore, any adaptive cutting edge geometry has to be coupled with the shortest possible overhang for maximum stiffness and thick core for the lowest possible deflection;

- At the early stage of cutting, the cutting edge micro geometry had no significant influence on the cutting stability. Once the tool wear deteriorated, cutting with tools with chamfered cutting edges led to a transitional stability within the cutting system;
- Smaller chamfer width resulted in shorter chip-tool contact length, lower cutting forces and relatively lower amount of heat generated during cutting;
- The surface roughness was found to be mostly correlated to the force acting in the axial direction (Fz). A larger chamfer width resulted in slightly higher surface roughness due to the vibrations associated with the increase in cutting forces;
- For the dry air cooling strategies utilized the maximum-flow settings for dry cooling resulted in better cutting performance than that obtained by the minimum-temperature settings. Using chilled-air as a cutting environment resulted in severe damage to the tool rake face. Utilizing a copious flow of dry air as a cutting environment was found to be the most effective dry cooling strategy for hard high speed milling applications. Sufficient air flow resulted in more predictable chip removal (i.e. proper chip evacuation) and adequate heat dissipation without activating the onset of thermal shocks. The adequate heat dissipation produced by the super-air nozzle was attributed to the balance between the corresponding higher heat transfer coefficient and higher heat-flux induced into the tool;
- Despite its beneficial lubricious and tribological effect, MQL was less effective than dry air cutting environment under conditions of high speed milling (400 m/min) of hardened steel. Dry cutting (using pressurized air as a cutting

environment) was found to be more favorable not only for the tool wear behavior of the coated carbide tools used in this cutting application but also for the deformation behavior of the working material;

- Higher cutting speed was always accompanied by shorter tool life under the tested range of cutting speeds. The highest cutting speed resulted in slightly lower resultant cutting force up to a machined length of 60 m. This was due to the thermally-reduced yield strength of AISI H13 as more heat flowed within the shear zone. This may correspond with an increase in the shear angle and a reduction in the shear flow stress within the deformation zone. A reduction in the chip thickness as cutting speed increased was also observed. Using higher cutting speeds did not lead to a distinguishable improvement in the surface finish. However, the reduction in cutting forces associated with the high cutting speed seemed to offset the effect of flank wear evolution, so as to favor the steadiness of the machined surface roughness throughout the cutting test;
- Post-treatment-polishing of TiAlCrN/NbN PVD coating surface yielded a coated-tool with poorer cutting performance as compared to the untreated one. The loss of the coating material during surface-treatment was believed to negatively alter the coating behavior despite its droplet-free surface morphology. This loss of coating material was found as micro-pores formation and coating layer delamination (bearing in mind that each coating layer is about 15 nm in thickness);

- Owing to its improved surface morphology, Supernitride-HSN[2] AlTiN PVD coating exhibited small flank wear patterns scattered along the cutting edge with minimal edge chipping intensity;
- In most of the observed flank wear evolutions, the maximum flank wear tended to be more localized around the highest contact point between the tool and the workpiece. The localization became even more evident as cutting speed increased. This particular type of flank wear was attributed to the intensified abrasion and attrition interactions between the tool and the burrs or the debris of hardened steel. These burrs usually formed along the outer leading edge of the machined surface. The incorporation of a small tilting angle or optimized cutting kinematics may diminish the detrimental effect of the burrs formed during milling;
- Severe tool wear was detected by excessive variation in the cutting force components throughout the cutting time. Excessive variation can be in the form of a sudden reduction in the magnitude of the resultant cutting force prior to the end of tool life. The sudden reduction in the resultant measured force data was related in one case to the fatigue thermal cracking and the excessive edge chipping. These forms of tool wear were suddenly followed by a catastrophic tool failure. Another sudden reduction was linked to the accelerated flank wear progression. There was a corresponding reduction in the yield strength of the working material which was due to the tremendous amount of heat generated and accumulated during the rapid wear stage. Therefore, the variation in cutting forces is still one of the most reliable approaches for in-process monitoring of tool wear and cutting stability;

- Detailed investigation of chip formation and configuration showed that deformed chip thickness, effective rake angle of the tool and tool wear have some influence on the formation of saw-tooth chips as well as the morphology of chip segmentation. The negative rake angle yielded "inhomogeneous deformed segmented chips" with uneven serrations due to higher strain and pressure imposed into the work-material under the negative rake angle effect. The investigation of the chip formation supported the theory reported by other researchers in the literature that the adiabatic shear theory can be used either as a stand-alone theory or be accompanied by the periodic fracture theory to describe the initiation and formation of saw-tooth chips. Closer examination of the cross sections of chips showed that some shear bands were initiated at the tool tip but they did not propagate sufficiently to the free surface so as to cause catastrophic thermoplastic instability.

5.2 Recommendations for Future Work

Future research in the area of high-speed milling of hardened steels is suggested to continue in order to address some of the open research issues discussed in this thesis, which can be summarized as follows:

- Further investigation of the integrated methodology for designing adaptive cutting edge micro-geometries for specific cutting applications: The results indicated that selecting the proper cutting edge preparation for certain cutting applications can lead to an improved tool wear behavior. These adaptive cutting edge micro-geometries must be supported by a well-engineered substrate design in order to achieve an optimum cutting performance. Therefore, further experimental and numerical applications are still needed to widely validate this methodology for hard high-speed milling applications.
- Applying MQL cutting conditions under a lower range of cutting speeds: Based on the results obtained in this investigation, utilizing a mist-oil as a cutting environment resulted in less seizure formation along the tool surfaces. However, the early activation of the onset of thermal shocks restrained the beneficial influence of mist lubrication. Therefore, applying MQL cutting conditions under lower range of cutting speeds may improve the cutting performance by avoiding this early activation of thermal shocks while enhancing the tribological performance of the deposited hard PVD coating;

- Investigation of the influence of chip segmentation on cutting dynamics: Due to the increased chip velocities attained under the cutting conditions applied in this thesis, the frequencies associated with the chip segmentation could not be recorded using the available data acquisition system. Therefore, other techniques such as acoustic/noise emission should be considered in the future for better detection of any vibrations that might be induced during cutting due to chip segmentation.

While not covered in this thesis, the finite element analysis (FEA) integration is also an important area of research. Due to the geometric complexity of ball end-milling, FEA iterations are mandatory to fully predict the cutting performance. These numerical iterations must involve the following:

- The cutting edge micro-geometry;
- The material behavior associated with higher values of strain rate attained under higher range of cutting speeds (300 - 600 m/min);
- The transition from continuous to segmented chips as flank wear deteriorates with a corresponding alteration in the temperature field.

Therefore, research and development are highly desired to seamlessly simulate this complex milling process under 2D and 3D configurations.

In addition to the advancements in the above areas, the continual development of new improved designs of hard PVD coatings would be essential for further industrial applicability of carbide tools for hard high-speed milling applications.

Bibliography

Acchar, W., Gomes, U.U., Kaysser, W.A., Goring, J., *Strength degradation of a tungsten carbide-cobalt composite at elevated temperatures*, Materials Characterization, v 43, n 1, 1999, pp. 27-32.

Almeida, F.A., Oliveira, F.J., Sousa, M., Fernandes, A.J.S., Sacramento, J., Silva, R.F., *Machining hardmetal with CVD diamond direct coated ceramic tools: Effect of tool edge geometry*, Diamond and Related Materials, Proceedings of Diamond 2004, the 15th European Conference on Diamond, Diamond-Like Materials, Nitrides and Silicon, v 14, n 3-7, 2005, pp. 651-656.

Altan, T., Lilly, B., Yen, Y.C., *Manufacturing of dies and molds*, Annals of the CIRP, v 50, n 2, 2001, pp. 405-423.

Armarego, E.J.A., Brown, R.H., *The Machining of Metals*, Prentice-Hall, 1969.

Arsecularatne, J.A., *On tool-chip interface stress distributions, ploughing force and size effect in machining*, International Journal of Machine Tools and Manufacture, v 37, n 7, 1997, pp. 885-899.

Arunachalam, R.M., Mannan, M.A., Spowage, A.C., *Surface integrity when machining age hardened Inconel 718 with coated carbide cutting tools*, International Journal of Machine Tools and Manufacture, v 44, n 14, 2004, pp. 1481-1491.

ASM Handbook, *Properties and Selection: Irons, Steels, and High Performance Alloys*, v 1, 10^{th} ed., 1990.

Axinte, D.A., Dewes, R.C., *Surface integrity of hot work tool steel after high speed milling-experimental data and empirical models*, Journal of Materials Processing Technology, v 127, n 3, 2002, pp. 325-335.

Banciu, D., *Cutting tool edge design for longer tool life*, M.Sc. Thesis, McMaster University, ON, 2005.

Barnett-Ritcey, D.D., *High-speed milling of titanium and gamma-titanium aluminide: An experimental investigation*, Ph.D. dissertation, McMaster University, ON, 2004.

Barry, J., Byrne, G., *The mechanisms of chip formation in machining hardened steels*, Journal of Solar Energy Engineering, Transactions of the ASME, v 124, n 3, 2002, pp. 528-535.

Beard, T., *Edge prep can make the difference – preparation of the insert's cutting edge-Emphasis: Cutting Tools*, Modern Machine Shop, 1993.

Benes, J.J., *Get an edge on tool performance*, American Machinist, v 149, n 12, 2005, pp. 42-44.

Bouzakis, K.D., Skordaris, G., Mirisidis, I., Mesomeris, G., Michailidis, N., Pavlidou, E., Erkens, G., *Micro-blasting of PVD films, an effective way to increase the cutting performance of coated cemented carbide tools*, Annals of the CIRP, v 54, n 1, 2005, pp. 95-98.

Braghini A., Coelho, R.T., *An investigation of the wear mechanisms of polycrystalline cubic boron nitride (PCBN) tools when end milling hardened steels at low/medium cutting speeds*, International Journal of Advanced Manufacturing Technology, v 17, n 4, 2001, pp. 244-251.

Byrne, G., Dornfeld, D., Denkena, B., *Advancing cutting technology*, Annals of the CIRP, v 52, n 2, 2003, pp. 483-507.

Chen, J., Huang, Y., Chen, M., *A study of the surface scallop generating mechanism in the ball-end milling process*, International Journal of Machine Tools and Manufacture, v 45, n 9, 2005, pp. 1077-1084.

Chen, L., El-Wardany, T.I., Harris, W.C., *Modeling the effects of flank wear land and chip formation on residual stresses*, Annals of the CIRP, v 53, n 1, 2004, pp. 95-98.

Chen, L., El-Wardany, T.I., Nasr, M., Elbestawi, M.A., *Effects of Edge Preparation and Feed when Hard Turning a Hot Work Die Steel with Polycrystalline Cubic Boron Nitride Tools*, Annals of the CIRP, v 55, n 1, 2006, pp. 89-92.

Conicity Technologies, *Conicity.com : Introduction to EMG.* http://www.conicity.com (28 March 2006).

Cselle, T., Barimani, A., *Today's applications and future developments of coatings for drills and rotating cutting tools*, Surface and Coatings Technology, v 76-77, n 1-3 pt 2, 1995, pp. 712-718.

Davies, M.A., Burns, T.J., Evans, C.J., *On the dynamics of chip formation in machining hard metals*, Annals of the CIRP, v 46, n 1, 1997, pp. 25-30.

Davies, M.A., Chou, Y., Evans, C.J., *On chip morphology, tool wear and cutting mechanics in finish hard turning*, Annals of the CIRP, v 45, n 1, 1996, pp. 77-82.

Davis, J. R., *Metals handbook*, 2nd ed., Materials Park, Ohio: ASM International Handbook Committee, 1998.

De Melo, A.C.A., Milan, J.C.G., Da Silva, M.B., Machado, A.R., *Some observations on wear and damages in cemented carbide tools*, Journal of the Brazilian Society of Mechanical Sciences and Engineering, v 28, n 3, 2006, pp. 269-277.

Diniz, A., Micaroni, R., *Cutting conditions for finish turning process aiming: The use of dry cutting*, International Journal of Machine Tools and Manufacture, v 42, n 8, 2002, pp. 899-904.

Dokainish, M.A., Elbestawi, M.A., Polat, U., Tole, B., *Analysis of stresses during exit in interrupted cutting with chamfered tools*, International Journal of Machine Tools and Manufacture, v 29, n 4, 1989, pp. 519-534.

Ducros, C., Benevent, V., Sanchette, F., *Deposition, characterization and machining performance of multilayer PVD coatings on cemented carbide cutting tool*, Surface and Coatings Technology, v 163-164, 2003, pp. 681-688.

Dumitrescu, M., *Critical assessment of carbide tool performance in high speed milling of hardened tool steel*, M.Eng. Thesis, McMaster University, ON, 1998.

Elbestawi, M.A., Chen, L., Becze, C.E., El-Wardany, T.I., *High-speed milling of dies and models in their hardened state*, Annals of the CIRP, v 46, n 1, 1997, pp. 57-62.

Elbestawi, M. A., Srivastava, A. K., El-Wardany, T. I., *A Model for chip formation during machining of hardened steel*, Annals of the CIRP, v 45, n 1, 1996, pp. 71-76.

Electronica Machine Tools Ltd. *Electronicacarbide.com*, Hard materials division, http://www.electronicacarbide.com/technical.html (21 September 2007).

El-Wardany, T.I., Mohammed, E., Elbestawi, M.A., *Cutting temperature of ceramic tools in high speed machining of difficult-to-cut materials*, International Journal of Machine Tools and Manufacture, v 36, n 5, 1996, pp. 611-634.

Erkens, G., *New approaches to plasma enhanced sputtering of advanced hard coatings*, Surface and Coatings Technology, v 201, n 9-11, 2007, pp. 4806-4812.

Erkens, G., Cremer, R., Hamoudi, T., Bouzakis, K.D., Mirisidis, I., Hadjiyiannis, S., Skordaris, G., Asimakopoulos, A., Kombogiannis, S., Anastopoulos, J., Efstathiou, K., *Properties and performance of high aluminum containing (Ti,Al)N based supernitride coatings in innovative cutting applications*, Surface and Coatings Technology, v 177-178, 2004, pp. 727-734.

Erkens, G., Cremer, R., Hamoudi, T., Bouzakis, K.-D., Mirisidis, J., Hadjiyiannis, S., Skordaris, G., Asimakopoulos, A., Kombogiannis, S., Anastopoulos, J., Efstathiou, K., *Supernitrides: A novel generation of PVD hardcoatings to meet the requirements of high demanding cutting applications*, Annals of the CIRP, v 52, n 1, 2003, pp. 65-68.

Endrino, J.L., Fox-Rabinovich, G.S., Gey, C., *Hard AlTiN, AlCrN PVD coatings for machining of austenitic stainless steel*, Surface and Coatings Technology, v 200, n 24, 2006, pp. 6840-6845.

Fang, N., Wu, Q., *The effects of chamfered and honed tool edge geometry in machining of three aluminum alloys*, International Journal of Machine Tools and Manufacture, v 45, n 10, 2005, pp. 1178-1187.

Fontaine, M., Devillez, A., Moufki, A., Dudzinski, D., *Predictive force model for ball-end milling and experimental validation with a wavelike form machining test*, International Journal of Machine Tools and Manufacture, v 46, n 3-4, 2006, pp. 367-380.

Fox-Rabinovich, G., Totten, G. (Eds.), *Self-organization during friction: Advanced surface-engineered materials and systems design*, CRC Press, Taylor and Francis, 2006.

Fox-Rabinovich, G.S., Yamamoto, K., Kovalev, A.I., Veldhuis, S.C., Ning, L., Shuster,L.S. and Elfizy, A., *Wear behavior of adaptive nano-multilayered TiAlCrN/NbN coatings under dry high performance machining conditions*, Surface and Coatings Technology, v 202, n 10, 2008, pp. 2015-2022.

Fox-Rabinovich, G.S., Yamomoto, K., Veldhuis, S.C., Kovalev, A.I., Dosbaeva, G.K., *Tribological adaptability of TiAlCrN PVD coatings under high performance dry machining conditions*, Surface and Coatings Technology, v 200, n 5-6, 2005, pp. 1804-1813.

Fox-Rabinovich, G.S., Yamamoto, K., Veldhuis, S.C., Kovalev, A.I., Shuster, L.S., Ning, L., *Self-adaptive wear behavior of nano-multilayered TiAlCrN/WN coatings under severe machining conditions*, Surface and Coatings Technology, v 201, n 3-4, 2006, pp. 1852-1860.

Gen, H., *Metal cutting and turning theory*, Manufacturing Engineering Handbook, New York: McGraw-Hill Professional, 2004.

Hirao, M., Tlusty, J., Sowerby, R., Chandra, G., *Chip formation chamfered tools,* Journal of Engineering for Industry, Transactions ASME, v 104, n 4, 1982, pp. 339-342.

Kennedy, B., *A better edge*, Cutting tool engineering magazine, v 56, n 2, 2004.

Kim, S.W., Lee, C.M., Lee, D.W., Kim, J.S., Jung, Y.H., *Evaluation of the thermal characteristics in high-speed ball-end milling*, Journal of Materials Processing Technology, v 113, n 1-3, 2001, pp. 406-409.

Kishawy, H.E.A., *Chip formation and surface integrity in high speed machining of hardened steel*, Ph.D. dissertation, McMaster University, ON, 1998.

Kishawy, H.A., Becze, C.E., *Morphology of chips formed during high speed milling of die and mold tool steel using ball end mills*, Society of Manufacturing Engineers., n MS02-199, 2002, pp. 1-8.

Kishawy, H.A., Rogers, R.J., Balihodzic, N., *A numerical investigation of the chip tool interface in orthogonal machining*, Journal of the Machining Science and Technology, v 6, n 3, 2002, pp. 397-414.

Klocke, F., Eisenblaetter, G., *Dry cutting*, Annals of the CIRP, v 46, n 2, 1997, pp. 519-526.

Koenig, W., Fritsch, R., Kammermeier, D., *New approaches to characterizing the performance of coated cutting tools*, Annals of the CIRP, v 41, n 1, 1992, pp. 49-54.

Komanduri, R., Brown, R.H., *ON the mechanics of chip segmentation in machining*, American Society of Mechanical Engineers, n 80, 1980.

Kovalev, A., Wainstein, D.L., Fox-Rabinovich, G., Yamamoto, K., Veldhius, S., *Impact of Al and Cr alloying of TiN-based PVD coatings on its cutting performance*, Surface and Interface Analysis, v 38, n 4, 2006, pp. 879-882.

Lamikiz, A., Lopez de Lacalle, L.N., Sanchez, J.A., Bravo, U., *Calculation of the specific cutting coefficients and geometrical aspects in sculptured surface machining*, Machining Science and Technology, v 9, n 3, 2005, pp. 411-436.

Lazoglu, I., Liang, S.Y., *Modeling of ball-end milling forces with cutter axis inclination*, Journal of Manufacturing Science and Engineering, v 122, n 1, 2000, pp. 3-11.

Lee, P., Altintas, Y., *Prediction of ball-end milling forces from orthogonal cutting data*, International Journal of Machine Tools and Manufacture, v 36, n 9, 1996, pp. 1059-1072.

Lee, L.C., Lee, K.S., Gan, C.S., *On the correlation between dynamic cutting force and tool wear*, International Journal of Machine Tools and Manufacture, v 29, n 3, 1989, pp. 295-303.

Lim, C.Y.H., Lim, S.C., Lee, K.S., *Wear of TiC-coated carbide tools in dry turning*, Wear, v 225-229, n 1, 1999, pp. 354-367.

Liu, X., Cheng, K., *Modeling the machining dynamics of peripheral milling*, International Journal of Machine Tools and Manufacture, v 45, n 11, 2005, pp. 1301-1320.

Liu, J., Kevin Chou, Y., *On temperatures and tool wear in machining hypereutectic Al-Si alloys with vortex-tube cooling*, International Journal of Machine Tools and Manufacture, v 47, n 3-4, 2007, pp. 635-645.

Löeffler, F.H.W., *Systematic approach to improve the performance of PVD coatings for tool applications*, Surface and Coatings Technology, v 68-69, 1994, pp. 729-740.

Luo, Q., Rainforth, W.M., Munz, W.D., *Wear mechanisms of monolithic and multicomponent nitride coatings grown by combined arc etching and unbalanced magnetron sputtering*, Surface and Coatings Technology, v 146-147, 2001, pp. 430-435.

Machado, A.R., Wallbank, J., *Effect of extremely low lubricant volumes in machining*, Wear, v 210, n 1-2, 1997, pp. 76-82.

Mativenga, P.T., Hon, K.K.B., *A study of cutting forces and surface finish in high-speed machining of AISI H13 tool steel using carbide tools with TiAlN based coatings*, Proceedings of the Institution of Mechanical Engineers, Part B: Journal of Engineering Manufacture, v 217, n 2, 2003, pp. 143-151.

Movahhedy, M.R., Altintas Y., Gadala, M.S., *Numerical analysis of metal cutting with chamfered and blunt tools*, Journal of Manufacturing Science and Engineering, Transactions of the ASME, v 124, n 2, 2002, pp. 178-188.

Nakayama, K, Arai, M, Kanda, T., *Machining Characteristics of Hard Materials*, Annals of the CIRP, v 37, n 1, 1988, pp. 89-92.

Ng, E., Aspinwall, D. K., *The effect of workpiece hardness and cutting speed on the machinability of AISI H13 hot work die steel when using PCBN tooling*, Journal of Manufacturing Science and Engineering, Transactions of the ASME, v 124, n 3, 2002, pp. 588-594.

Ning, Y., Rahman, M., Wong, Y.S., *Investigation of chip formation in high speed end milling*, Journal of Materials Processing Technology, v 113, n 1-3, 2001, pp. 360-367.

Ning, L., Veldhuis, S.C., Yamamoto, K., *Investigation of nano-structured PVD coatings for dry high-speed machining*, Machining Science and Technology, v 11, n 1, 2007, pp. 45-59.

Ning, L., Veldhuis S.C., Yamamoto, K., *Investigation of wear behavior and chip formation for cutting tools with nano-multilayered TiAlCrN/NbN PVD coating*, International Journal of Machine Tools and Manufacture, v 48, n 6, 2007, pp. 656-665.

Özel, T. , Hsu, T., Zeren, E., *Effects of cutting edge geometry, workpiece hardness, feed rate and cutting speed on surface roughness and forces in finish turning of hardened AISI H13 steel*, International Journal of Advanced Manufacturing Technology, v 25, n 3-4, 2005, pp. 262-269.

Poulachon, G., Moisan, A.L., Jawahir, I.S., *Evaluation of chip morphology in hard turning using constitutive models and material property data*, Transactions of the ASME. Journal of Manufacturing Science and Engineering, v 129, n 1, 2007, pp. 41-47.

Rahman, M., Kumar, A. Senthil, Manzoor-Ul-Salam, Ling, M.S., *Effect of Chilled Air on Machining Performance in End Milling*, International Journal of Advanced Manufacturing Technology, v 21, n 10-11, 2003, pp. 787-795.

Rahman, M., Senthil Kumar, A., Salam, M.U., *Experimental evaluation on the effect of minimal quantities of lubricant in milling*, International Journal of Machine Tools and Manufacture, v 42, n 5, 2002, pp. 539-547.

Ren, H., Altintas, Y., *Mechanics of machining with chamfered tools*, Journal of Manufacturing Science and Engineering, v 122, n 4, 2000, pp. 650-659.

Sandvik Coromant, *Modern metal cutting: A practical handbook*, Sweden, 1994.

Santhanaml, A. T., *Carbides, Cemented*, Kirk-Othmer Encyclopedia of Chemical Technology, 5th ed., v 4, 2003, pp. 655-674.

Shatla, M., Kerk, C., Altan, T., *Process modeling in machining. Part II: Validation and applications of the determined flow stress data*, International Journal of Machine Tools and Manufacture, v 41, n 11, 2001, pp. 1659-1680.

Shaw, M. C., *Metal cutting principles*, 2nd ed., Oxford University Press, 2005.

Shaw, M. C., Vyas, A., *Chip formation in the machining of hardened steel*, Annals of the CIRP, v 42, n 1, 1993, pp. 29-33.

Shaw, M. C., Vyas, A., *The mechanism of chip formation with hard turning steel*, Annals of the CIRP, v 47, n 1, 1998, pp. 77-82.

Sikdar, C., Paul, S., Chattopadhyay, A. B., *Effect of variation in edge geometry on wear and life of coated carbide face milling inserts*, Wear, v 157, n 1, 1992, pp. 111-126.

Stephenson, D. A., Agapiou, J.S., *Metal cutting theory and practice*, New York: Marcel Dekker, 1997.

Su, Y., He, N., Li, L., Iqbal, A., Xiao, M.H., Xu, S., Qiu, B.G., *Refrigerated cooling air cutting of difficult-to-cut materials*, International Journal of Machine Tools and Manufacture, v 47, n 6, 2007, pp. 927-933.

Suh, C.S., Khurjekar, P.P., Yang, B., *Characterization and identification of dynamic instability in milling operation*, Mechanical Systems and Signal Processing, v 16, n 5, 2002, pp. 853-872.

Thiele, J.D. , Melkote, S.N., *Effect of cutting edge geometry and workpiece hardness on surface generation in the finish hard turning of AISI 52100 steel*, Journal of Materials Processing Technology, v 94, n 2, 1999, pp. 216-226.

Thomson, W. T., Dahleh, M. D., *Theory of Vibration with Applications*, 5th ed. Upper Saddle River, New Jersey: Prentice Hall, 1998.

Tlusty, G., *Manufacturing process and equipment*, Upper Saddle River, New Jersey: Prentice Hall, 1999.

Tlusty, J., Masood, Z., *Chipping and breakage of carbide tools*, Journal of Engineering for Industry, Transactions of the ASME, v 100, n 4, 1978, pp. 403-412.

Toenshoff, H.K., Arendt, C., Amor, R.B., *Cutting of hardened steel*, Annals of the CIRP, Manufacturing Technology, v 49, n 2, 2000, pp. 547-566.

Toh, C.K., *Comparison of chip surface temperature between up and down milling orientations in high speed rough milling of hardened steel*, Journal of Materials Processing Technology, v 167, n 1, 2005, pp. 110-118.

Toh, C.K., *Vibration analysis in high speed rough and finish milling hardened steel*, Journal of Sound and Vibration, v 278, n 1-2, 2004, pp. 101-115.

Trent, E. M., Wright, P. K., *Metal cutting*, 4th ed. Boston: Butterworth-Heinemann, 2000.

Urbanski, J.P., Koshy, P., Dewes, R.C., Aspinwall, D.K., *High speed machining of moulds and dies for net shape manufacture*, Materials and Design, v 21, n 4, 2000, pp. 395-402.

Venkatesh, V.C., Zhou, D.Q., Xue, W., Quinto, D.T., *Study of chip surface characteristics during the machining of steel*, Annals of the CIRP, v 42, n 1, 1993, pp. 631-636.

Vyas, A., Shaw, M.C., *Mechanics of saw-tooth chip formation in metal cutting*, Journal of Manufacturing Science and Engineering, Transactions of the ASME, v 121, n 2, 1999, pp. 163-172.

Wang, J.Y., Liu, C.R., *Effect of tool flank wear on the heat transfer, thermal damage and cutting mechanics in finish hard tuning*, Annals of the CIRP, v 48, n 1, 1999, pp. 53-58.

Wang, J.J., Zheng, M.Y., *On the machining characteristics of H13 tool steel in different hardness states in ball end milling*, International Journal of Advanced Manufacturing Technology, v 22, n 11-12, 2003, pp. 855-863.

Weinert, K., Inasaki, I., Sutherland, J.W., Wakabayashi, T., *Dry machining and minimum quantity lubrication*, Annals of the CIRP, v 53, n 2, 2004, pp. 511-537.

Yamamoto, K., Kujime, S., Takahara, K., *Properties of nano-multilayered hard coatings deposited by a new hybrid coating process: Combined cathodic arc and unbalanced magnetron sputtering*, Surface and Coatings Technology, v 200, n 1-4, 2005, pp. 435-439.

Yamamoto, K., Sato, T., Takahara, K., Hanaguri, K., *Properties of (Ti,Cr,Al)N coatings with high Al content deposited by new plasma enhanced arc-cathode*, Surface and Coatings Technology, v 174-175, 2003, pp. 620-626.

Yen, Y.C., Jain, A., Altan, T., *A finite element analysis of orthogonal machining using different tool edge geometries*, Journal of Materials Processing Technology, v 146, n 1, 2004, pp. 72-81.

Yeo, S.H., Ong, S.H., *Assessment of the thermal effects on chip surface*, Journal of Materials Processing Technology, v 98, n 3, 2000, pp. 317-321.

Zhang, H.T., Liu, P.D., Hu, R.S., *Three-zone model and solution of shear angle in orthogonal machining*, Wear, v 143, n 1, 1991, pp. 29-43.

Zhou, J. M., Walter, H., Andersson, M., Stahl, J. E., *Effect of chamfer angle on wear of PCBN cutting tool*, International Journal of Machine Tools and Manufacture, v 43, n 3, 2003, pp. 301-305.

Zhu, R., Kapoor, S., Devor, R.E., *Mechanistic modeling of the ball end milling process for multi-axis machining of free-form surfaces*, Journal of Manufacturing Science and Engineering, Transactions of the ASME, v 123, n 3, 2001, pp. 369-379.

Appendix A: Frequency Modes

- Tooth passing frequency (*i.e. cutting frequency*) and its harmonics:

$\omega_{n\,tooth} = \dfrac{ZN}{60}$ Where,

N is the Spindle speed in (RPM);

Z is the Number of flutes.

- Frequency associated with chip formation process (*i.e. chip segmentation*):

$\omega_{n\,chip}(Hz) = \dfrac{r_{chip} V_c}{60\, st_p}$ Where,

r_{chip}

r_{chip} [16] is the cutting ratio, $r_{chip} = st_p/st_h$;

V_c is the cutting speed in (m/min);

st_p and st_h are the average saw-tooth pitch and height respectively, as shown in Figure (A.1).

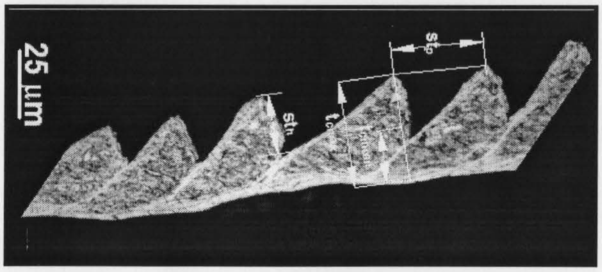

Figure (A.1) Saw-tooth chip produced in hard ball end-milling of AISI H13 (HRC 55)

[16] The cutting ratio is the ratio between uncut-chip thickness and chip thickness or the ratio between chip length and uncut-chip length. For saw-tooth chips, the cutting ratio can be considered as the ratio between uncut-chip thickness and maximum saw-tooth chip thickness, [Elbestawi et al., 1996] or the ratio between uncut-chip thickness and mean chip thickness, [Shaw and Vyas, 1993] or the ratio between the average tooth pitch and average tooth height, [Shaw, 2005].

- Frequencies associated with oscillations arising from the tool-clamping system:

The tool holding system can be approximated as clamped-free beam and longitudinal rod, as shown in Figure (A.2).

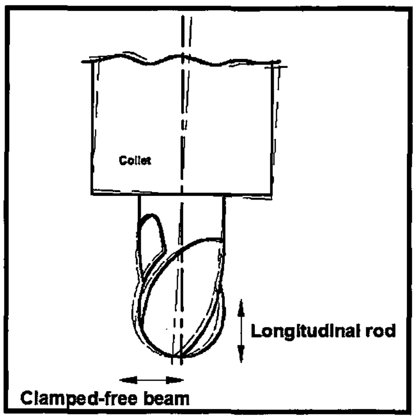

Figure (A.2) Approximated tool-clamping system

Hence, natural frequencies of the nth mode will be, [Thomson and Dahleh, 1998]

$$\omega_{n\,beam} = (2n-1)\frac{\pi}{2\ell}\sqrt{\frac{E}{\rho}} \quad \textit{(for longitudinal rod)}$$

For the first pattern of vibration mode shapes; $n=1$

Then, $\omega_{n\,beam}(Hz) = \dfrac{\pi}{2\ell}\sqrt{\dfrac{E}{\rho}}$

$$\omega_{n\,rod} = (\beta_n \ell)^2 \sqrt{\frac{EI}{m\ell^4}} \quad \textit{(for clamped-free beam)}$$

For the first pattern of vibration mode shapes;

$(\beta_n \ell)^2 = 3.516$

$$\text{Then, } \omega_{n\,rod}(Hz) = 3.516\sqrt{\frac{EI}{m\ell^4}}$$

Where; ℓ : Tool holding overhang length (m)

E : Modulus of elasticity (GPa) for fine micro-grain tungsten carbide tools (≈ 620 GPa)

I : Second moment of area (m^4)

m : Mass density per unit length (Kg/m)

ρ : Mass density (Kg/m^3) for fine micro-grain tungsten carbide tools (≈ 14600 Kg/m^3)